Politecnico di Torino

Politecnico di Torino

Corso di Laurea Magistrale in Ingegneria Biomedica
A.a. 2024/2025
Sessione di Laurea Marzo 2025

The role of low-frequency activity in BCIs motor decoding

A comparison
between invasive (ECoG) and non-invasive (EEG) brain recordings during repetitive finger movements

Supervisors:
Dr. Marco Ghislieri
Prof. Marc Van Hulle

Candidate:
Erik Lupi 316661

ABSTRACT

Brain-Computer Interfaces (BCIs) enable direct communication between the brain and external devices by interpreting neural signals. BCIs can utilize both invasive signals, such as electrocorticogram (ECoG), and non-invasive signals, like electroencephalogram (EEG). This work aims to compare EEG and ECoG signals during repeated finger flexion-extension.

First, it examines CorticoKinematic Coherence (CKC) at low frequencies, analyzing Low Motor Potentials (LMPs). Then, it assesses neural decoding for BCIs by predicting finger trajectories, comparing LMPs and higher frequency bands, as well as a basic (Multiple Linear Regressor, MLR) and a more complex model (Temporal Convolutional Network, TCN).

ECoG data comes from the publicly available Stanford ECoG dataset, which includes recordings from nine subjects performing repeated self-paced, single-finger flexion-extension. For EEG data, an experiment was designed, recording signals during repeated finger flexion-extension at 1 Hz and 3 Hz, with movement frequency guided by a shrinking circle. Six subjects' EEG signals were recorded using a 64-electrodes cap, while finger movements through a sensor glove. ECoG data were provided already preprocessed, with only an additional Common Average Reference (CAR) applied. For the EEG data, preprocessing included removing noisy intervals, applying Notch filters, bandpass filtering, removing eye movement artifacts, and re-referencing with CAR.

CKC was then calculated for both datasets.

ECoG showed an average coherence of 0.45 ± 0.2, consistent across fingers but varying between subjects, ranging from 0.15 (Subject 5) to over 0.6 (Subjects 2, 3, and 6). EEG exhibited lower coherence, with a mean of 0.02 ± 0.01 across subjects, and 0.03 for Subject 2. Additionally, while CKC frequency trends and topographic distributions for ECoG matched expectations, with EEG, it happened only in a few instances. These results suggest that achieving optimal frequency stability in repeated movements is crucial for analyzing CKC with EEG, while this issue is less impactful with ECoG, highlighting the need for high-quality signals.

For the decoding, signals were lowpass filtered at 4 Hz for LMPs, 40 Hz for full-band EEG, and 200 Hz for full-band ECoG. Finger trajectories were predicted using a 0.5 second-brain signal time window preceding the corresponding time instant. Results are reported for the best-performing subject for conciseness. As regards ECoG, the best correlation values between original and predicted trajectories were obtained with the LMPs (0.56 to 0.78 across fingers), with no significative difference using the MLR or TCN. Using the full band, MLR exhibited correlations of 0.44-0.68, while TCN between 0.54 and 0.73. EEG, as expected from the coherence analysis, showed generally low decoding performances with LMPs, with MLR correlations ranging from 0.04 to 0.07 across fingers. TCN did not provide a notable improvement (0.05-0.10). However, some discrete results have been reached by applying TCN to full band data, with correlations between 0.08 and 0.31, while MLR failed. Results suggest that LMPs provide valuable decoding information, with even a simple MLR performing well

when the LMPs are clear. If they are unclear, TCN can be useful using instead raw signals with higher frequencies.

Future works could focus on ensuring consistent movement frequency during repeated finger movements when analyzing CKC. Moreover, for both signals there seems to be a positive correlation between CKC and decoding performance.

List of abbreviations

CAR	Common Average Reference
CKC	CorticoKinematic Coherence
CNN	Convolutional Neural Network
CNS	Central Nervous System
ECoG	Electrocorticogram
EEG	Electroencephalogram
ICA	Independent Component Analysis
MEG	Magnetoencephalographic
MLR	Multiple Linear Regression
MSE	Mean Squared Error
PCA	Principal Component Analysis
PNS	Peripheral Nervous System
PSD	Power Spectral Density
RNN	Recurrent Neural Network
SNR	Signal-to-Noise Ratio
TCN	Temporal Convolutional Network

Table of contents

1 Introduction

1.1 Brain electrical activity

Brain electrical activity refers to the ensemble of electrical signals generated by neurons in the brain, essential for communication, information processing, and the execution of cognitive, motor, and sensory functions.

This electrical activity is part of the broader functioning of the nervous system, which is responsible for processing and transmitting information throughout the body. The nervous system is primarily divided into two main parts: the central nervous system (CNS) and the peripheral nervous system (PNS). The CNS, consisting of the brain and spinal cord, serves as the main control center for integrating and interpreting neural signals. The PNS comprises the network of nerves that extends from the CNS to the rest of the body, enabling communication between the brain, spinal cord, muscles, and sensory organs.

At the core of this system are neurons, the fundamental units of neural communication. Each neuron consists of a cell body (soma), which contains the nucleus and essential organelles; dendrites, which receive signals from other neurons; and an axon, a long projection that transmits electrical impulses away from the cell body to other neurons or muscles. These electrical impulses, known as action potentials, are generated through the rapid opening and closing of voltage-gated ion channels along the neuron's membrane, causing rapid changes in membrane potential. This process enables neurons to efficiently transmit signals across neural networks, allowing for complex functions such as movement control, perception, and cognition.

Figure 1: Visualization of neuronal electrical activity.

When groups of neurons fire synchronously, they produce rhythmic oscillations known as brain waves, which form the basis of brain electrical activity, that can be recorded and analyzed to study brain function and diagnose neurological disorders [1]. The ability to measure brain electrical activity was pioneered by Hans Berger, who, in 1929, recorded the first electroencephalogram (EEG). This breakthrough opened new avenues for research in brain

function and neurological disorders. Nowadays, the electrical activity of the brain can be recorded by different types of electrical signals, which can be classified as invasive or non-invasive, or by magnetic signals. Non-invasive methods, such as EEG, record brain activity from electrodes placed on the scalp, while invasive techniques, such as Electrocorticogram (ECoG) and intracortical recordings, involve electrode implantation at different depths inside the head, ranging from the brain surface to deep within the cortex [2] (Figure 2). Magnetic signals, such as the non-invasive Magnetoencephalogram (MEG), record the magnetic field accompanying the electrical activity of the brain. In this work, the signals that were analyzed and compared are EEG and ECoG.

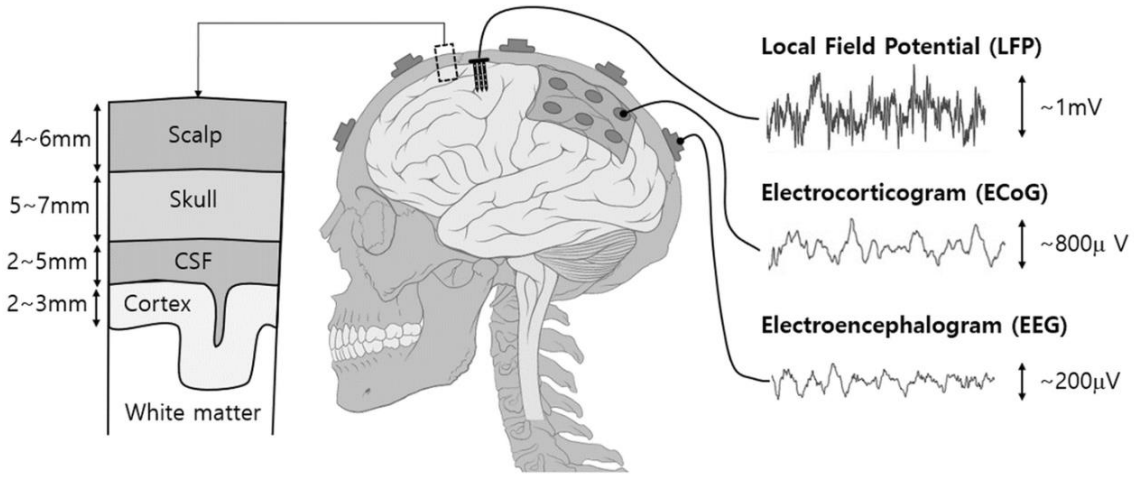

Figure 2: Types of electrical signals recorded from the brain cortex. From [2].

1.2 EEG signal

EEG is an electrical recording of brain electrical activity, by which we mean the just described voltage fluctuations resulting from ionic current flows within the neurons of the brain [3]. EEG is an essential tool for diagnosing conditions such as epilepsy and sleep disorders, while also providing insights into cognitive processes, learning, and memory [4]. This signal is recorded using electrodes placed on the scalp, which detect the small voltage fluctuations generated by

neuronal activity. This technique is non-invasive, meaning it does not require surgical procedures or direct access to brain tissue, making it safe and widely applicable for clinical and research purposes. The electrodes used for EEG recordings can be of different types, including wet electrodes, which require conductive gel to reduce impedance and enhance signal quality, and dry electrodes, that eliminate the need for conductive gel and allow for faster and more comfortable setup, although they may have slightly lower signal quality compared to gel-based electrodes.

The amplitude of the EEG signal ranges between 10 - 200 mV with a frequency falling approximately in the range 0.5 Hz - 60 Hz. EEG waves are classified into five frequency bands (alpha, beta, theta, delta, and gamma bands). Delta (δ) waves (0.5 - 4 Hz) are the slowest EEG waves, normally detected during deep and unconscious sleep. Theta (θ) waves (4 - 8 Hz) are observed during some states of sleep and quiet focus. Alpha (α) band (8 - 14 Hz) originates during periods of relaxation with eyes closed but still awake. Beta (β) band (14 - 30 Hz) originates during normal consciousness and active concentration. Finally, Gamma (γ) waves (over 30 Hz) are known to have stronger electrical signals in response to visual stimulation [5]. However, each frequency band also contains a wide range of other information and can be observed during various brain activities beyond those typically associated with them. Different cognitive, sensory, and motor processes can modulate these oscillations.

EEG signals are affected by the various tissues and fluids in the head, which introduce distortions and attenuations as the electrical activity propagates from its cortical origin to the scalp. This phenomenon, known as volume conduction, causes the signals detected by scalp electrodes to be influenced by multiple overlapping neural sources rather than reflecting purely localized activity. As a result, each EEG electrode typically captures a mixture of signals from different brain regions, while the activity of a single neural source is often recorded by multiple

electrodes [6], as it is possible to see in Figure 3. This results in a low spatial resolution of approximately 6 - 9 cm [7].

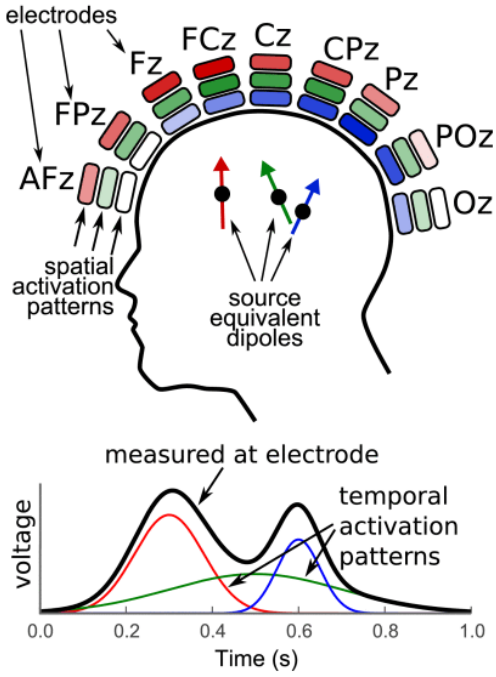

Figure 3: Sketch showing how signals generated at different dipole generators are captured by the EEG electrodes. Activity at the three generators is drawn in blue, red, and green. Each electrode records a mixture of the three generators. (Top) Spatial activation patterns produced by the generators are shown as rectangles with different color intensities. (Bottom) Temporal activation patterns of the generators are shown as curves in different colors. The black curve represents the summation of these patterns as captured by a single EEG electrode. From [6].

Additionally, it leads to a weaker signal-to-noise ratio (SNR), making it more challenging to extract relevant brain activity from background noise. Furthermore, artifacts from non-neuronal sources, such as muscle activity, eye movements, and environmental noise, further contaminate the EEG signal, requiring careful preprocessing and filtering techniques to improve data quality.

1.3 ECoG signal

ECoG is recorded with electrodes on the surface of the cerebral cortex (Figure 2) and represents the cerebral activity just beneath the electrodes. Since this technique requires electrodes to be implanted, it is considered invasive, which greatly limits its use to specific medical and research applications. ECoG is typically used in clinical contexts where high spatial and temporal resolution is essential, such as pre-surgical epilepsy monitoring to precisely locate seizure foci, or in certain Brain-Computer Interfaces applications for patients who already require electrode implantation. On the other hand, ECoG presents with much better spatial resolution (<1 cm) and comparable temporal resolution (ms) as compared to EEG, as it does not require the signal to pass through the scalp and skull [8]. For example, Agrita Dubey et al. [9] calculated the spatial resolution of the ECoG signal, obtaining a spatial spread surprisingly local (diameter ∼3 mm). This higher spatial resolution allows for better differentiation of neuronal sources, minimizing the signal mixing and volume conduction effects that affect EEG recordings. The frequency bands of ECoG signals are generally similar to those of EEG (delta, theta, alpha, beta, and gamma). However, ECoG provides access to higher-frequency components, including higher frequencies in the gamma band (60–100 Hz), and the high-gamma band (100–300 Hz) [10], which is often not detectable in scalp EEG due to attenuation and noise. This high-gamma activity is particularly relevant as it is closely related to local neuronal population activity and is commonly used in motor and cognitive research.

1.4 BCIs

Brain-Computer Interfaces (BCIs) are systems that establish a direct communication pathway between the brain and an external device, bypassing traditional neuromuscular output channels.

BCIs function by detecting and interpreting neural activity, recorded through non-invasive methods like EEG or invasive techniques such as ECoG. Depending on their purpose, BCIs can be classified into different categories, including communication BCIs, which enable individuals with severe disabilities to convey messages; neurofeedback BCIs, used for cognitive training and rehabilitation; and motor BCIs, designed to restore or assist movement in individuals with motor impairments [11]. Motor BCIs, which are the focus of this study, aim to decode movement-related brain signals to control external devices such as robotic limbs, exoskeletons, or computer interfaces. These systems hold significant potential for individuals with neuro-motor disorders, such as spinal cord injuries or stroke. The effectiveness of motor BCIs depends on accurately extracting relevant features from brain activity, particularly from the motor and somatosensory cortices, where movement-related information is encoded. Understanding the neural signatures associated with voluntary movement is therefore crucial for enhancing the reliability and precision of motor BCIs.

Despite significant advancements, BCIs still face several challenges that limit their widespread adoption. Non-invasive BCIs, such as those based on EEG, suffer from low spatial resolution and susceptibility to noise, reducing accuracy. Invasive BCIs, like ECoG-based systems, offer higher signal quality but pose surgical risks and long-term stability concerns. Additionally, the high inter- and intra-subject variability in neural signals presents a major hurdle, requiring extensive calibration and individualized training for each user [12]. In many cases, the user must also learn how to interact with the BCI correctly, which is not always intuitive and can require prolonged training. Other limitations include the need for real-time processing with minimal latency, the difficulty of decoding complex movements with high accuracy, and the influence of cognitive and physiological states on BCI performance.

1.5 Sensorimotor cortex activity

The present study focuses on the activity of the sensorimotor cortex, as it is responsible for encoding movement-related information within brain signals. Different parts of the brain are associated with distinct motor and sensory functions, as represented by the homunculus of Wilder Penfield. This mapping, first published in 1937, achieved through direct electrical stimulation of the brain, reveals a distorted human figure known as the homunculus, where each body part corresponds to a specific cortical area dedicated to its motor or somatosensory function (Figure 4). The distortions in the homunculus reflect the varying density of neural representations, with body parts requiring finer motor control or greater sensory sensitivity, such as the hands and lips, occupying disproportionately larger cortical areas.

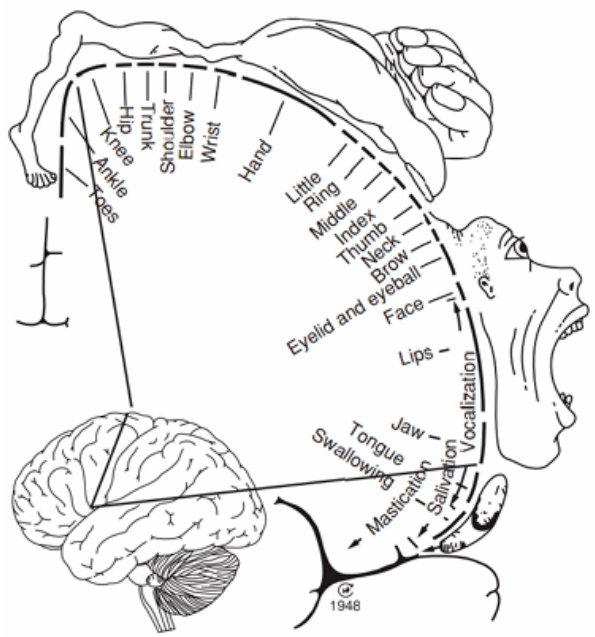

Figure 4: Representation of the somatosensory and motor homunculus by Wilder Penfield, illustrating the cortical areas dedicated to different body parts.

The somatosensory cortex is located in the postcentral gyrus of the parietal lobe, directly posterior to the central sulcus, while the motor cortex resides in the precentral gyrus of the

frontal lobe, anterior to the central sulcus (Figure 5). The primary motor cortex (M1) is responsible for initiating voluntary movements, whereas the primary somatosensory cortex (S1) processes sensory feedback such as proprioception, touch, and kinesthetic information, all of which are part of movement execution and control. These regions are highly interconnected, allowing for continuous sensorimotor integration. Given their role, activity within sensorimotor cortex is particularly relevant for BCIs designed for motor decoding.

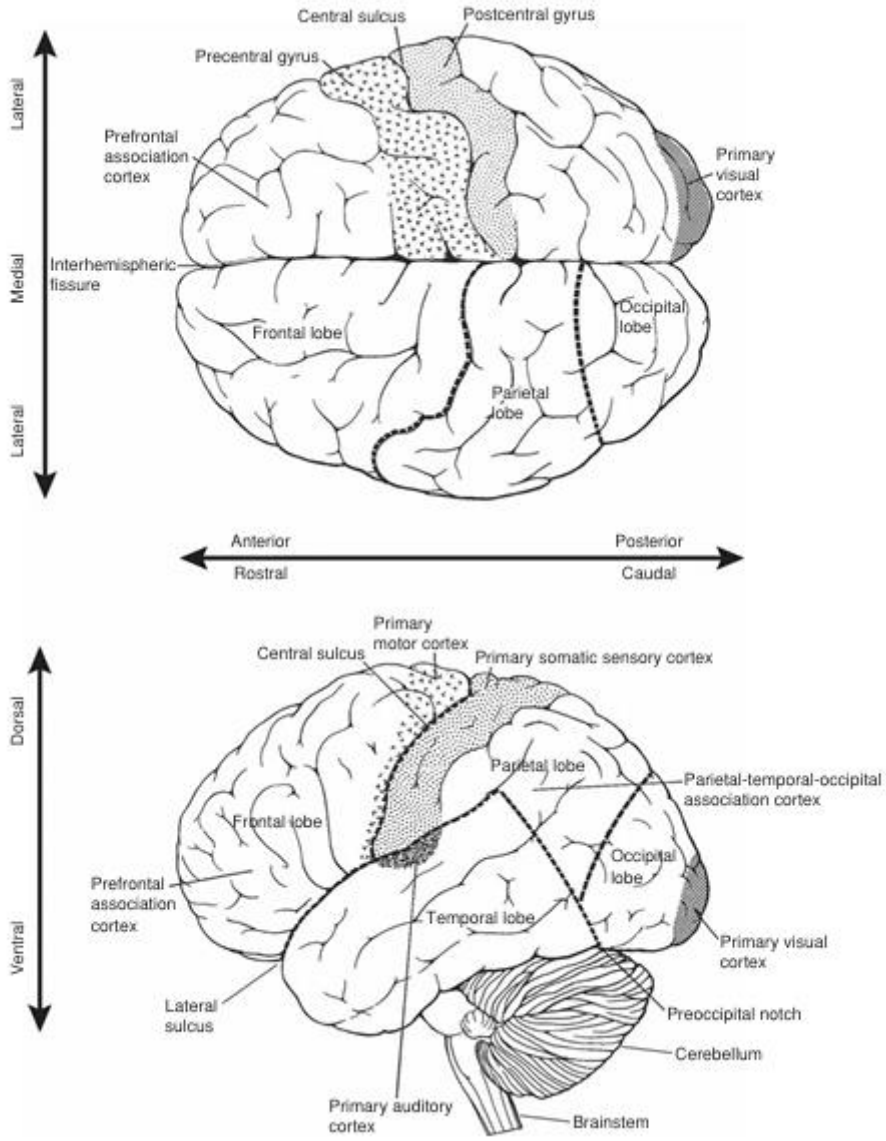

Figure 5: Major divisions of the human cerebral cortex in dorsal (from above) and lateral views. Somatosensory cortex is shown in the postcentral gyrus, while motor cortex in the precentral gyrus.

Neural activity in these regions manifests in various electrophysiological patterns that have been extensively studied for their role in motor decoding. In this work, we specifically analyzed Low/Slow Motor Potentials (LMPs) related to active movement execution, which are slow cortical potentials (low-frequency components) associated with the preparation and execution of voluntary movements. They reflect shifts in the cortical electrical activity lasting from several hundreds milliseconds to several seconds [13] and they share similarities with readiness potentials, which are explained below, but persist throughout the movement, reflecting sustained neural engagement. LMPs are often used in scientific literature for motor decoding applications, as they provide valuable information on movement-related brain activity and have been successfully employed in both invasive and non-invasive BCIs [14] [15] [16] [17]. Furthermore, They appear to be particularly suited for tracking slow movements but are less effective in distinguishing movement from a no-movement state [18] [19].

Other relevant features extracted from ECoG and EEG signals that are usually exploited for BCIs include:

- Sensory-motor rhythms, characterized by two distinct neural phenomena: event-related desynchronization and event-related synchronization. Desynchronization refers to a decrease in the amplitude of oscillatory activity in the alpha (8–12 Hz) and beta (13–30 Hz) bands during movement execution or motor imagery. Conversely, synchronization represents an increase in oscillatory power in these frequency bands, typically occurring during movement cessation or rest.
- Readiness potentials, that are slow cortical potentials that precede voluntary movements. They typically appear as a gradual negative shift in electrical activity, beginning up to one second before movement onset.

- High-gamma activity (100–300 Hz), observable only in ECoG, that correlates strongly with active movement and motor imagery. Unlike low-frequency oscillations, high-gamma power increases during voluntary movement and is spatially localized to motor-relevant cortical areas [20]. Unlike LMPs, high-gamma activity seems to be more effective in distinguishing movement from a no-movement state but is less suited for accurately tracking movement trajectories [18] [19].

1.6 CorticoKinematic coherence as a reflection of low frequency activity

Coherence is a quantitative indicator to measure the phase coupling between two signals [21], reflecting the degree of synchronization between their oscillatory components at a given frequency. It can be defined also as the degree of linear dependence between two signals at a specific frequency [22]. It can range from 0 (i.e., no correlation at a given frequency) to 1 (i.e., perfect correlation), following this formula:

$$C_{xy}(f) = \frac{\left|G_{xy}(f)\right|^2}{G_{xx}(f)G_{yy}(f)}$$

Equation 1

- The numerator $\left|G_{xy}(f)\right|^2$ represents the shared power (square of cross-spectrum) between the two signals at frequency f, capturing how much they co-vary in the frequency domain.
- The denominator $G_{xx}(f)G_{yy}(f)$ normalizes this shared power by the total power of each individual signal at the same frequency, ensuring coherence values range from 0 to 1.

For coherence to be high (close to 1), the two signals must share the same frequencies and also maintain a consistent relationship in phase over time. If they contain different frequency components, or their phase relationship fluctuates randomly, coherence will be low (close to 0).

CorticoKinematic coherence (CKC), instead is defined as the coherence calculated between limb kinematics and cortical neurophysiological signals [21]. The concept of CorticoKinematic coherence (CKC) was first introduced by Jerbi et al. (2007) [23], who investigated the coherence between magnetoencephalographic (MEG) signals and hand velocity. Their finding suggested a role for slow (≤5 Hz) oscillations in motor cortex in the neural mechanisms underlying the neural control of limb speed, that may also be interpreted as evidence for the existence of a neural representation of low-frequency components of limb kinematics. Later, Bourguignon et al. (2011) [24] further explored this phenomenon, demonstrating a strong coherence between cortical activity recorded with MEG and hand acceleration during rhythmic movements. These pioneering studies provided fundamental insights into CKC, highlighting the coupling between primary sensorimotor cortex activity and movement kinematics. Subsequently, most studies on CKC have been conducted using the MEG signal, with in particular Bourguignon and Piitulainen extensively studying this phenomenon over the years [22] [23] [24] [25] [26] [27] [28]. In this work, however, we will focus on EEG and ECoG signals to investigate this phenomenon. Some studies about CKC were done using EEG, obtaining lower coherence values respect to the MEG [21] [29] [30] [31]. Indeed, CKC is widely known to be reproducible when estimated with MEG, while feasibility and reproducibility of CKC based on EEG is still unclear [21]. However, using these different signals to calculate the same metrics (CKC) is justified by the fact that all three signals reflect brain activity, although it is important to consider the differences between them, which also influence the observed CKC. MEG is a non-invasive technique that measures magnetic fields generated by neuronal activity in the brain, providing high temporal resolution and good spatial

localization of brain signals [32]. Unlike EEG, which is affected by the conductivity of the skull, MEG directly detects magnetic fields, avoiding this issue. Similarly, ECoG, which involves direct cortical electrode placement, avoids this problem. While all the signals measure neuronal activity, ECoG provides higher spatial resolution [8] [9], as it captures the electrical signals closer to the source. This suggests that we could obtain better coherence values with ECoG, because the signal detected from an electrode placed on the sensorimotor cortex is more likely to stronger detect the activity of the region of interest.

2 Materials

To investigate the two signals used in this work during the repetitive fingers flexion-extension, two different datasets were used:

- For the ECoG signal a public dataset provided by the Stanford University [33].
- As regards the EEG signal, data were recorded during an experiment conducted at the Computational Neuroscience Laboratory of the KU Leuven (Belgium).

2.1 ECoG Stanford Dataset

ECoG data used are from the public ECoG Stanford Dataset. It contains both finger flexion kinematic data and the corresponding ECoG data from 9 healthy subjects (mean age of 26.8 with a standard deviation of 9.2, 4 males and 2 females), details of which are summarized below (Table 1).

	Age	Sex	Handedness	Array location
Subject 1	18	F	R	L Fronto-parietal
Subject 2	21	M	R	R Fronto-temporal
Subject 3	27	F	R	L Fronto-temporal-parietal
Subject 4	35	F	R	L Fronto-temporal
Subject 5	26	M	R	L Parietal - Temporal - Occipital
Subject 6	45	F	R	L Fronto-temporal
Subject 7	32	M	R	L Fronto-temporal-parietal
Subject 8	19	F	R	R Fronto-parietal
Subject 9	18	F	R	L Frontal

Table 1: subjects details of the Stanfod ECoG dataset

Each subject had a different number of electrodes implanted in varying positions, but always covering at least part of the left sensorimotor cortex (that corresponds to the contralateral cortex side respect to the right hand moved). Figure 6 shows an example of electrodes placement for Subject 1 of Stanford ECoG dataset.

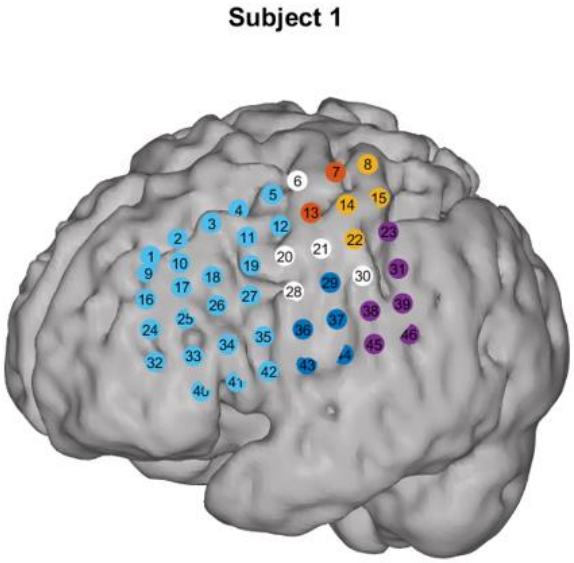

Figure 6: Electrodes placement for Subject 1 of Stanford ECoG dataset.

Ethics statement: All patients participated in a purely voluntary manner, after providing EASYinformed written consent, under experimental protocols approved by the Institutional Review Board of the University of Washington (12193). All patient data was anonymized according to IRB protocol, in accordance with HIPAA mandate. These data originally appeared in the manuscript *"Human Motor Cortical Activity Is Selectively Phase- Entrained on Underlying Rhythms"* published in PLoS Computational Biology in 2012 [33].

During the finger flexion task, subjects were cued with a word displayed on a bedside monitor indicating which finger to move during 2- second movement trials. The subject performed self-paced movements in response to each of these cues, and they moved each finger at least 2–5

times during each trial, but some trials included many more movements. A 2-second rest trial (blank screen) followed each movement trial. There were 30 movement cues for each finger, and trials were interleaved randomly. The total recording time of each subject varies from around 3 minutes to around 10 minutes. Finger positions were recorded using a 5 degree-of-freedom dataglove sensor (5 dt, Irvine, CA).

2.2 EEG experiment

2.2.1 Participants

We recruited 6 healthy students participants (mean age of 26.2 ± 2.6, 4 males and 2 females). All subjects are right-handed.

2.2.2 Paradigm for EEG

The experiment was designed on the one hand to have data comparable with the ECoG dataset and on the other hand, so that they could be used for decoding and to investigate the role of the movement frequency. For the first purpose the experiment paradigm was organized so that it had the same conditions as in the ECoG dataset. Participants again consisted of 9 healthy subjects, whose details are given in the table:

Also in this experiment, finger flexions were performed, but in this case the movement wasn't totally self-paced. In particular, there were two different target frequencies of movement: 1 Hz and 3 Hz. These frequencies were selected since studies in literature demonstrated that among slow motor potentials frequencies, 3 Hz is appropriate and efficient for robust CKC estimation

[28]. Furthermore, only the Thumb and Index were moved independently, while the movement of the other three fingers was merged into two movement classes: the 'Point' movement, which includes flexion of the third finger, Ring finger and Little finger and the 'Fist' flexion of all fingers. In total there were therefore 4 types of movement, all performed at 2 different speeds, bringing the total number of classes to 8. Subjects were helped to flex their fingers at the correct frequency by projecting a shrinking circle on the screen in front of them (Figure 7). This circle contained a cross on whose axes there were dashes. Dashes were at such a distance that the circle, as it tightened, touched each consecutive dash at a frequency equal to the required frequency of movement.

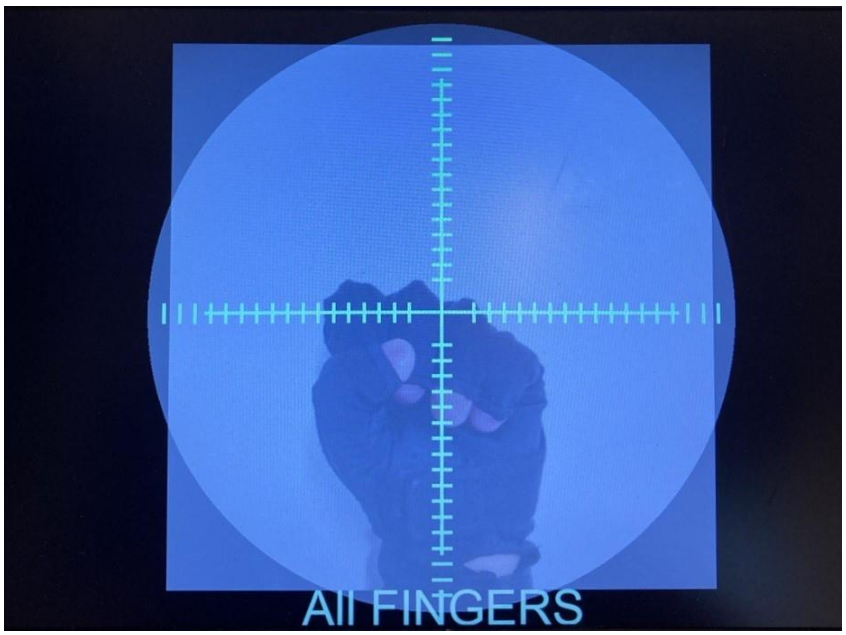

Figure 7: Layout of the experimental setup that was showed on the screen to the subjects during the experiment. Dashes on the cross were at such a distance that the circle, as it tightened, touched each consecutive dash at a frequency equal to the required frequency of movement. 'All fingers' refers to the type of movement to perform, always written below the circle.

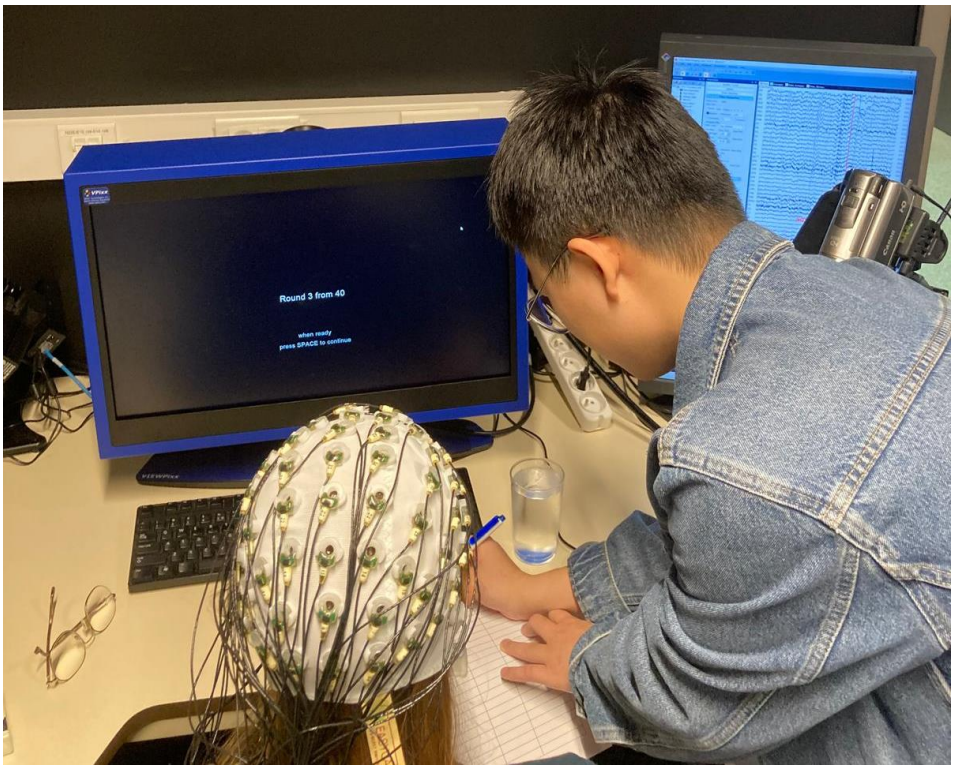

Figure 8: Experimental setup during the explanation of the experiment to a subject. A screen in front of subjects showed the instructions of the experiment, while the screen on the right was turned off during the recording and used only to assess signal quality before the recordings.

The number of trials performed by each subject ranged from 12 to 15. From the twelfth trial onwards, the subject could decide whether to end the experiment by pressing a button at the end of each trial. Each trial consisted of 8 blocks of 20 seconds each, comprising a movement class. The block included an initial fixation of the screen of 1 second, a task cue of 1 second, in which the movement class to be performed was projected on the screen, a preparation period of 3 seconds, the task that lasted 15 seconds, and a final rest of 2 seconds (Figure 9). Before all recordings, a glove calibration phase was done, required for the acquisition of kinematic signals with the glove.

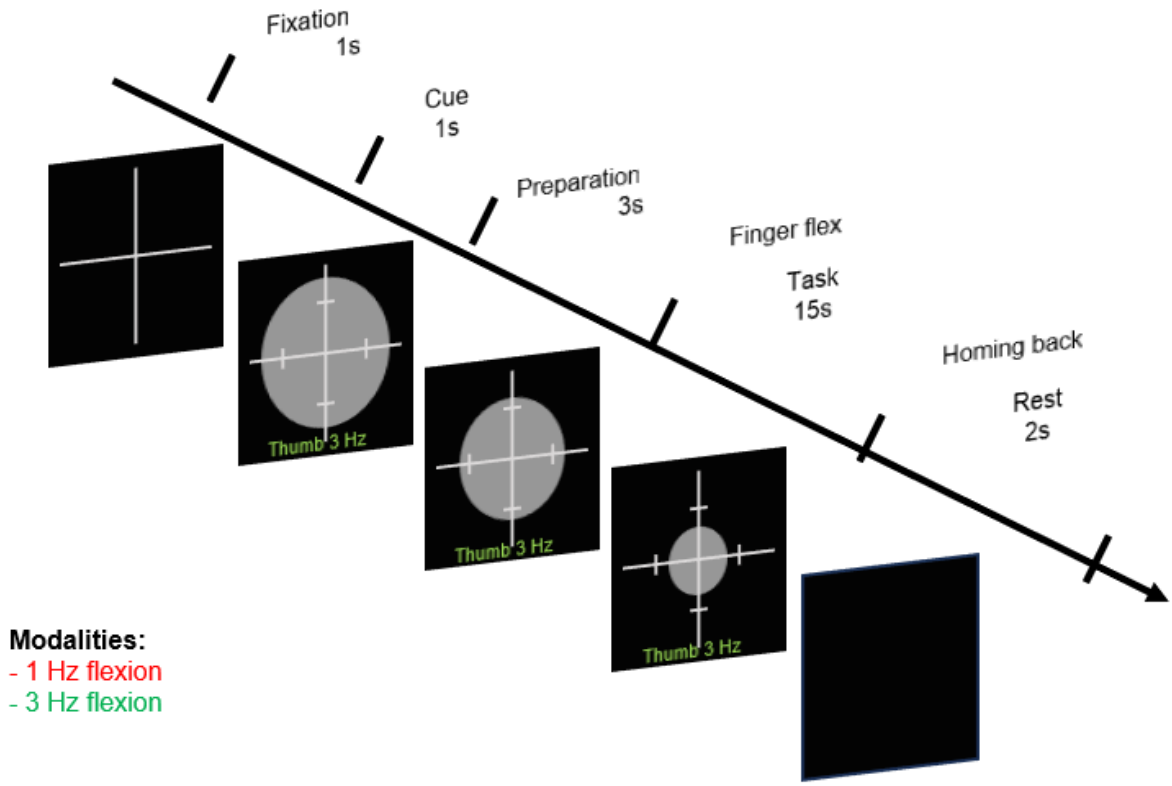

Figure 9: EEG experiment paradigm scheme. For the correctness, there were also dashes within the circle relating to the flexion-extension period, not shown in the figure for visual clarity.

The first difference from the ECoG dataset then concerns the frequency/speed of finger flexion. The ECoG data presents self-paced movements, but actually looking at the data, each subject maintained an almost constant movement frequency, in a wide range of about 1-2 Hz. This happened in the same way with the EEG experiment, having a similar and sometimes smaller range around the main movement frequency, even if in this case the movements were not self-paced. Subsequently the main difference is just that in the EEG case two different frequency of movement were performed. This decision was made to study whether there were differences in the results according to the speed of movement. The layout to help the subject perform movements at the correct frequency was designed to give only a reference to the subject, avoiding the introduction of stimuli that could cause variations in the EEG signal due to the stimuli themselves. For example, using a repeated visual or sound stimulus at the frequency of

movement would certainly have led to movements at more precise frequencies, but it would also have introduced variations in the EEG signal due to the perception of such stimuli.

The second difference from the ECoG dataset relates to different movements class. Indeed, flexion-extensions of each finger were performed individually for the ECoG dataset. The choice of combining the flexion of the third finger, Ring finger and Little finger in the 'Point' movement was made because it is physiologically impossible to move these three fingers individually. For this reason, the ECoG dataset contains periods in which theoretically only one of these three fingers had to move, but in the end the others were also flexed to a greater or lesser extent. In addition, the simultaneous flexion of all fingers ('Fist') was included, under the hypothesis that such a movement could enhance the motor task's impact on the signal, making it more suitable for decoding.

During the acquisition, specific markers were sent from the execution code as input to the recorder device. These markers were numbers designed to be unique identifiers of the various relevant intervals in the experiment: the entire acquisition interval, the intervals of each trial, those of each block, and those of each interval within a block following the initial preparation and preceding the final rest. Thanks to the markers, it was possible to define each interval in the subsequent data processing.

2.2.3 Instrumentation

The instrumentation used for the acquisitions was the same for each subject and included:

- An EEG cap of the *easycapM11* type, designed for 64 electrodes (Figure 10) that follows the standard 10-10 electrodes configuration. The 10-10 electrode system is an extension

of the internationally recognized 10-20 system used for EEG. In the 10-10 system, additional electrodes are placed between those of the 10-20 system, reducing the distance between adjacent electrodes to 10% of the total front-back or right-left distance of the skull. This results in a higher density of electrodes, allowing for more detailed spatial resolution of brain activity [34]. The abbreviated names used for the electrodes are based on their anatomical location on the scalp and their position relative to the brain regions they measure. Each abbreviation includes a letter indicating the brain region and a number representing the electrode's position:

- F: Frontal region
- T: Temporal region
- C: Central region
- P: Parietal region
- O: Occipital region
- Fp: Frontopolar (most anterior frontal region)
- Z: Midline electrodes (central axis)

Numbers indicate the position of the electrodes relative to the midline (Z). Even numbers are in the right hemisphere, and odd numbers are in the left hemisphere. Then, with EEG signals there was a common electrodes setup for all participants, unlike ECoG dataset in which electrodes were implanted in different positions.

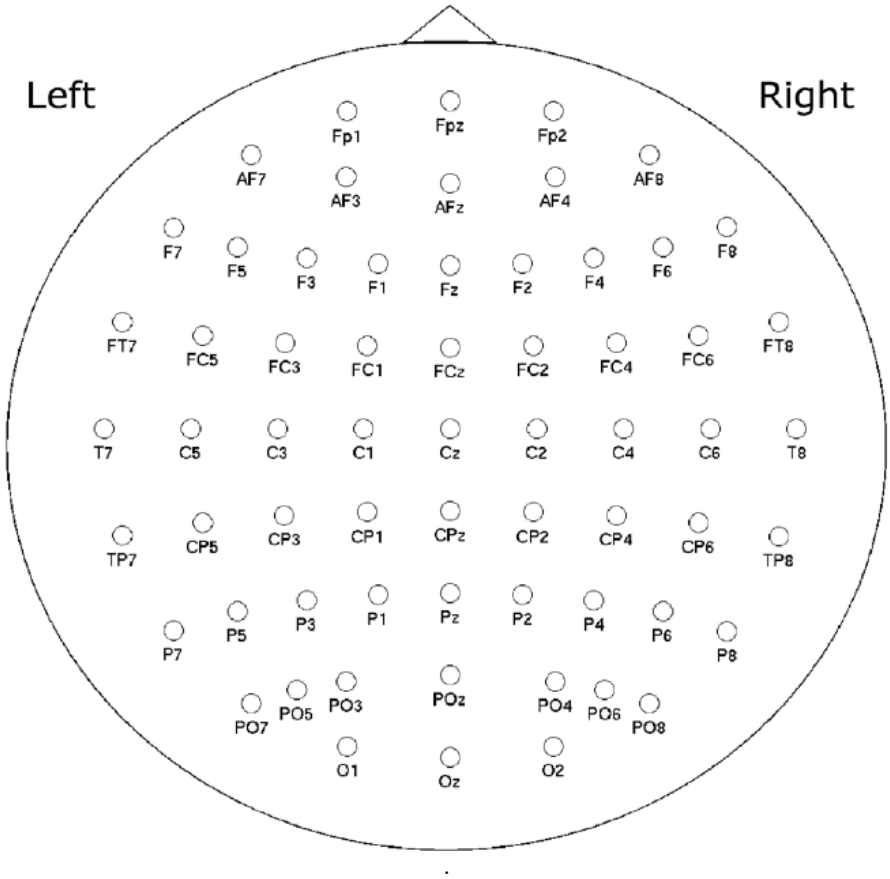

Figure 10: 64 electrodes configuration of the EEG cap.

- A *ViewPixx* stimulator device, that also included the monitor placed in front of the subject. It transmitted the outputs of the code executed to conduct the acquisition, i.e. everything that was projected on the screen and the various markers. Matlab software was utilized to write and execute the code for the experiment. The script was designed to display instructions and the layout for the task on the screen, guiding the participant during the experiment. Additionally, the code was responsible for sending event markers to the recording system through the stimulator, to ensure synchronization between the experimental events and the recorded data. The ViewPixx monitor is a screen used to perform this kind of experiments due to the high RGB (red, green and blue) channels resolution refresh rate

- An EEG recorder that was the *Neuroscan SynAmps RT* device (Compumedics). It also received as input the various markers with their time instant, in addition to the EEG signals. It includes a SynAmps RT 64-channel Amplifier, details of which are given in the table below:

Specifications SynAmps RT 64-channel Amplifier	
Max Number of Channels	*70*
EEG Channels	*64*
Bipolar Channels	*4*
Analog Inputs (HLI)	*2*
DC/AC	*DC, AC (2 modes)*
Max Sampling Rate	*20 kHz*
Sampling Rate (Hz)	*100, 200, 250, 500, 1000, 1250, 2000, 2500, 5000, 10000, 20000*
Bandwidth	*DC-3500 Hz*
Resolution	*24-bit*
Input Range	*400 mV (DC mode), 1.9 mV (AC mode)*
Sensitivity	*24 nV (DC mode), 3 nV (AC mode)*
Input Impedance	*>10 GOhm*
Common Mode Rejection (CMRR)	*>110 dB*
Noise (peak-to-peak)	*<0.5 uV (DC mode)*
Impedance Check	*Yes*
Trigger	*16-bit TTL*

Table 2: Specifications of the EEG recorder amplifier used.

- 64 Ag/AgCl (silver/silver chloride) wet electrodes (easycap), connected to the recorder, with a conductive gel (*Signagel*, highly conductive, multi-purpose electrolyte). By using wet electrodes, a gel or saline liquid is applied to increase the conductivity value [35] (and therefore decrease the impedance value). The ground electrode was set at AFz, and the reference electrode was at FCz.
- A digital data glove (*5 Ultra MRI, 5DT*, Irvine CA, USA) connected to the stimulator. This glove consists of 5 Fiber Optic based sensors (one per finger). Other details are

showed in Figure 11. The glove used a variable sampling frequency that depended on the speed of the movement detected. The management of this issue is explained in the data processing section.

Specifications

	5DT Data Glove 5 Ultra	5DT Data Glove 14 Ultra
Material	Black Stretch Lycra	Black Stretch Lycra
Sensor Resolution	12-bit A/D (typical range 10 bits)	12-bit A/D (typical range 10 bits)
Flexure Sensors	Fiber Optics Based 5 Sensors in total 1 Sensor per finger, measures average of knuckle and first joint.	Fiber Optics Based 14 Sensors in total 2 Sensors per finger, one sensor for knuckle and one for first joint. Abduction sensors between fingers.
Computer Interface	Full-speed USB 1.1 RS-232 (via optional serial interface kit)	Full-speed USB 1.1 RS-232 (via optional serial interface kit)
Power Supply	Via USB Interface	Via USB Interface
Sampling Rate	Minimum 75Hz	Minimum 75Hz

Figure 11: Data glove specifications. The model used for recording kinematic data is the 5DT Data Glove 5 Ultra (second column of the table).

2.2.4 Acquisition steps

Before each recording, the following steps were followed:

1. The size of the subject's head was measured, so that the cap was as similar in size as possible.
2. Electrodes were mounted on the cap, according to the easycapM11 layout.
3. The glove was connected to the stimulator, while electrodes were connected to the recorder. All the electronic devices were turned on.
4. The conductive gel was applied to the holes of each electrode using a syringe, first trying to move the hairs below the hole to reach the skin. This was done by monitoring the impedance value measured on each electrode using the software Curry 7. This software allows to visually check the impedance value of each electrode through both a color

map and showing the value of each impedance. The process continued until an impedance below 5 kΩ was achieved for all electrodes, also making sure that there were no impedances equal to 0 Ω caused by electrodes shorting/bridging. In addition, the trend of EEG signals themselves were also monitored, visually ensuring that they had a reasonable time course, identifying noisy channels. For example, two tests were usually performed: the eye blinking, which was supposed to cause a spike if the signal was correct, and keeping the eyes closed, which should have caused a frequency increase in alpha rhythms (8 Hz -12 Hz) especially between the occipital and parietal electrodes.

5. Finally, the paradigm was explained to the participant and a trial run was performed to allow the participant to become familiar with the task.
6. During the recording, the signal was visually monitored, noting electrodes that showed noisy signals and intervening with conductive gel in the case of serious problems with some electrodes. The sampling rate was set at 1000 Hz.

3 Methods

3.1 Analysis Software

Two software were used for data processing and analysis:

1. Matlab: it is a high-level programming language and a numeric computing environment developed by MathWorks [36]. It is designed for scientists and engineers to work with matrix manipulations, data-plotting, develop algorithms and create models. The data analysis was carried out using various Matlab toolboxes, which will be mentioned later.

2. Python on Google Colab: Python is a high-level, general-purpose programming language that supports object-oriented programming and is widely used for data analysis, scientific computing, and machine learning due to its simplicity, readability, and extensive libraries [37]. Only the part concerning the Temporal Convolutional Neural Network (TCN) decoder was realized with Python. The code was not actually executed by software, but within Google Colab's cloud-based online platform [38].

3.2 Data Preprocessing ECoG

An initial preprocessing was applied to ECoG and EEG data, previously to both coherence analysis and decoding.

ECoG data from the Stanford dataset were provided already preprocessed. Specifically, a bandpass filter from 0.15 Hz to 200 Hz was applied. This filter consisted of a single pole, so there was no sharp corner at 200 Hz. The sampling frequency was equal to 1000 Hz and the data were provided with a scale factor such that 1 amplifier unit = 0.0298 μV.

The only preprocessing operation that was carried out consisted of a **Common Average Reference** (CAR). This method re-references each electrode's potential to the average potential of all electrodes, reducing noise and highlighting local brain activity. CAR is commonly used in EEG, where it is necessary to identify small signal sources in very noisy recordings [39].

$$V_i^{CAR} = V_i - \frac{1}{N}\sum_{j=1}^{N} V_j$$

Equation 2

Where:

- V_i^{CAR}: potential referring to the common average for electrode i.
- V_i : original electrode potential.
- N: total number of electrodes.
- $\frac{1}{N}\sum_{j=1}^{N} V_j$: average value of the potential calculated on all electrodes.

3.3 Data Preprocessing EEG

EEG data were recorded at a frequency of 1000 Hz and subsequently preprocessed using the FieldTrip toolbox. It is an open-source software for advanced analysis of MEG, EEG, and Invasive Electrophysiological data [40]. The preprocessing included the following steps:

1. Firstly, for each subject **noisy intervals were removed**. These could include periods that were noted as noisy during the acquisition itself, or that were later deemed noisy by a visual inspection of the signals.
2. After, all data were **down sampled to 250 Hz**.
3. **Two Notch filters** were applied: the first had cut-off frequencies of 49.5 Hz and 50.5 Hz to remove the first harmonic line noise, while the second one had cut-off frequencies of 99.5 Hz and 100.5 to remove the second harmonic line noise. Both the filters were Butterworth type of 3th order.

4. Then a **bandpass filter between 0.2 Hz and 120 Hz** was applied to remove a part of the signal that is not included in the signal band. Once again, both the filters used were of the 3th order Butterworth type.
5. After these steps, signals were visually inspected to remove channels that showed noisy behavior, also according to the notes taken during the measurements.
6. Subsequently an Independent Component Analysis (ICA) algorithm was used to identify and **remove eye movement components**. The ICA is a computational method for finding additive and statistically independent components from multivariate/multi-dimensional statistical data. It is based on the assumption that the observed signals are linear mixtures of non-Gaussian source signals. ICA is widely applied in fields like signal processing, particularly for tasks such as artifact removal and blind source separation. For performing ICA, the 'runica' algorithm was used, which implements the Infomax ICA algorithm by Bell and Sejnowski [41] with the natural gradient feature introduced by Amari, Cichocki, and Yang [42], and the Extended-ICA algorithm of Lee, Girolami, and Sejnowski [43]. Additionally, it applies also PCA (Principal Component Analysis) dimensionality reduction, and the spectrogram preprocessing, as suggested by Zibulevsky [44]. The algorithm was used to extract a number of components equal to the number of channels. Then, these components were visually analyzed in order to find two particular components:
    - One component related to the eye blink, that usually appears as in Figure 12 in the 4th row (component runica004), showing a peak in correspondence with the eye blink [45]. The topographic map of this component over the scalp shows that it appears mostly in the central frontal area of the head.
    - The other eye movement component, caused by horizontal eye movement performed by the subject. It appears as in Figure 12 at about 132 seconds, with a rising or falling front maintained for a longer period respect to the eye blink.

This component is instead located in one of the two lateral regions of the scalp, therefore corresponding to one temporal lobe, with a symmetrical distribution with respect to the two temporal lobes, as can be seen from the topographic map.

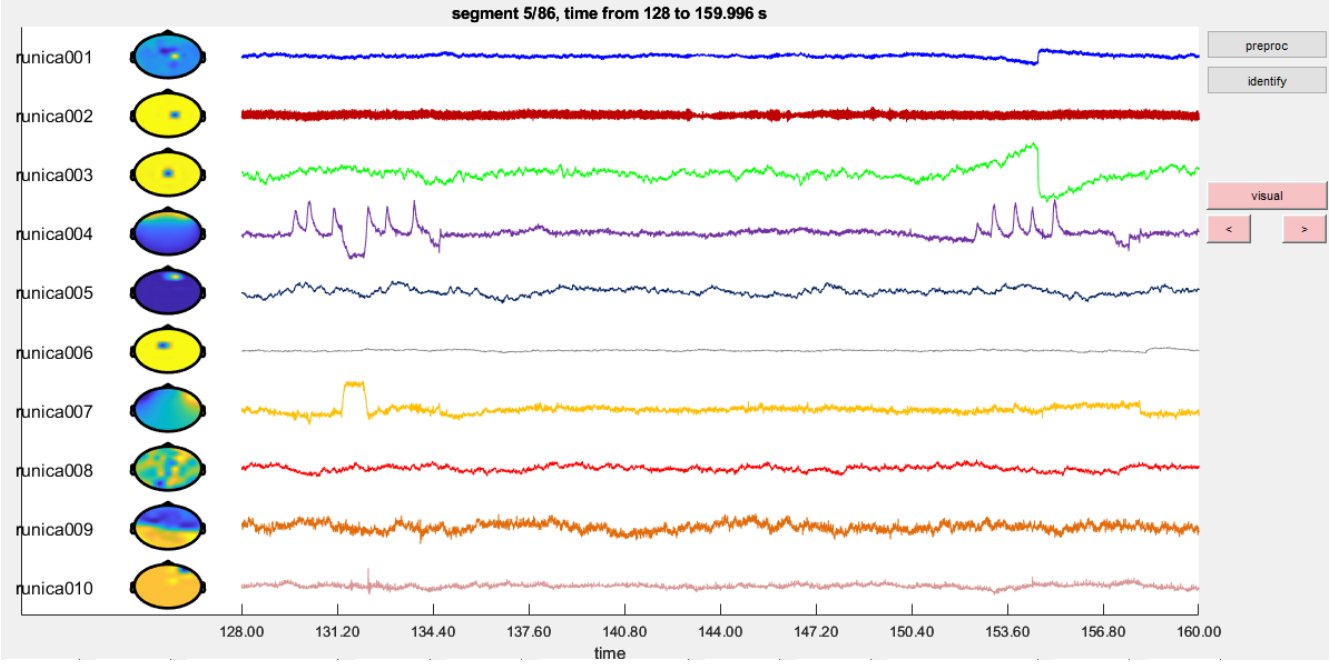

Figure 12: ICA components of an EEG signal of one subject. Each row represents a time window of one of the components extracted. The components 4 and 6 show respectively the component related to eye blinks and the ones caused by horizontal eye movements.

7. Subsequently all the signals of each electrode were referenced again using **CAR referencing** (Equation 2).
8. Finally, a visual inspection was carried out again to check whether there were noisy channels after the preprocessing.

3.4 Coherence analysis

Firstly, a coherence analysis was performed on ECoG and EEG data. Both the data were still processed in order to properly calculate the coherence for different cases.

3.4.1 Kinematics data preprocessing and labelling

Both the kinematic data from the ECoG Stanford dataset and the acquired ones were processed following the same method, as the purpose was a comparison of the coherences obtained with the two types of brain signals. Sometimes there was some slight difference, as shown below.

- **Preprocessing**: The kinematic data from the dataglove were acquired already normalized between 0 and 1, thanks to the calibration phase that preceded every recording. Kinematic data of the ECoG dataset were also provided normalized. The only preprocessing applied was an offset removal. The operation was done because in the non-movement pashes the subjects kept their fingers relaxed and fully extended, so the kinematic signal is supposed to have an almost constant 0 value, but sometimes the kinematic signal in these resting phases showed values slightly different from 0. The offset was calculated as the median value of the data of each finger. Using the median instead of the mean allows for a value less influenced by peak movements, as we are interested in obtaining an average value of the non-movement periods only.

- **Segmentation and labelling**: This procedure was done in order to correctly identify the movement intervals. In fact, the actual movement intervals differed from those defined by the theoretical cues in the ECoG dataset. This difference was not of the same magnitude for the EEG data, but the same processing was nevertheless applied because it was important to select precisely these intervals in view of the coherence analysis. The labelling was done based on the method used in the work of Yao (2022) [46], with some modifications. They used the same data from the Stanford ECoG dataset. Basically, a threshold-based signal segmentation was performed, following these steps:

1. *First threshold*: a threshold was applied, therefore values higher than the threshold were identified. This parameter was chosen to select almost only the movement intervals and exclude the effect of fluctuating noise during the rest state.
2. *Second threshold*: another threshold, based only on previously identified intervals. was applied, obtaining the start and end of a finger movement. In the work of Yao (2022) [46], they set the first threshold at 0.2 times the maximum amplitude of each trajectory, and the second one at the half of the average amplitude of the preselected values. The same approach was used for the ECoG dataset, while for EEG data the threshold values changed between subjects. This choice was done by analyzing the segmentation results and adjusting the value retrospectively to get more accurate results, however starting from the same values just mentioned.

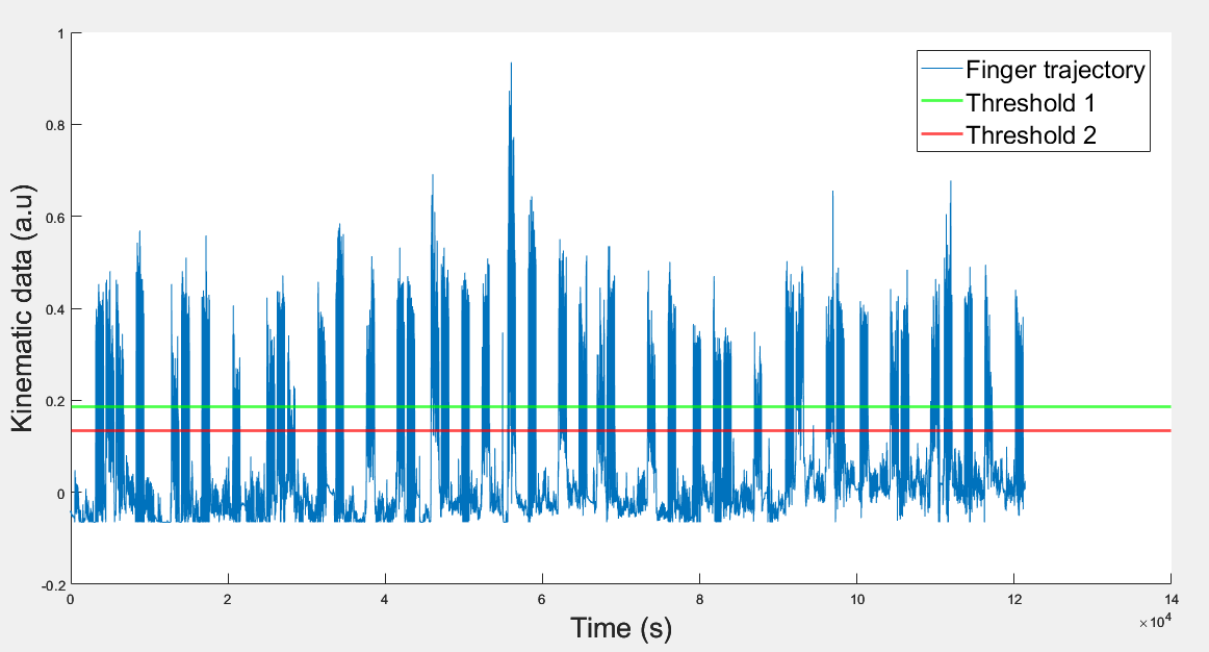

Figure 13: Example of kinematic data of a subject's finger with relative thresholds.

3. *Union of too close intervals*: intervals that were too close were joined, because in these cases the division into different intervals was caused by fluctuations. For the ECoG data

intervals below 0.8 seconds of distance were joined, while for the EEG data the ones that were less than 2 seconds apart. Indeed, by knowing that there was much more temporal distance between the end of one movement block and the beginning of the next one, it was impossible to have intervals that close.

4. *Higher threshold*: another threshold was applied to remove any remaining false activation intervals. In fact, movements were sometimes carried out in periods where movement was not required, for several possible reasons.
5. *Labelling*: Each identified interval was labelled with its movement class number.

   With regard to the ECoG data, the label numbers simply correspond to the number of the moved finger (1: Thumb, 2:Index, 3:Middle, 4:Ring, 5:Little fingers).

   With the EEG data there were 4 different movements performed at 2 different frequencies. Subsequently, the first 4 classes correspond to the different movements executed at 1 Hz, while the classes from 5 to 8 include the same movements at 3 Hz (1: Thumb 1 Hz, 2:Index 1 Hz, 3:Point 1 Hz, 4:Fist 1 Hz, 5: Thumb 3 Hz, 6:Index 3 Hz, 7:Point 3 Hz, 8:Fist 3 Hz). There were, however, periods when several fingers were moved at the same time. Two different approaches were used for the two datasets:

   - With the ECoG data, there were individual flexions of each finger. Then to correctly classify each movement, the relative amplitude maximum was extracted in each obtained interval, calculated as:

$$\frac{Max(movement\ interval)}{Max(whole\ finger\ trajectory)}$$

Equation 3

.

The finger with the highest relative amplitude maximum was treated as the moving finger in these intervals.

- In the EEG experiment there were instead two classes involving the simultaneous movement of several fingers (Point and Fist flexion). When one of these movements was performed, we expected to have more than one finger above the threshold, while in the other two classes we wanted to have just one finger labelled as activated. For this reason, the initial thresholds had been optimized, as reported above, to avoid having fingers that exceeded the threshold in intervals where they should not have been flexing. By detecting all the fingers activated in each interval, labelling was initially done using only four classes for the four movements, without considering the frequency of flexion: class 1 if only the Thumb was above the threshold, class 2 if only the Index was, class 3 if Middle, Ring and Little fingers exceeded the threshold and class 4 if all fingers were above the threshold.

6. *Removal of too short intervals*: intervals shorter than 0.2 seconds for the ECoG data and shorter than 1 seconds for the EEG data were removed, while they were caused by oscillations that didn't belong to the repetitive finger flexion.
7. *Labelling based on the frequency (only for EEG data)*: At this point, ECoG related trajectories were fully labelled, while each class of the EEG kinematic data were still split into 2 different classes depending on the frequency of flexion-extension performed. To do this, the Power Spectral Density (PSD) of each interval was calculated. The PSD represents how the power of a signal is distributed over different frequencies [47]. It can be estimated through two main approaches: parametric methods, which assume a predefined model for the data, and non-parametric methods, which rely on the discrete Fourier transform (DFT) or the signal's autocorrelation function. According to the Wiener-Khintchine theorem, it can be obtained by taking the Fourier transform of the autocorrelation function (correlogram method). However, PSD can also be directly

computed from the Fourier transform of the signal itself by squaring its magnitude, which is the basis of the periodogram method. In this case, it was calculated through the Welch periodogram method, using 0.5 overlapped Hamming windows. If the PSD in the 0.5-1.5 Hz band was greater than the PSD in the 2-3.5 Hz band, then the movement was classified as flexion-extension at 1 Hz, otherwise at 3 Hz. These asymmetrical extremes were chosen by observing that often the movement theoretically at 1 Hz was performed somewhat faster, while that at 3 Hz slightly slower. The final classes are those listed above in the '*Labelling*' section.

8. *Manual corrections*: The labeling process was designed to be as automated as possible, following the steps described above. However, any errors were manually corrected through visual inspection of the data. An example of the final EEG dataset labelling is shown in Figure 14, where the black line corresponds to the theoretical movement intervals, while the blue lines to the obtained. When these lines are equal to 0 it means there is no movement, while the value of the step in the movement intervals equals the number with which the class was labelled divided by 10.

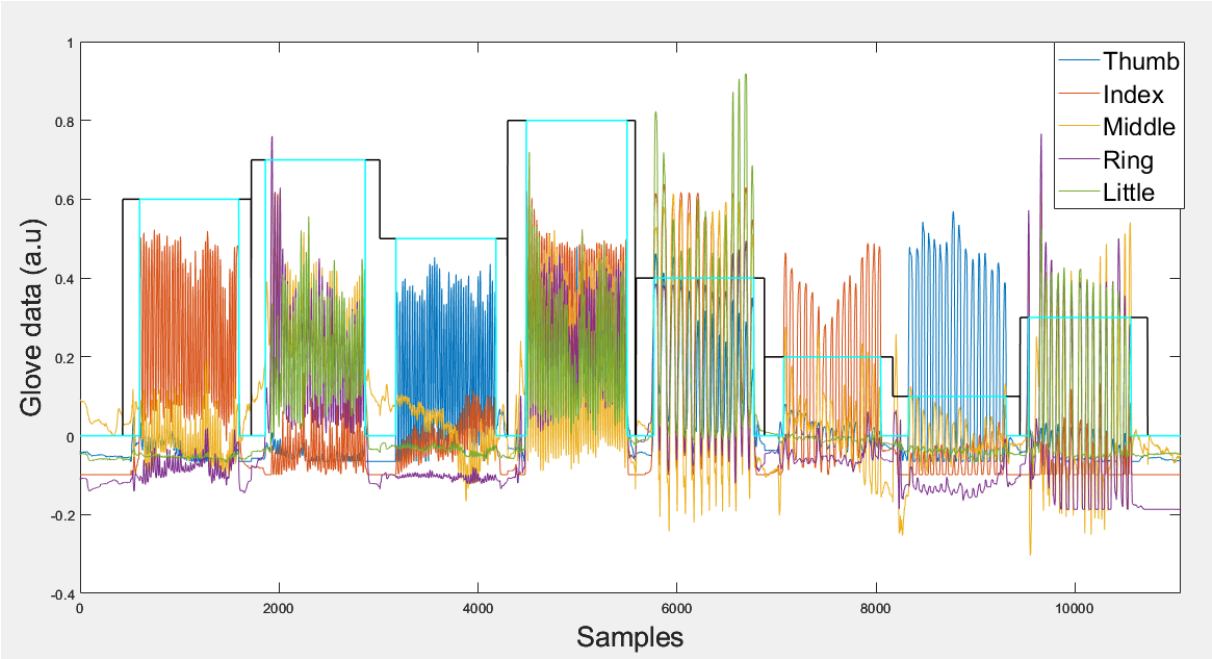

Figure 14: Kinematic data segmentation and labelling. Black line corresponds to the theoretical movement intervals, while the blue lines to the obtained. When these lines are equal to 0 it means there is no movement, while the value of the step in the movement intervals equals the number with which the class was labelled divided by 10.

3.4.2 Synchronization with brain data

The intervals of the different types of movements were then paired with the corresponding intervals of the brain signals (EEG and ECoG respectively).

For the ECoG dataset, this operation was simpler, while the sampling frequency of the kinematic data was the same as the ECoG signal (1000 Hz), therefore the intervals of the kinematic and ECoG signals were easily matched.

Concerning the EEG, however, the sampling frequency was different from that of the dataglove. A simple conversion between the two frequencies was not sufficient to align the kinematic and EEG intervals in time, as the dataglove recorded kinematic data with a variable sampling frequency. This variability primarily occurred between periods of relevant movement and those where no significant motion was recorded, while in movement intervals (where CKC was

calculated), the sampling frequency was about constant. As a result, a more complex synchronization process was required. Having the markers corresponding to each interval, along with their respective sample indices for the two signals, the theoretical movement intervals of the kinematic signals and those of the EEG were first matched. Subsequently, knowing the temporal duration of these theoretical intervals (as defined during the experiment), the sampling frequency within each theoretical interval of the kinematic data was calculated as follows:

$$f_s^{kinematic} = \frac{Number\ of\ samples\ \ of\ the\ interval}{Temporal\ duration\ of\ the\ interval}$$

Equation 4

Then, having obtained the kinematic sampling frequency, it was possible to interpolate the Dataglove intervals to obtain signals with the same sampling frequency as the EEG. A cubic interpolation was used, ensuring a smoot transition and preserving the continuity of the first and second derivative.

3.4.3 Coherence calculation

All the intervals belonging to a movement class were concatenated into a single signal. CorticoKinematic coherence was then calculated for each class of movement, splitting concatenated data into 2 s epochs with 1.6 s epoch overlap, leading to a frequency resolution of 0.5 Hz. A significant overlap was used as this allows for a more stable coherence, with a lower variance and bias [48]. Regarding EEG, since the Point and Fist movements involve the flexion-extension of multiple fingers, coherence was calculated using the kinematic signal of the Middle

and Ring fingers, respectively, as only one trajectory could be used. However, additional attempts were made using other moving fingers to ensure the reliability of the results.

3.5 Decoding

The second aim of this work, beyond the coherence analysis, was to decode movements from brain signals. By "decoding," we refer to reconstructing finger trajectories using ECoG or EEG signals. This reconstruction relies on segments of cerebral signals preceding the corresponding finger position; therefore, it is more accurate to describe it as a prediction of the upcoming movement rather than a reconstruction. Having analyzed the coherence within the low frequencies, the approach was to use the low frequency band (Low Motor Potentials) of the signals for decoding. The goal was to investigate whether Low Motor Potentials, that are responsible for the CKC, enable the decoding of repetitive movements from ECoG and/or EEG signals. The finger trajectory prediction from brain signals was first performed using a Multiple Linear Regression (MLR) model. Subsequently, a Temporal Convolutional Network (TCN) model was also employed to investigate whether a more complex model could achieve better performance. However, given the poor coherence and decoding results obtained with EEG, it was decided to further explore it using the TCN with a broader frequency band that included the entire spectrum for both ECoG and EEG signals. Using almost raw signals with Deep Learning models makes sense because these models are capable of automatically extracting relevant features from the data, eliminating the need for manual feature extraction beforehand. In addition, the use of additional frequency bands is justified by various characteristics of brain signals that could help for the decoding, such as Movement-Related Potentials in EEG and High Gamma activity (both described in Section 1.5). Therefore, the idea was that, since these models

can autonomously extract features, incorporating higher frequency bands might help the model uncover new useful information for decoding.

In addition, decoding was performed using both the entire original dataset and a "**corrected**" version, in which intervals where subjects moved fingers other than the target finger for training were removed. This means that, for instance, when training the model to decode the thumb trajectory, intervals where other fingers were moving were excluded, retaining only the segments where the thumb was moved or no movement was performed at all. This approach was used because, in both the ECoG and EEG datasets, movements of different fingers were performed sequentially. As a result, when using the full cerebral signal, intervals were included where the trajectory of the target finger (the one being decoded) remained nearly flat, while other fingers were actually moving. The idea was that such movements of other fingers were detectable in the brain signals but not in the kinematic signals, leading the model to associate characteristic movement patterns with the target finger even when its trajectory showed no movement, increasing prediction errors. The underlying hypothesis is that repeated movements of different fingers are represented similarly in brain signals, making it likely that the model would recognize these same patterns when other fingers were moved. This assumption is also supported by findings in the literature, which highlight the challenges of classifying movements between different fingers [18]. Furthermore, this idea was confirmed by the results reported in results Section 4.2, which showed improved performance when using these “corrected data”. A **0.5-second window** of brain signals was used as input for decoding to simulate a BCI with feasible real-time (or near real-time) application.

To evaluate the decoding performance, the **Pearson correlation coefficient** was used as the primary metric.

The Pearson correlation measures the linear relationship between two variables, in this case, the predicted and actual finger trajectories. It ranges from -1 to 1, where:

- A value of 1 indicates a perfect positive correlation, meaning the predicted trajectory closely follows the actual movement.
- A value of -1 represents a perfect negative correlation, where the predicted trajectory is the inverse of the actual one.
- A value close to 0 suggests no linear relationship between the predicted and original trajectories.

The Pearson correlation coefficient r is defined as:

$$r = \frac{\sum(x_i - \bar{x})(y_i - \bar{y})}{\sqrt{\sum(x_i - \bar{x})^2 \sum(y_i - \bar{y})^2}}$$

Equation 5

where x_i and y_i are the two variables, that correspond to predicted and actual trajectory in this case, while $\bar{x}$ and $\bar{y}$ are their respective means.

This metric provides an intuitive way to assess how well the model captures the temporal variations of finger movements, and can be written also as:

$$r = \frac{\sigma_{xy}}{\sigma_x \sigma_y}$$

Equation 6

Where σ_{xy} is the covariance between the two variables, while σ_x and σ_y are the standard deviations of the two variables, corresponding to the square root of their variances. This formulation shows that correlation is a normalized measure of covariance, making it possible to compare linear relationships between variables regardless of their scales.

3.5.1 Preprocessing

Both ECoG and EEG data had previously undergone the initial preprocessing described in Sections 3.2 and 3.3. Subsequently, the two data filtered differently were extracted, in order to compare the decoding performance in the two cases:

- **LMPs**: Data were further filtered to extract the Low Motor Potentials. A 7th order Butterworth lowpass filter with a cutoff frequency of 4 Hz was applied to both ECoG and EEG signals. Subsequently, data were downsampled in an integrative way to 25 Hz to reduce computational load. According to the Nyquist-Shannon sampling theorem, the sampling frequency must be at least twice the maximum frequency present in the signal to avoid aliasing. Since we had previously removed frequencies above 4 Hz, downsampling at 25 Hz was sufficient, as this is well above the Nyquist frequency of 8 Hz. In this case, downsampling was performed by integrating multiple consecutive samples into one, where instead of selecting a single sample every 'n' samples, we summed the 'n' samples and used their sum as the new sample (Equation 7). This method helps retain the signal's key characteristics while reducing its dimensionality for computational efficiency

$$y[N] = \sum_{(N-1)n+1}^{Nn} x[k]$$

Equation 7

where:

- $y[N]$ is the resampled signal.
- $x[k]$ is the original signal.
- n is the downsampling factor, calculated as *original sampling frequency / new sampling frequency*.
- N is the index of the new resampled signal.
- k is the index of the original signal.

- **Whole band**: To retain the entire frequency range of interest of the EEG signals, the same type of lowpass filter used for LMPs was applied, but with a different cutoff frequency. Specifically, a 40 Hz cutoff frequency was chosen, as the EEG band typically ranges from approximately 0.1 to 40 Hz [5]. (frequencies below 0.1 Hz had already been removed during initial preprocessing). This range includes important bands for Movement Related Potentials, such as the Alpha (8-13 Hz) and Beta (14-30 Hz) bands. Regarding ECoG signals, they were initially provided filtered between 0.15 and 200 Hz, so the full available band up to 200 Hz was retained. In fact, the High Gamma band can extend beyond 200 Hz, reaching up to 300 Hz [10]. Once again, both EEG and ECoG data were downsampled to reduce computational load while adhering to the Nyquist-Shannon theorem. EEG signals were downsampled to 83.3 Hz, ensuring a sampling rate above the Nyquist frequency of 80 Hz. This specific frequency was chosen due to the integrated downsampling approach, which requires an integer downsampling factor. Given that the data had been previously downsampled to 250 Hz during initial preprocessing, a factor of 3 was the smallest integer that resulted in a sampling frequency above the Nyquist limit.

These data were given as input to the model that performed the decoding. Specifically, the two models mentioned before were tested:

- A Multiple Linear Regressor (MLR)
- A Temporal Convolutional Network (TCN)

Both the models can be used to perform a regression problem like this one. Regression involves predicting continuous numerical values and must be distinguished from classification, where the goal is to assign discrete labels or categories. However, these models differ significantly in complexity and approach. Linear Regression is one of the simplest and most fundamental models for regression problems. It is often considered the foundation of predictive modeling, serving as a core concept in both machine learning and artificial intelligence. On the other hand, the Temporal Convolutional Network is a Deep Learning model, meaning it is designed to automatically extract relevant features from raw data during training, rather than relying on manually selected input features, as is common in traditional machine learning approaches. The rationale behind using these two models is to compare a simple and interpretable model with a more complex one, in order to assess the contribution of the model itself to decoding performance. Meanwhile, the influence of the input features is analyzed by comparing Low Motor Potentials and the whole band signals, as described above.

The same training approach was applied to both models, utilizing a **3-Fold Cross-Validation** technique. This method involves splitting the dataset into three subsets (folds). In each iteration, two folds are used for training, while the remaining fold is reserved for model selection and evaluation. This process is repeated three times, ensuring that each subset is used for validation once. This approach allows for both hyperparameter tuning and an unbiased estimation of the model's generalization performance [49]. A separate training was performed for each fold of a finger of a subject, resulting in distinct models trained for each specific case.

3.5.2 Multiple Linear Regression

Linear Regression establishes a relationship between a dependent and one or more independent variables through a linear function and serves as the foundation for more complex predictive models [50], as mentioned in the previous section. The accuracy of the regression then depends on how well the relationship between the dependent and independent variables can be approximated by a linear model. Mathematically, a simple linear regression model is expressed as:

$$y = a + bx + \epsilon$$

Equation 8

where:

- y is the dependent variable (output).
- x is the independent variable (input).
- a is the intercept of the straight line.
- b is the slope coefficient of the straight line.
- ϵ represents the residual error, the difference between the predicted and the actual values.

Linear Regression is based on the Least Squares Error method, which aims to find the best-fitting line that approximates a given set of points by minimizing the sum of squared differences between the predicted and actual values. The Least Squares method finds the optimal values of a and b by minimizing the Mean Squared Error (MSE), defined as:

$$MSE(a,b) = \frac{1}{N}\sum_{i=1}^{N}(y_i - \hat{y_i})^2$$

Equation 9

where:

- N is the number of data points.
- y_i are the actual values.
- $\hat{y_i}$ are the predicted values from the model.

Equation 9 refers to a traditional linear regression model, where a single independent variable is used to predict a dependent variable. However, in this study the regression was performed using a Multiple Linear Regression, which involves multiple independent variables to predict a single dependent variable. Specifically, a temporal window approach combined with a channel selection was exploited. In this method, each sample of the predicted trajectory was obtained by feeding the model with a time window of 0.5 second of the cerebral signal, prior to the target sample, from a certain number of selected channels. This approach transforms the input into a matrix, where each row corresponds to a specific time instance, and contains the 0.5 second windows of brain data from all the selected channels preceding that time instance. This model can be described by the following modified version of the Equation 9 [51]:

$$y = a + \sum_{n=1}^{N}\sum_{k=0}^{L} b_i x_i(t-k) + \epsilon$$

$$y = XW + \epsilon$$

Equation 10

where:

- y is again the vector of predicted trajectory values (output).
- a is again the intercept.
- N is the number of channels used to predict the dependent variable.
- L corresponds to the number of signal lags used to predict the dependent variable.
- b_i is the weight of the model that multiplies the independent variable x_i.
- X is the input matrix of independent variables, with dimensions N x (TC). N refers again to the number of samples of the predicted trajectory, T represents the number of samples in the 0.5 second window (equal to $0.5f_{sample}$), while C is the number of selected channels.
- W is the weight vector, that includes all the coefficients of each independent variable.

The estimation of the optimal weight vector W, which represents the model training process and involves the minimization the Mean Squared Error, as described in traditional Linear Regression, is obtained using the following equation:

$$W = (X^T X)^{-1} X^T y$$

Equation 11

The channels to give as input to the model were instead selected based on a modified **Sequential Forward Selection**. This method follows a bottom-up search strategy, starting with an empty feature set and progressively adding features based on an evaluation function that minimizes the Mean Square Error. At each iteration, the next feature is selected from the remaining available ones, but it is added to the set only if its inclusion leads to a lower prediction error

compared to any other possible addition [52]. This ensures that each newly added feature contributes to improving the model's performance. In this case, the evaluation function used to add new channels was the correlation between the original and predicted trajectories of the validation set. At each iteration, all remaining channels were tested one by one, computing the correlation for each and selecting only the channel that led to the greatest improvement in coherence. The process continued until a maximum of 10 channels was reached or until no further improvement was observed.

Given the very low decoding performance with EEG signals, a **permutation test** was conducted on the best-performing participant. The purpose of this test is to assess whether the observed decoding results exceed what could be expected by chance. This test was applied to determine whether decoding results in this case were above chance level, that corresponds to the results obtained with the permutation test. There are different ways to perform a permutation test, but since the data consists of time series representing finger trajectories, it was important to preserve the temporal structure of the samples. To achieve this, the permutation was performed by *circularly shifting* the predicted trajectories by a random amount while keeping the overall sequence intact. This approach disrupts the direct alignment between the predicted and actual trajectories while maintaining the temporal dependencies within each trial, making it a suitable way to estimate the chance level [53].

3.5.3 Temporal Convolutional Network

Temporal Convolutional Networks are powerful Convolutional Neural Network-based architecture for modeling sequential data, exploiting causal and dilated convolutions. As mentioned previously, being a Deep Learning architecture, they automatically extract relevant

features from raw data that are useful for prediction. Originally, Convolutional Neural Networks (CNNs) were developed primarily for image processing, as their convolutional operations are well-suited for capturing spatial patterns. However, by adapting these operations to process temporal dependencies instead of spatial ones, CNN-based architectures like TCNs have been successfully applied to time-series analysis and other sequential data tasks. For years, the most commonly used models for time series analysis have been Recurrent Neural Networks (RNNs) and their variants, with TCNs that have emerged as an alternative. Compared to RNNs, TCNs offer advantages such as parallel processing, a flexible receptive field size (which determines how many past time samples influence the current prediction), stable gradients that avoid the vanishing/exploding gradient problem (where weights either shrink to near zero or grow uncontrollably during backpropagation), and lower memory requirements during training [54]. The mathematic operation underlying this model is the **convolution**, that for discrete bidimensional data can be mathematically expressed as following [55]:

$$A[i_a, j_a] * B[i_b, j_b] = C[i_c, j_c] = \sum_{\tau_1=0}^{i_a-1} \sum_{\tau_2=0}^{j_a-1} A[\tau_1, \tau_2] B[i - \tau_1, j - \tau_2]$$

Equation 12

where:

- $C[i_c, j_c]$ is the resulting element in the output matrix C after convolving matrices A and B. Each element of matrix C is calculated as a weighted sum of the corresponding elements from matrices A and B at indices i_c, j_c.

- $A[i_a, j_a]$ is the element from the input matrix A that is convolved with matrix B. The indices i_a and j_a represent the positions (row and column) of the elements of A being combined with elements from matrix B.
- $B[i_b, j_b]$ is the filter or kernel matrix applied to the input matrix A, with indices i_b and j_b represent the positions of the elements of kernel matrix B.
- τ_1, τ_2 are the parameters used to iterate over and multiply the elements of matrices A and B during the convolution operation.

This formulation can be seen as one matrix sliding over the other one unit at a time, with the sum of the element-wise products of the two matrices as the result. Figure 15 [55] shows the convolution of a matrix (A) and a kernel (B) at a single coordinate of the matrix: $A[i_a, j_a]$. The complete convolution is found by repeating this process until the kernel has passed over every possible pixel of the source matrix

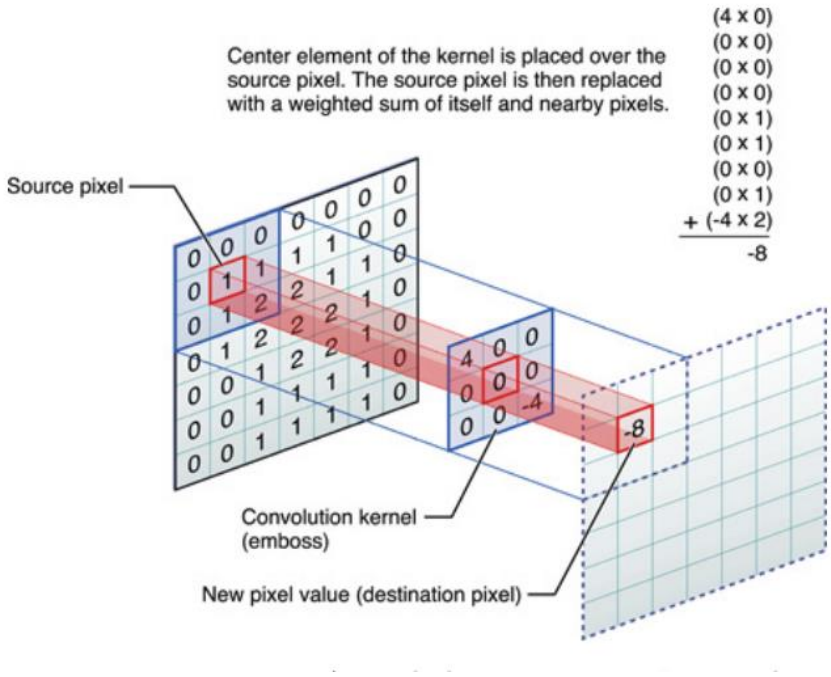

Figure 15: Convolution of a matrix and a kernel at a single coordinate [55].

A TCN exploits this operation in a more complex architecture, that includes dilated convolutions and residual connections. In the case of a TCN, the input matrix A consists of sequential data structured in a way that preserves temporal dependencies. Specifically, each row of A represents a time window, while columns correspond to different features extracted from the input signal over time. A simple causal convolution can only access a limited history proportional to the network's depth, which can be restrictive for tasks requiring a longer memory. To overcome this limitation, TCNs employ **dilated convolutions**, a technique that exponentially increases the receptive field, the range of input data influencing each output. A dilated convolution introduces gaps between sampled input points, controlled by a dilation factor d, allowing the network to model long-range dependencies without significantly increasing the number of layers. The effective **receptive field** of a TCN layer depends on both the **filter size** k and the **dilation factor** d. There are several layers, each with its own dilation factor, with an exponential increase of d at deeper layers ($d = 2^i$ at layer i). In this way, the network ensures that every relevant input within the receptive field is captured without passing through too many layers and maintaining computational efficiency. To further improve performance and stability, TCNs incorporate **residual connections**, where each residual block contains a certain number of layers of dilated causal convolutions followed by nonlinear activation functions, typically ReLU. This block contains a direct link that takes the initial block input and adds it directly to the final output. If the output has a different dimension respect to the summed input, because of the previous convolutions, a 1x1 convolution is added before the sum to ensure that the tensors have the same form. Additionally, techniques such as weight normalization and spatial dropout can be applied for regularization. This architectural design allows TCNs to efficiently capture long-term dependencies while maintaining stable gradients during training [55]. A schematic representation of a generic TCN is shown in Figure 16.

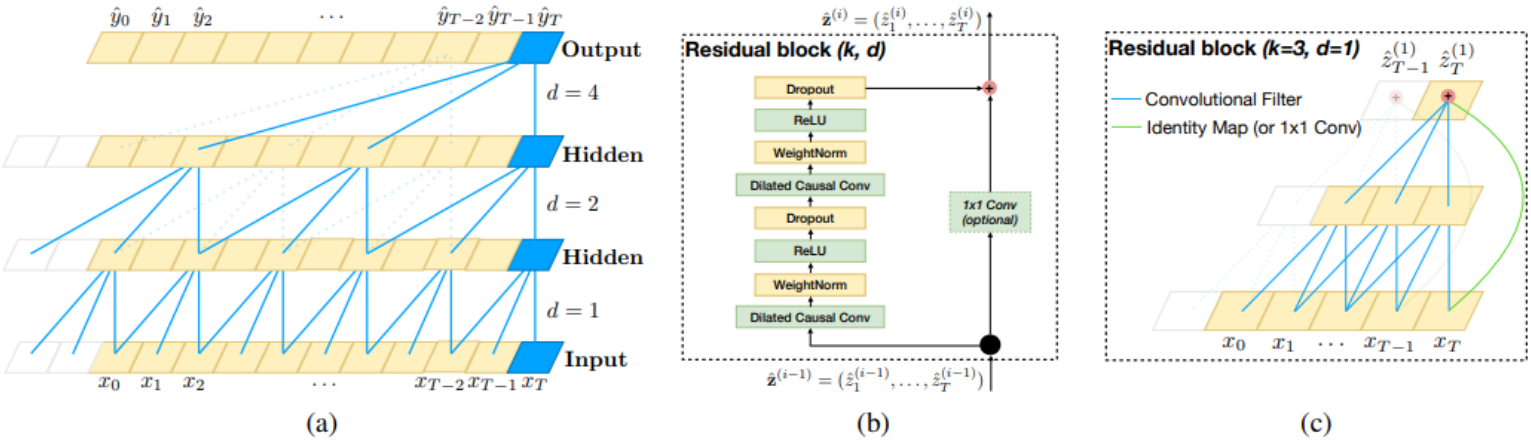

Figure 16: Architectural elements in a TCN. (a) A dilated causal convolution with dilation factors d = 1, 2, 4 and filter size k = 3. (b) TCN residual block. An 1x1 convolution is added when residual input and output have different dimensions. (c) An example of residual connection in a TCN. The blue lines are filters in the residual function, and the green lines are identity mappings.

In this work, the TCN model implemented by Philippe Remy was utilized [56]. This model is available in Python as part of the Keras library, a widely used deep learning framework built on top of TensorFlow. **Some hyperparameters were optimized** for this task, while others were left as default. Specifically, the number of convolutional filters per layer (*nb_filters*), the kernel size used in each convolution (*kernel_size*), and the dilation rates for the dilation levels (*dilations*) were tuned to achieve the best performance. The default values for the other parameters are documented in the Keras-TCN GitHub repository [56], considering that the three parametres just cited were settled as described. Note that, unlike Figure 16, in this model there are 2 sequential convolutional layers for each dilatation level, with the output of the first convolutional layer that is the input of the second one. The optimization was performed using the *GridSearchCV* function in Python, which systematically tested all possible combinations within a predefined set of values for the three parameters, finding the best combination based on the Mean Squared Error on the Validation Set. Given the four different types of signals considered: ECoG with LMPs, ECoG up to 200 Hz, EEG with LMPs, and EEG up to 40 Hz,

this optimization process was repeated separately for each signal type. However, due to the high computational cost of evaluating all combinations across all subjects and conditions, the optimization was conducted using data from only one finger of a single subject, keeping the obtained parameter values to train also other subjects data. This approach aimed to provide an initial indication of the best-performing parameters, acknowledging that optimal values could vary across subjects due to the high intra-subject variability of neural signals. Additionally, it was observed that slight variations in these parameters did not lead to significant differences in performance. Table 3 shows the values of the hyperparameters for each type of signal:

	ECoG LMP	EEG LMP	ECoG 200 Hz	EEG 40 Hz
nb_filters	64	128	32	32
kernel_size	3	3	3	3
dilations	[1, 2, 4]	[1, 2, 4]	[1, 2, 4, 8, 16, 32]	[1, 2, 4, 8]

Table 3: TCN hyperparameters used for each type of data.

The approach was to consistently use a 0.5-second signal window to ensure a fair comparison of results across different datasets while maintaining the same temporal window for prediction. To achieve this, the kernel size and dilation layers were selected so that the receptive field would always cover 0.5 seconds of input signal. The receptive field is determined by the formula [56]:

$$Receptive\ Field = 1 + \ 2(kernel\ size - 1)\sum_{i=0}^{L-1} d_i$$

where L is the number of layers, d_i represents the dilation rate at layer i. The factor '2' comes from the two sequential convolutions per layer. If the calculated receptive field exceeded the required time window, zero-padding was applied to the missing samples, as the input signal length remained fixed at 0.5 seconds.

Training was conducted with an **early stopping** criterion using a patience of 6, meaning that if the loss function (MSE) on the validation set did not improve for 6 consecutive epochs, the training was stopped. Although the maximum number of training epochs per fold was set to 50, this limit was never reached. Furthermore, a **learning rate annealing** strategy was applied, halving the learning rate when the validation loss did not improve for 3 consecutive epochs (patience = 3). The annealing method helps to adjust the learning rate during training, gradually reducing it to allow the model to converge more smoothly and avoid getting stuck in local minima of the loss function gradient, which can happen when the learning rate is too low. On the other hand, if the learning rate is too high, there is a risk of skipping local minima. Therefore, this strategy helps to avoid both these issues and can lead gradient descent to minima with better generalization than using a small learning rate throughout [57].

Regarding channel selection, a Sequential Forward Selection approach would have been impractical for TCN due to its high computational cost and time. Therefore, all channels covering the contralateral sensorimotor cortex (always corresponding to the left hemisphere) were included in the input tensor, based on the knowledge that finger movement-related information originates from this region. Specifically, for ECoG signals, the electrodes included in decoding varied across subjects, as the number and location of electrodes differed between

individuals. For EEG signals, the selected channels were FC5, FC3, FC1, C5, C3, C1, CP5, CP3, and CP1.

4 Results and Discussions

4.1 Coherence results and discussions

4.1.1 ECoG

Below are the results of the coherence analysis obtained from the ECoG data. Figure 17, Figure 18, Figure 19, Figure 20 and Figure 21 show the coherences computed for all subjects. Each figure is related to the results of each subject obtained for a specific finger flexion-extension, as it was not possible to calculate an average coherence across subjects and fingers. This limitation arises because the frequency of flexion-extension movements was not consistent across cases, as the movements were self-paced. For this reason, coherence peaks are located at different frequencies in different cases, making an overall averaging meaningless. The black line represents the PSD of the kinematic signal. It was added in order to be aware where the coherence peak is expected, i.e. at the peak of the PSD. This peak represents the main frequency at which the subject performed the movement of that finger. Given that the movement frequency was not perfectly controlled, there is actually a certain frequency band where the flexion-extension occurred, with a corresponding peak. Furthermore, since coherence was computed for each electrode, for each case (Subject and Finger), the channel showing the highest coherence value within the movement frequency band was selected. This band was defined as:

$$Movement\ Band = PSD\ Peak\ \pm Frequency\ Resolution$$

Equation 3

Each plot corresponds to a different subject. Specifically, the plots are arranged in a 3×3 grid, where each row represents three subjects in order. For example, the plot in the first row, first column corresponds to Subject 1, the second column to Subject 2, and so on.

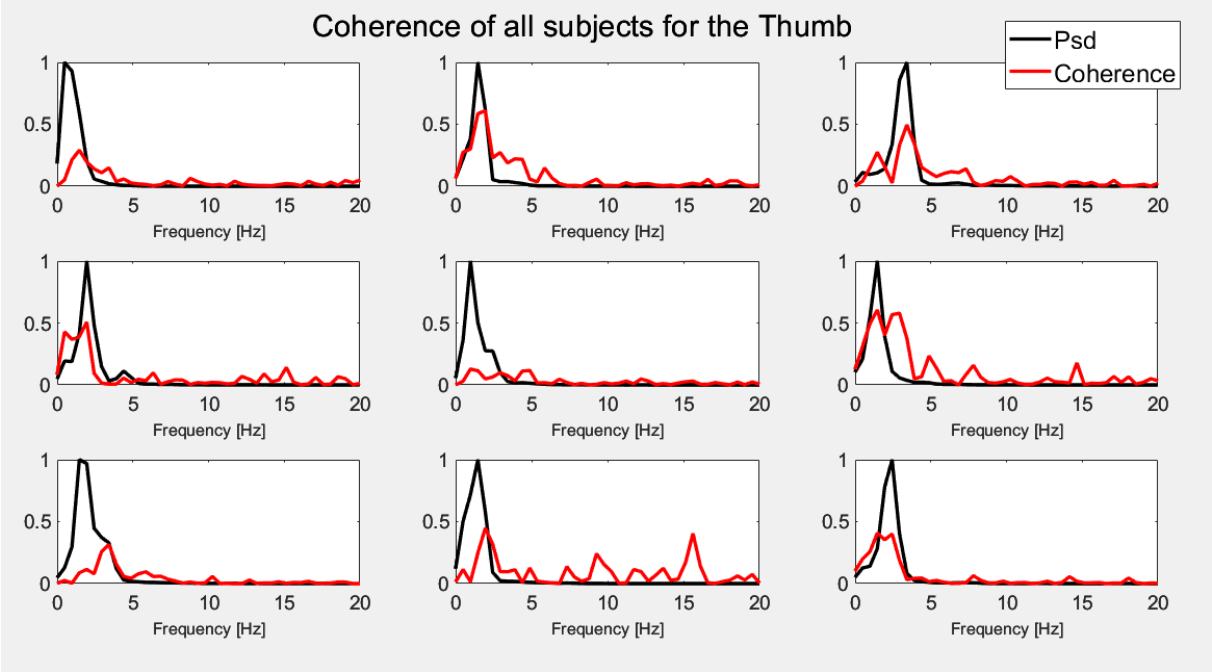

Figure 17: Coherence of the electrode with higher coherence in the movement frequency band for each subject for the Thumb. Each plot corresponds to a different subject. Specifically, the plots are arranged in a 3×3 grid, where each row represents three subjects in order. For example, the plot in the first row, first column corresponds to Subject 1, the second column to Subject 2, and so on.

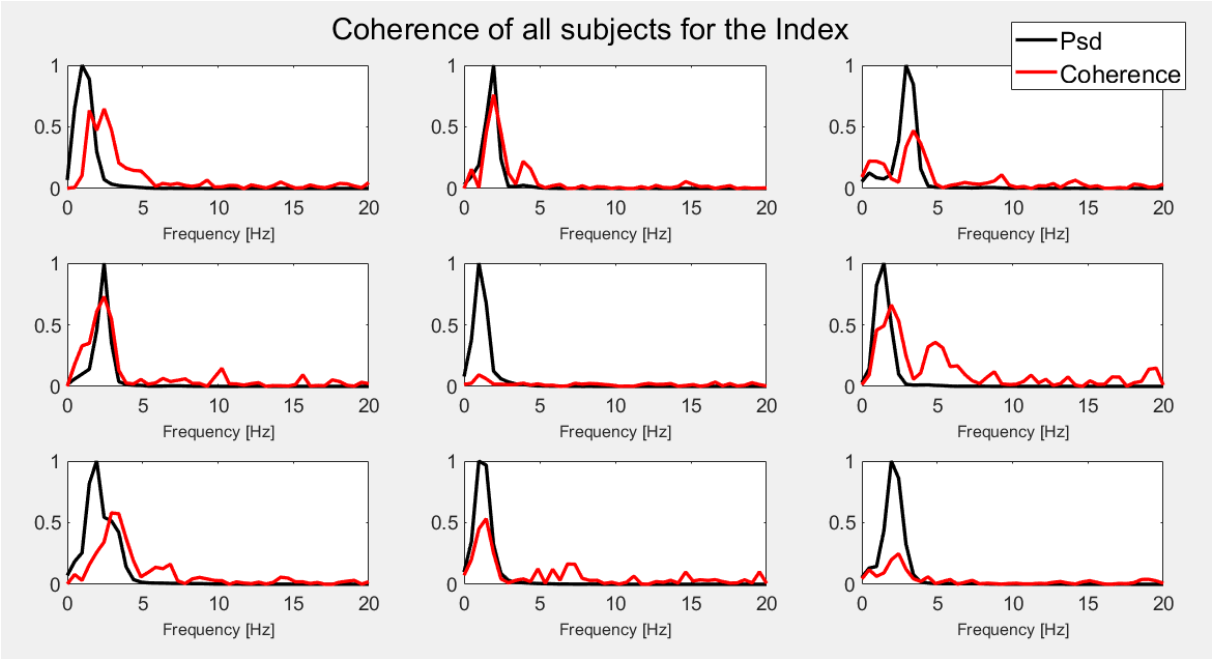

Figure 18: Coherence of the electrode with higher coherence in the movement frequency band for each subject for the Index finger. Each plot corresponds to a different subject. Specifically, the plots are arranged in a 3×3 grid, where each row represents three subjects in order. For example, the plot in the first row, first column corresponds to Subject 1, the second column to Subject 2, and so on.

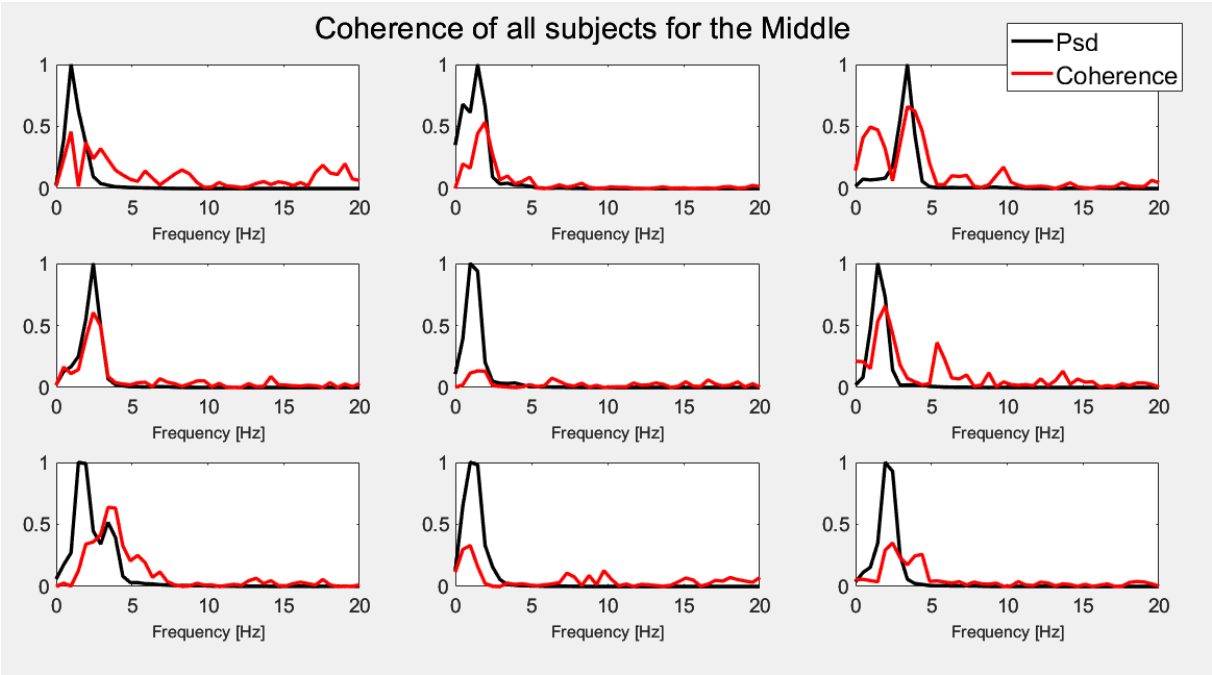

Figure 19: Coherence of the electrode with higher coherence in the movement frequency band for each subject for the Middle finger. Each plot corresponds to a different subject. Specifically, the plots are arranged in a 3×3 grid, where each row represents three subjects in order. For example, the plot in the first row, first column corresponds to Subject 1, the second column to Subject 2, and so on.

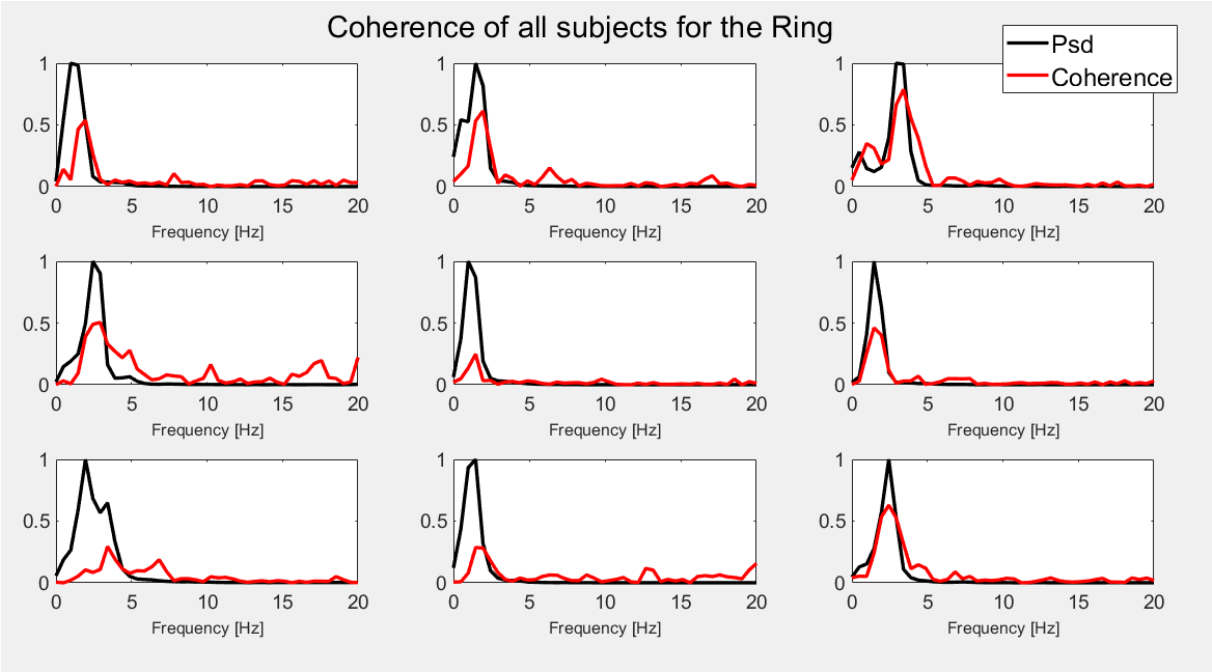

Figure 20: Coherence of the electrode with higher coherence in the movement frequency band for each subject for the Ring finger. Each plot corresponds to a different subject. Specifically, the plots are arranged in a 3×3 grid, where each row represents three subjects in order. For example, the plot in the first row, first column corresponds to Subject 1, the second column to Subject 2, and so on.

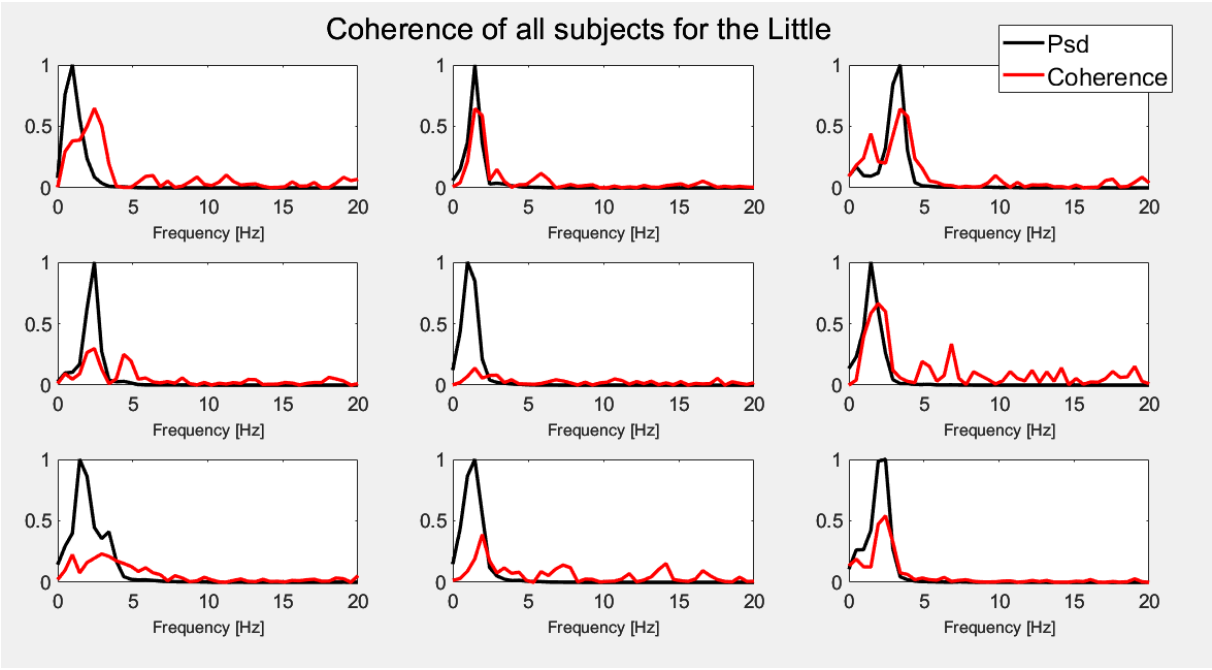

Figure 21: Coherence of the electrode with higher coherence in the movement frequency band for each subject for the Little finger. Each plot corresponds to a different subject. Specifically, the plots are arranged in a 3×3 grid, where each row represents three subjects in order. For example, the plot in the first row, first column corresponds to Subject 1, the second column to Subject 2, and so on.

It can be observed that high coherence values are present at the expected movement frequencies for almost all subjects, except for Subject 5. Coherence follows the expected trend in almost all cases, i.e. a peak at the movement frequency and much lower values at other frequencies. This indicates that the ECoG signal indeed follows, at least partially, the oscillations of the flexion-extension movements. It is sometimes possible to notice peaks around the second harmonic of the motion frequency, usually smaller in magnitude than the main peak. This aligns with findings in the literature, where CKC analyses consistently report peaks at the second harmonic and, in some cases, at higher-order harmonics. These harmonics likely reflect specific aspects of movement kinematics, such as sudden variations or discontinuities in finger position [24].

Boxplots were used to represent the distribution of coherence values across different experimental conditions. All boxplots in this work were generated following the same structure: the red line in the center of each boxplot represents the median of the distribution. The size of the box is determined by the interquartile range (IQR), spanning from the first to the third quartile, indicating where the central 50% of the data lies. The outer lines extend to the most extreme values within 1.5 times the IQR, while any data points beyond this range are considered outliers and are shown as individual dots. A general overview of the maximum coherence values in the movement band obtained for each subject is shown in Figure 22. Each boxplot contains these coherence values for all 5 fingers of the subject. Similarly, in Figure 23 the coherence between the different fingers was compared. In this case, each boxplot contains the values of all subjects for that finger.

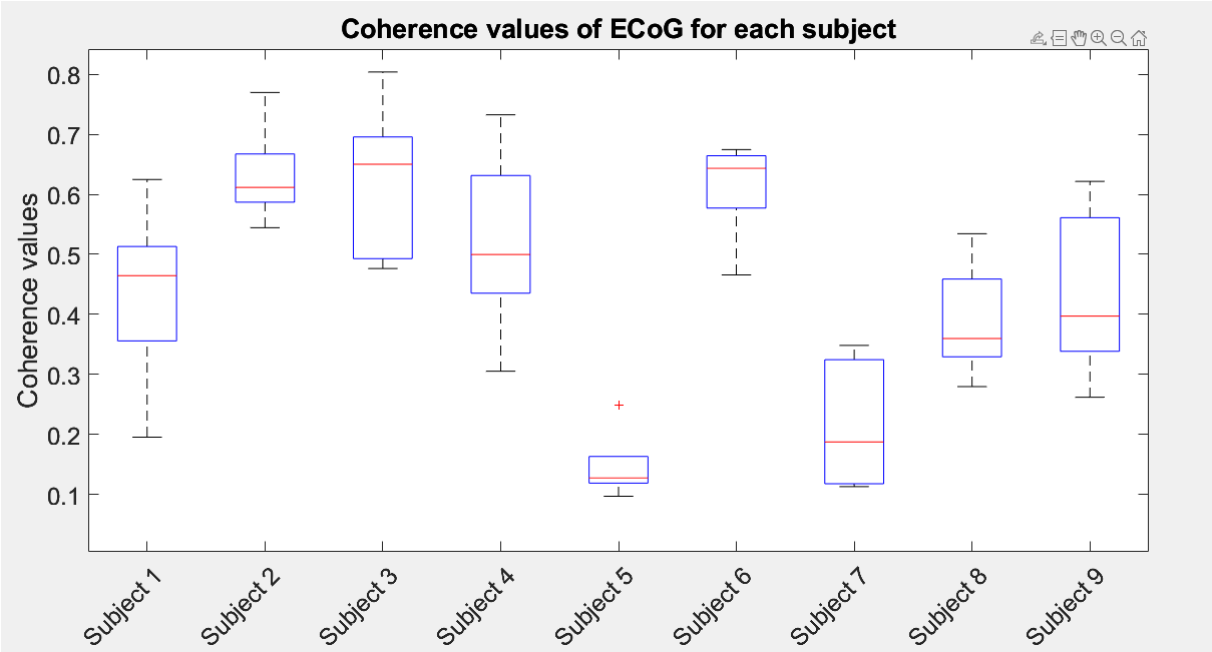

Figure 22: Coherence peak values for each subject with ECoG. The coherence peak is the higher coherence value of the electrode with the higher coherence in the movement frequency band.

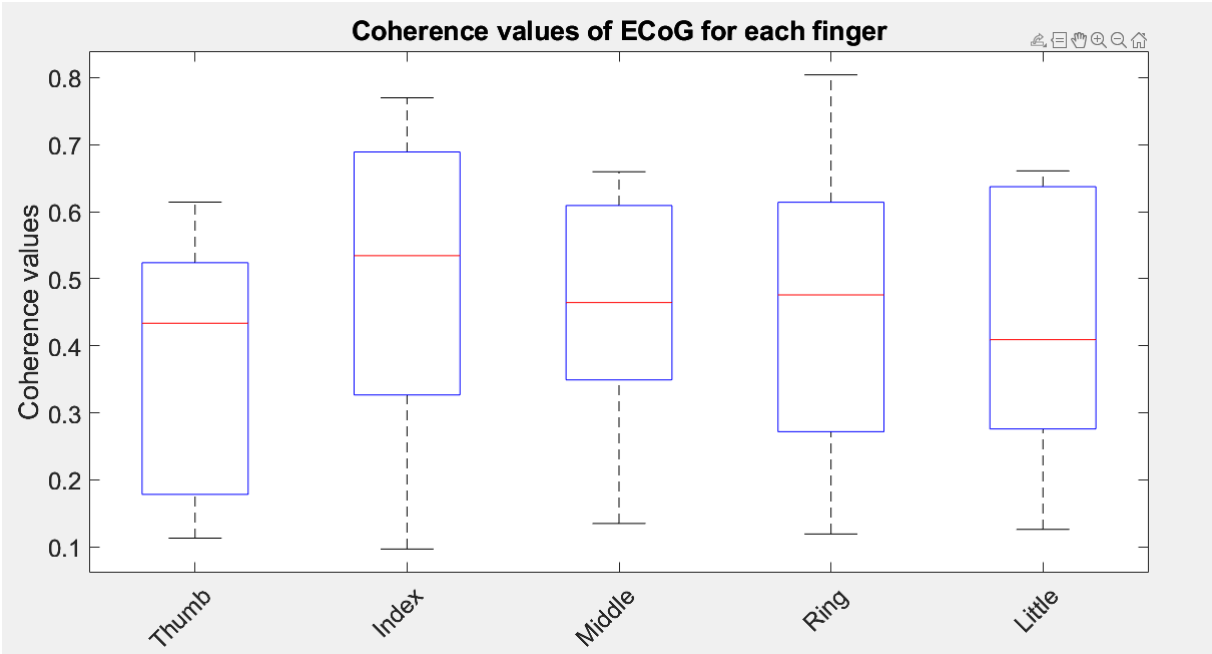

Figure 23: Coherence peak values across subjects for each finger with ECoG. The coherence peak is the higher coherence value of the electrode with the higher coherence in the movement frequency band.

These results show that, in general, good coherence values are obtained between the ECoG and kinematic signals. There are differences between subjects, particularly Subjects 5 and 7, who exhibit average values respectively of 0.15 and 0.22 (Figure 22). On the other hand, considering all the subjects, the average value is 0.45, with coherence reaching up to 0.80.

No significant differences were observed between the movements of different fingers (Figure 23), suggesting that CKC is generalizable to all fingers.

The obtained coherence results are fairly consistent with findings reported in the literature, although most studies have analyzed it using the magnetoencephalographic (MEG) signal. For example, Piitulainen et al. (2013) reported a mean coherence of 0.25 between the MEG signal and hand acceleration during self-paced flexion–extension movements of the right-hand fingers [25]. Since the experimental condition (active and self-paced flexion–extension) is about the same as in the present study, we can hypothesize that ECoG may yield higher coherence values compared to MEG. The only difference is that their experiment included a touch between the Thumb and the other fingers at the end of each flexion. However, the effect of touch on coherence remains controversial, as two different studies have reported conflicting results. In Piitulainen et al. (2013) [26], the presence of touch did not significantly affect coherence, suggesting that the two conditions (with and without touch) could be considered equivalent. In contrast, Bourguignon et al. [27] found significantly higher coherence in the active-touch condition compared to the active-no-touch (self-paced) condition, likely due to increased tactile input. Specifically, they reported group-level coherence values of 0.55 for the touch condition and 0.31 for the no-touch condition. Regardless of which hypothesis holds true, the fact that the experimental conditions of the present study did not involve touch, suggests again that the coherence values obtained with ECoG are superior to those reported with MEG. This is because

results of this current work exceed the no-touch condition in both studies and are comparable to the touch condition reported by Bourguignon et al.

In order to identify the brain regions where greater coherence was observed, topographic maps are presented in Figure 24, Figure 25, Figure 26, Figure 27 and Figure 28. The plots for each subject are arranged as in Figure 17, illustrating the coherence distribution over the scalp during fingers flexion-extension. The maps follow the colormaps shown on the below, with colors representing the peak coherence values in the motion band for each electrode. As previously mentioned, each subject has a different number of electrodes implanted in varying positions, but always covering at least part of the left sensorimotor cortex. Additionally, the graphical representation of each brain (provided with the dataset) also differs across subjects.

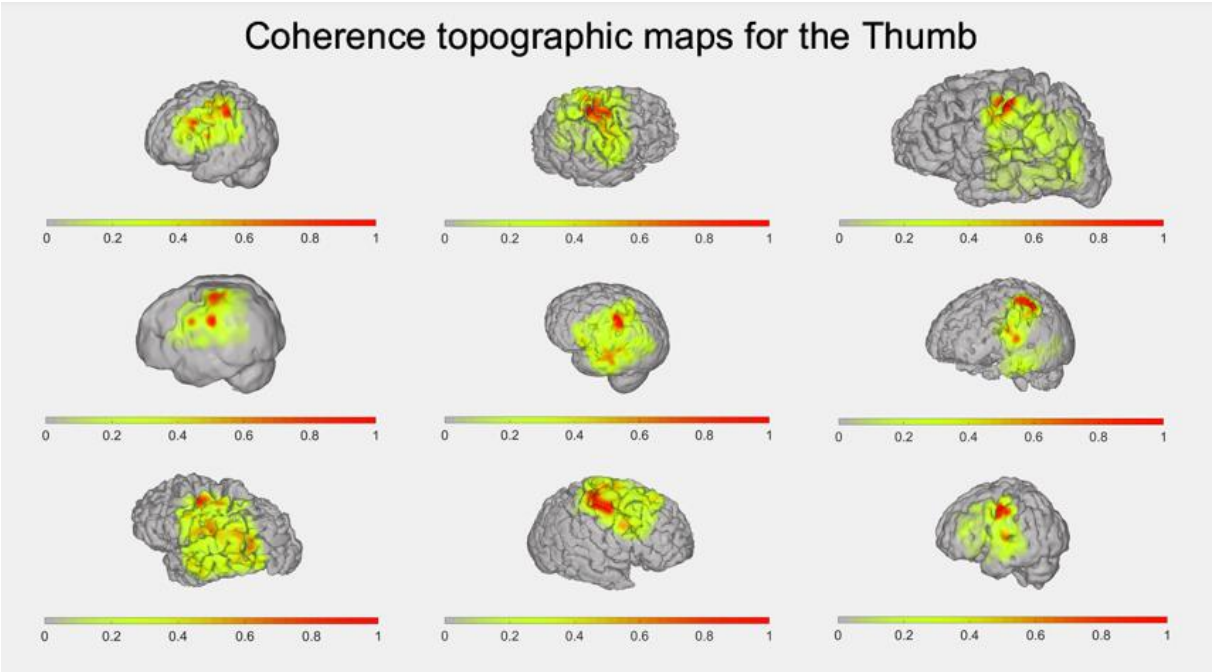

Figure 24: Coherence topographic maps of the ECoG of each subject for the Thumb finger. Each electrode shows the coherence in the movement band. Each plot corresponds to a different subject. Specifically, the plots are arranged in a 3×3 grid, where each row represents three subjects in order. For example, the plot in the first row, first column corresponds to Subject 1, the second column to Subject 2, and so on.

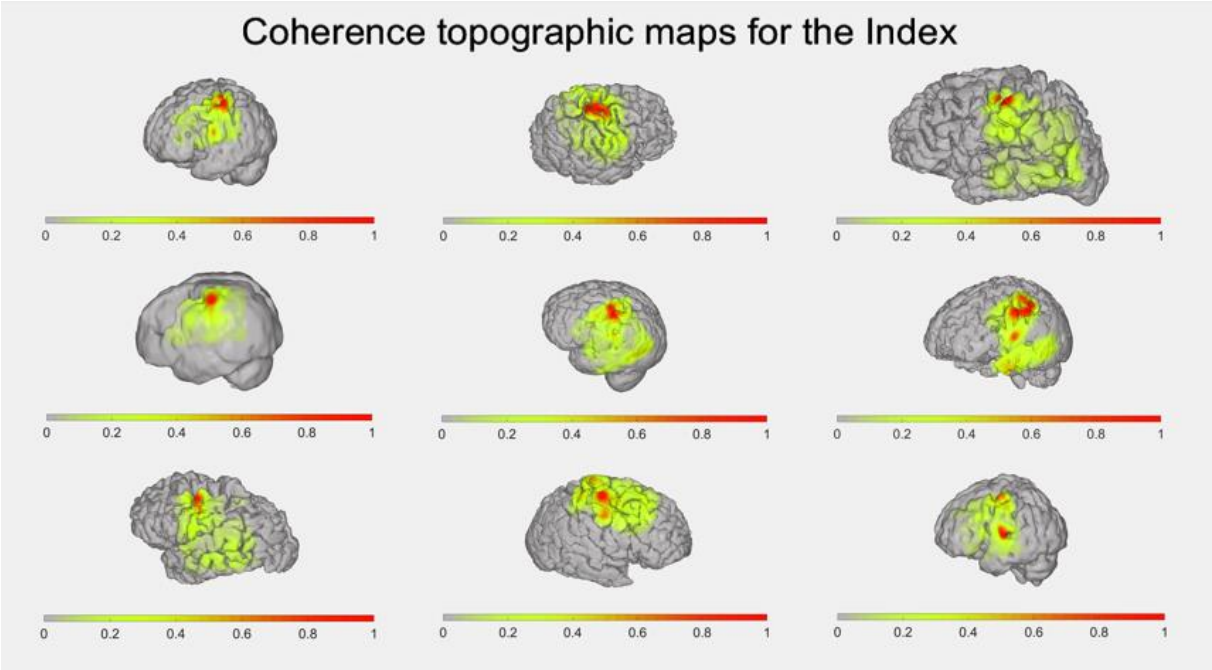

Figure 25: Coherence topographic maps of the ECoG of each subject for the Index finger. Each electrode shows the coherence in the movement band. Each plot corresponds to a different subject. Specifically, the plots are arranged in a 3×3 grid, where each row represents three subjects in order. For example, the plot in the first row, first column corresponds to Subject 1, the second column to Subject 2, and so on.

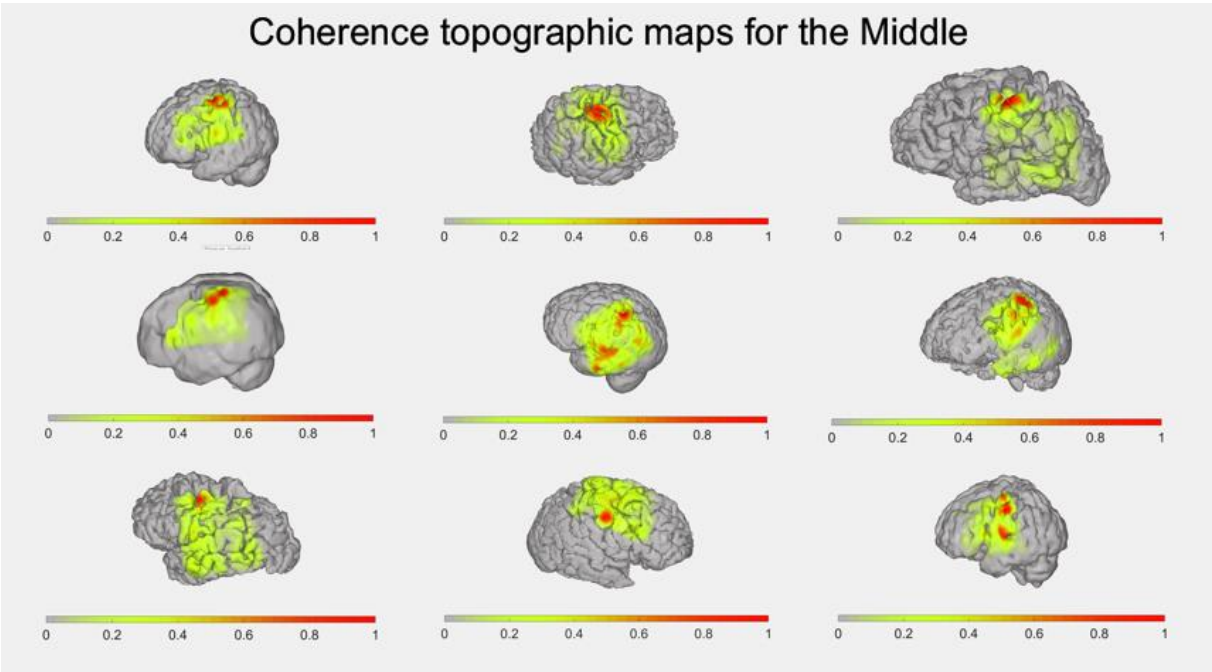

Figure 26: Coherence topographic maps of the ECoG of each subject for the Middle finger. Each electrode shows the coherence in the movement band. Each plot corresponds to a different subject. Specifically, the plots are arranged in a 3×3 grid, where each row represents three subjects in order. For example, the plot in the first row, first column corresponds to Subject 1, the second column to Subject 2, and so on.

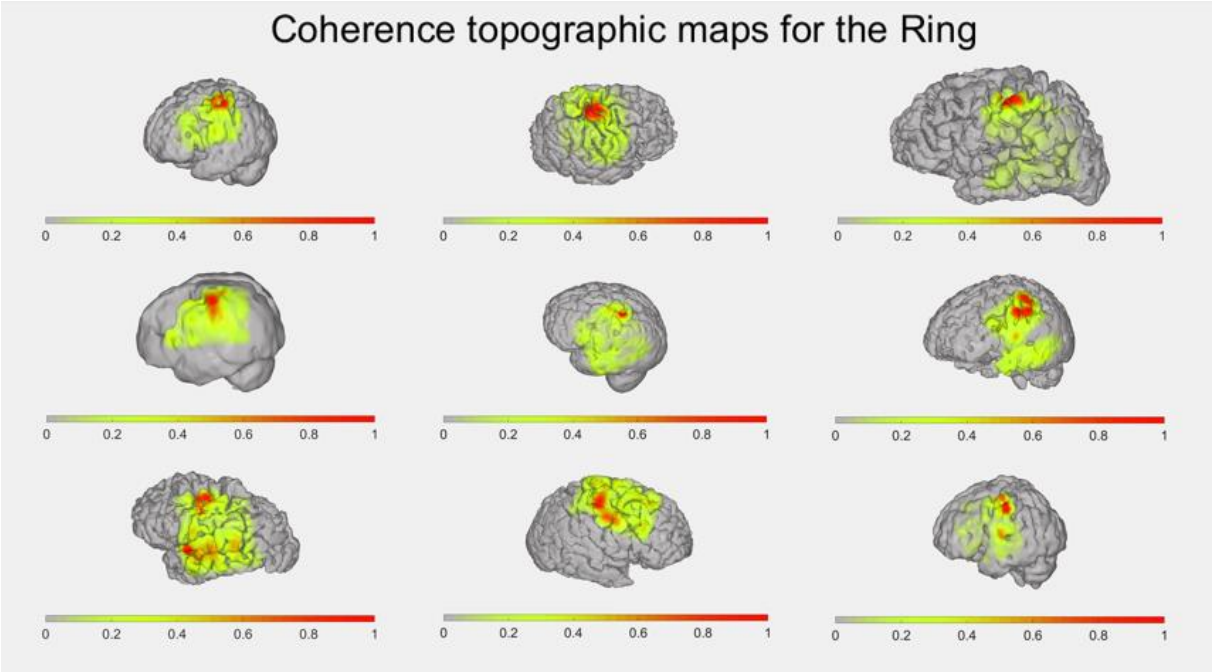

Figure 27: Coherence topographic maps of the ECoG of each subject for the Ring finger. Each electrode shows the coherence in the movement band. Each plot corresponds to a different subject. Specifically, the plots are arranged in a 3×3 grid, where each row represents three subjects in order. For example, the plot in the first row, first column corresponds to Subject 1, the second column to Subject 2, and so on.

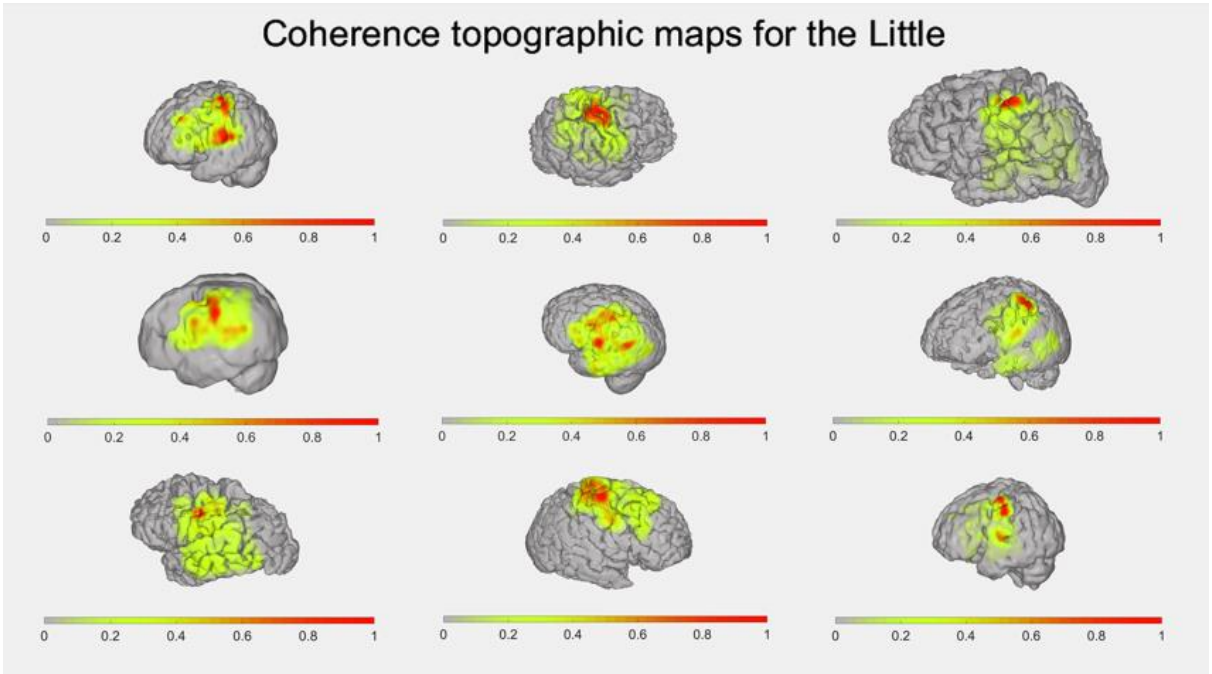

Figure 28: Coherence topographic maps of the ECoG of each subject for the Little finger. Each electrode shows the coherence in the movement band. Each plot corresponds to a different subject. Specifically, the plots are arranged in a 3×3 grid, where each row represents three subjects in order. For example, the plot in the first row, first column corresponds to Subject 1, the second column to Subject 2, and so on.

It can be observed that, in almost all cases, the highest coherence values are located in the electrodes over the left sensorimotor cortex, which corresponds to the hemisphere contralateral to the moving hand. This is expected and reasonable, as this region is responsible for controlling the movement of the contralateral limb [58]. Moreover, this finding is consistent with the results of all previously cited studies on CKC.

4.1.2 EEG

Here are the same coherence analysis results, but this time obtained using the EEG signal.

In Figure 29, Figure 30, Figure 31, Figure 32, Figure 33, Figure 34, Figure 35 and Figure 36 the coherence obtained from all six subjects is shown, one figure for each movement class. As in the previous case, calculating an average coherence across subjects and fingers was not feasible for the same reasons mentioned earlier. Once again, the coherence of the electrode with the highest coherence within the movement frequency band is shown.

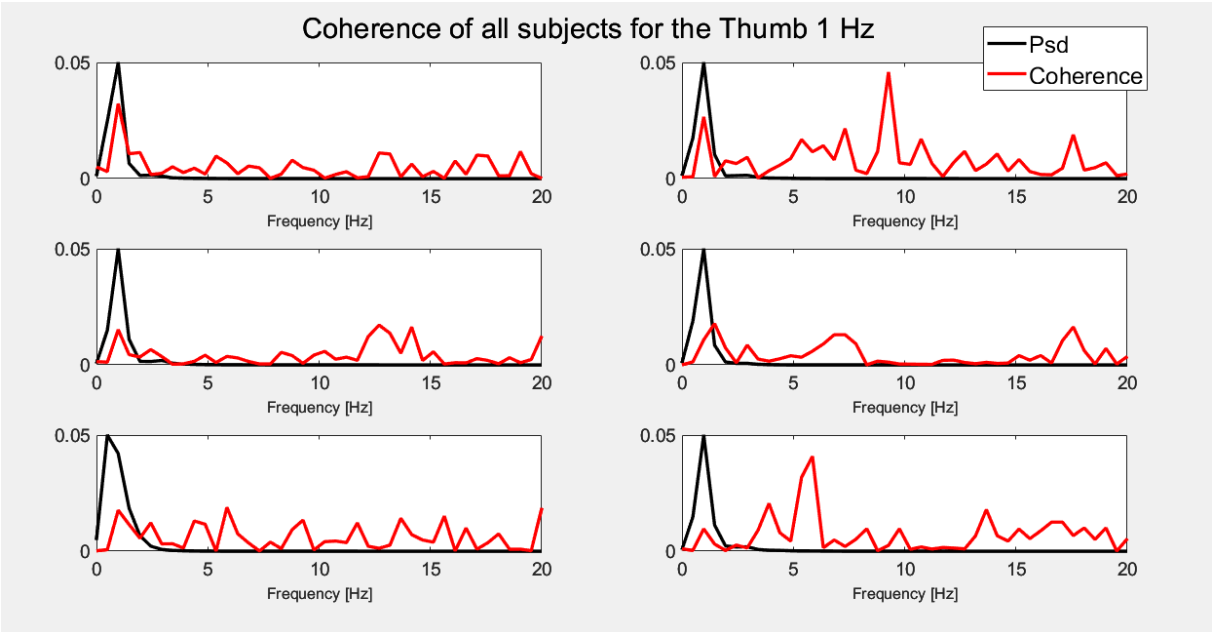

Figure 29: Coherence of the electrode with higher coherence in the movement frequency band for each subject for the Thumb flexion-extension at 1 Hz. Each plot corresponds to a different subject. Specifically, the plots are arranged in a 3×2 grid, where each row represents two subjects in order. For example, the plot in the first row, first column corresponds to Subject 1, the second column to Subject 2, and so on.

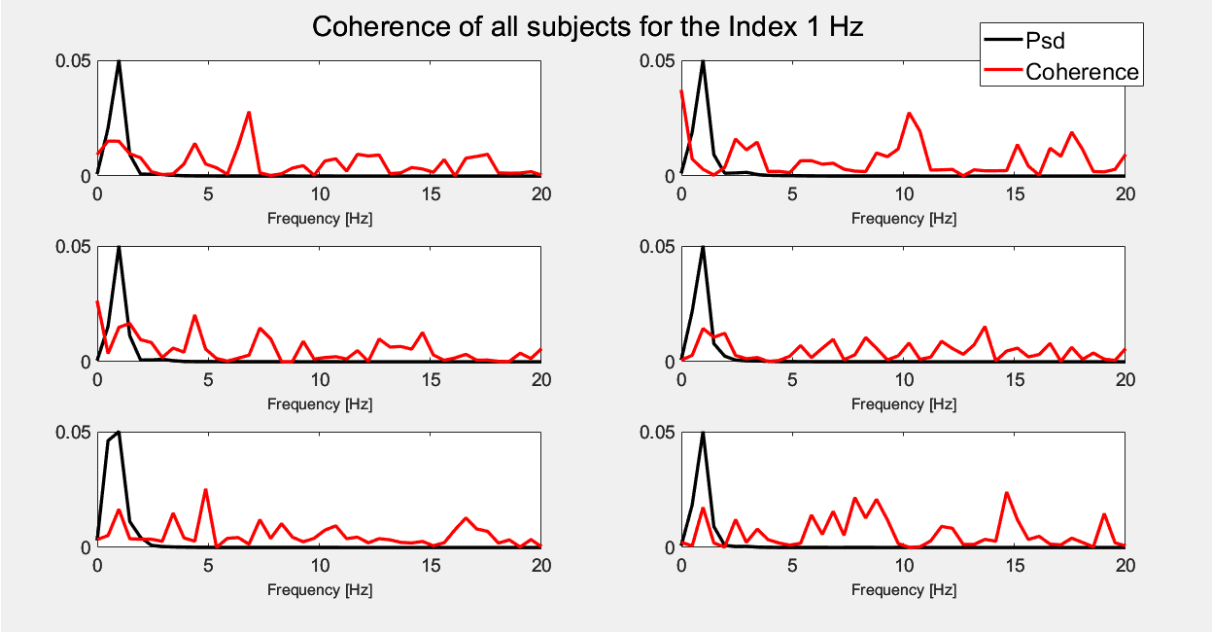

Figure 30: Coherence of the electrode with higher coherence in the movement frequency band for each subject for the Index flexion-extension at 1 Hz. Each plot corresponds to a different subject. Specifically, the plots are arranged in a 3×2 grid, where each row represents two subjects in order. For example, the plot in the first row, first column corresponds to Subject 1, the second column to Subject 2, and so on.

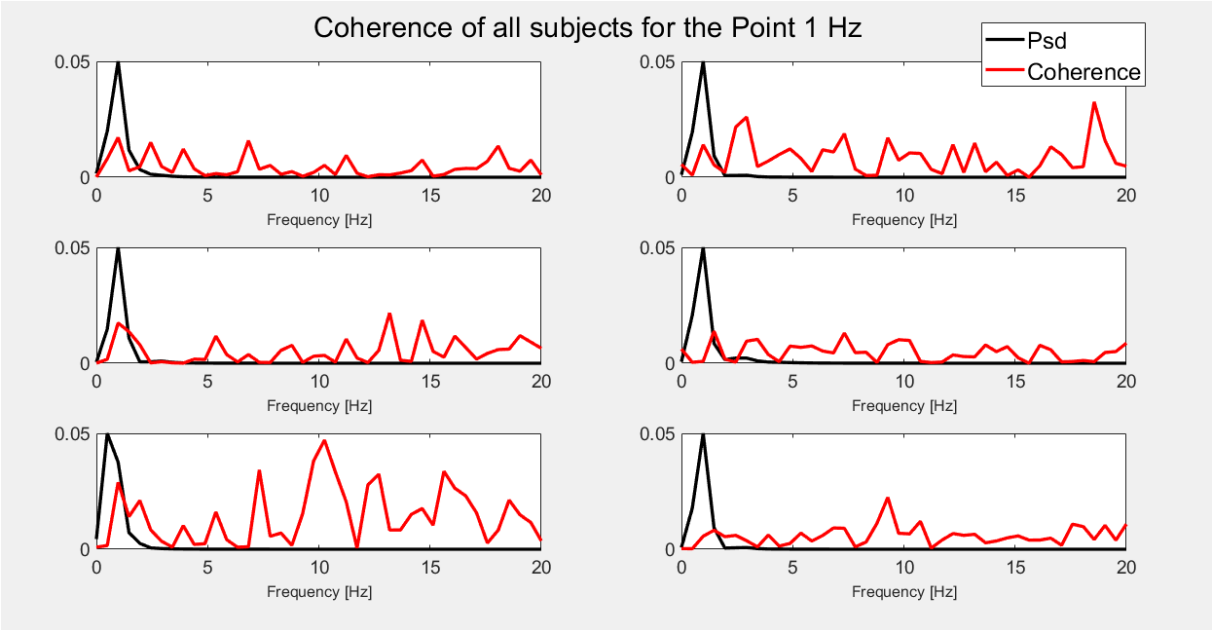

Figure 31: Coherence of the electrode with higher coherence in the movement frequency band for each subject for the Point flexion-extension at 1 Hz. Each plot corresponds to a different subject. Specifically, the plots are arranged in a 3×2 grid, where each row represents two subjects in order. For example, the plot in the first row, first column corresponds to Subject 1, the second column to Subject 2, and so on.

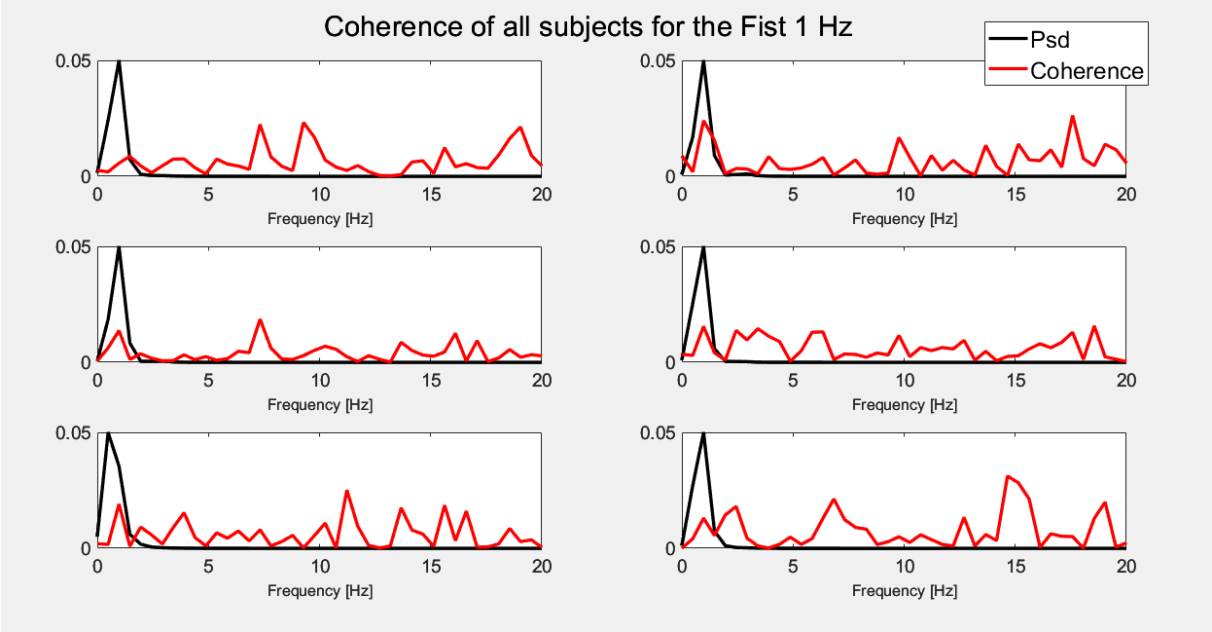

Figure 32: Coherence of the electrode with higher coherence in the movement frequency band for each subject for the Fist flexion-extension at 1 Hz. Each plot corresponds to a different subject. Specifically, the plots are arranged in a 3×2 grid, where each row represents two subjects in order. For example, the plot in the first row, first column corresponds to Subject 1, the second column to Subject 2, and so on.

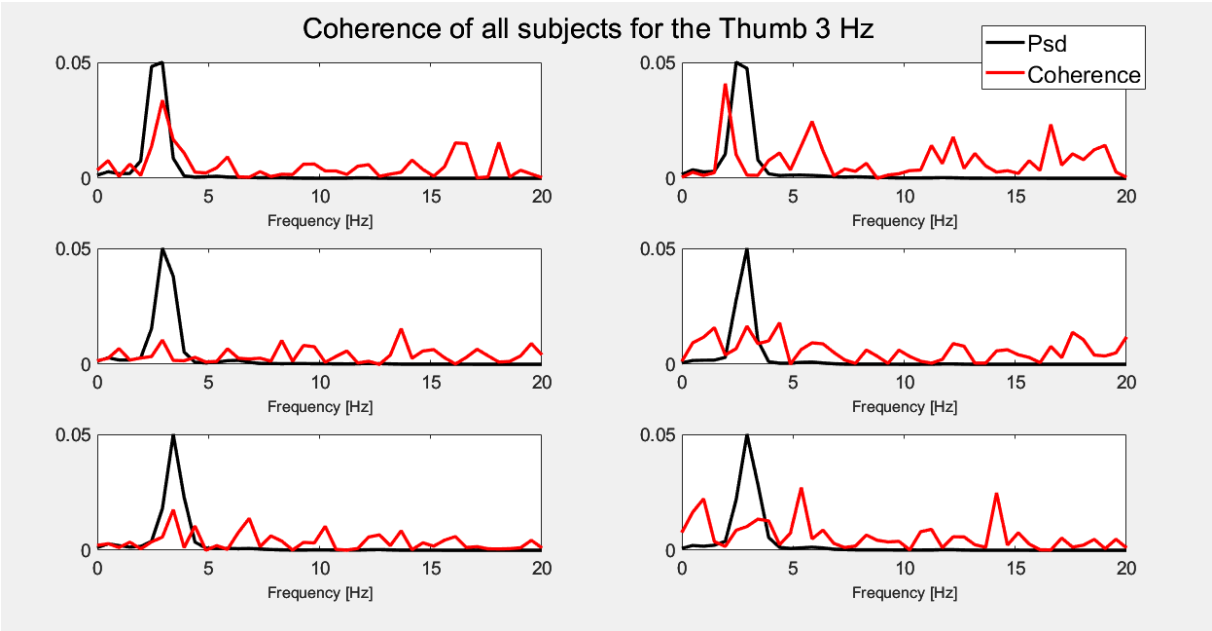

Figure 33: Coherence of the electrode with higher coherence in the movement frequency band for each subject for the Thumb flexion-extension at 3 Hz. Each plot corresponds to a different subject. Specifically, the plots are arranged in a 3×2 grid, where each row represents two subjects in order. For example, the plot in the first row, first column corresponds to Subject 1, the second column to Subject 2, and so on.

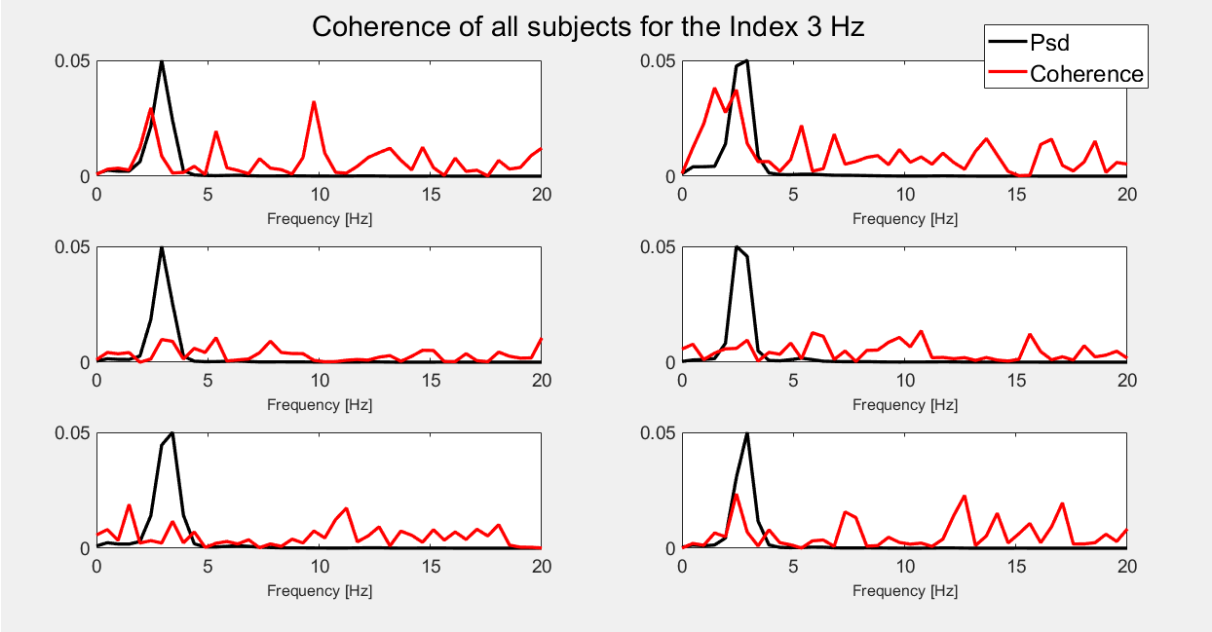

Figure 34: Coherence of the electrode with higher coherence in the movement frequency band for each subject for the Index flexion-extension at 3 Hz. Each plot corresponds to a different subject. Specifically, the plots are arranged in a 3×2 grid, where each row represents two subjects in order. For example, the plot in the first row, first column corresponds to Subject 1, the second column to Subject 2, and so on.

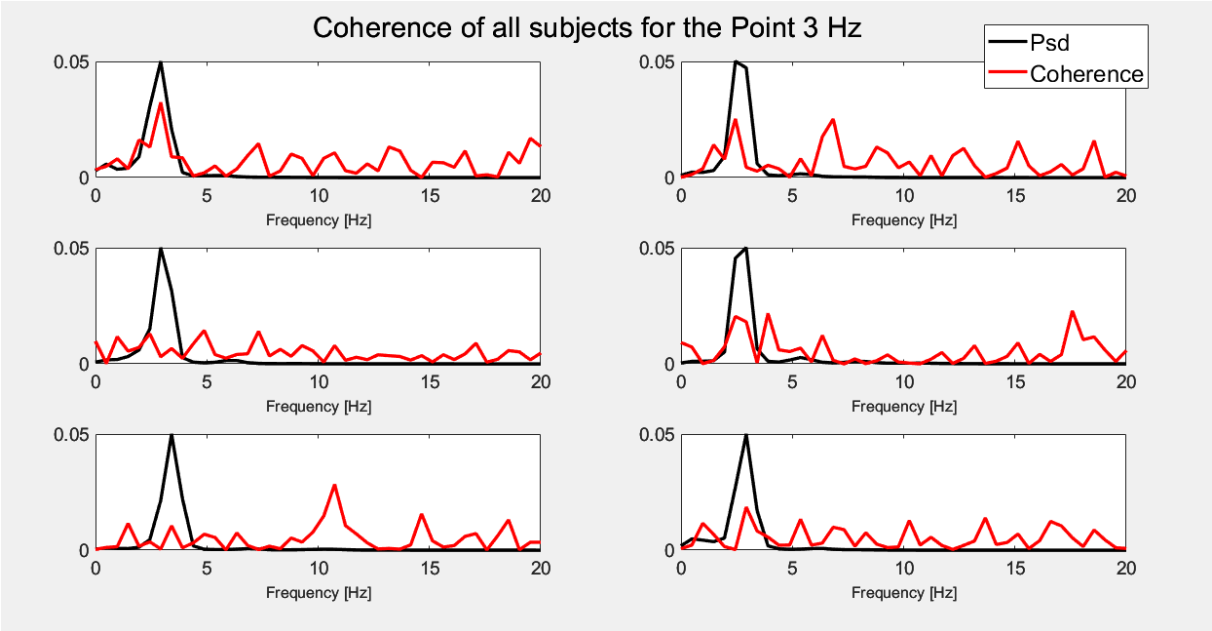

Figure 35: Coherence of the electrode with higher coherence in the movement frequency band for each subject for the Point flexion-extension at 3 Hz. Each plot corresponds to a different subject. Specifically, the plots are arranged in a 3×2 grid, where each row represents two subjects in order. For example, the plot in the first row, first column corresponds to Subject 1, the second column to Subject 2, and so on.

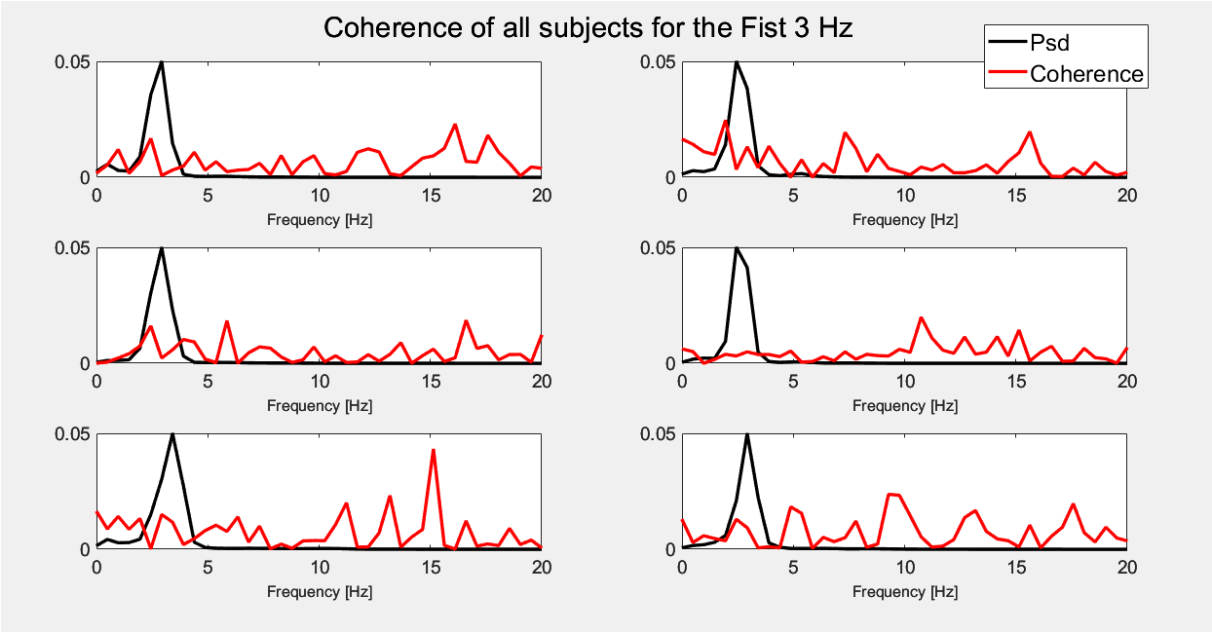

Figure 36: Coherence of the electrode with higher coherence in the movement frequency band for each subject for the Fist flexion-extension at 3 Hz. Each plot corresponds to a different subject. Specifically, the plots are arranged in a 3×2 grid, where each row represents two subjects in order. For example, the plot in the first row, first column corresponds to Subject 1, the second column to Subject 2, and so on.

It can be observed that, with the EEG signal, coherence does not always follow the expected pattern, and in some cases, the peak at the movement frequency is not clearly detectable respect to the other frequencies. This is likely due to the generally lower maximum coherence values within the movement frequency band, which prevents the peak from standing out. Indeed, looking at the Figure 37 and Figure 38, the peak coherence values within the movement band are very low compared with the previous ones of ECoG.

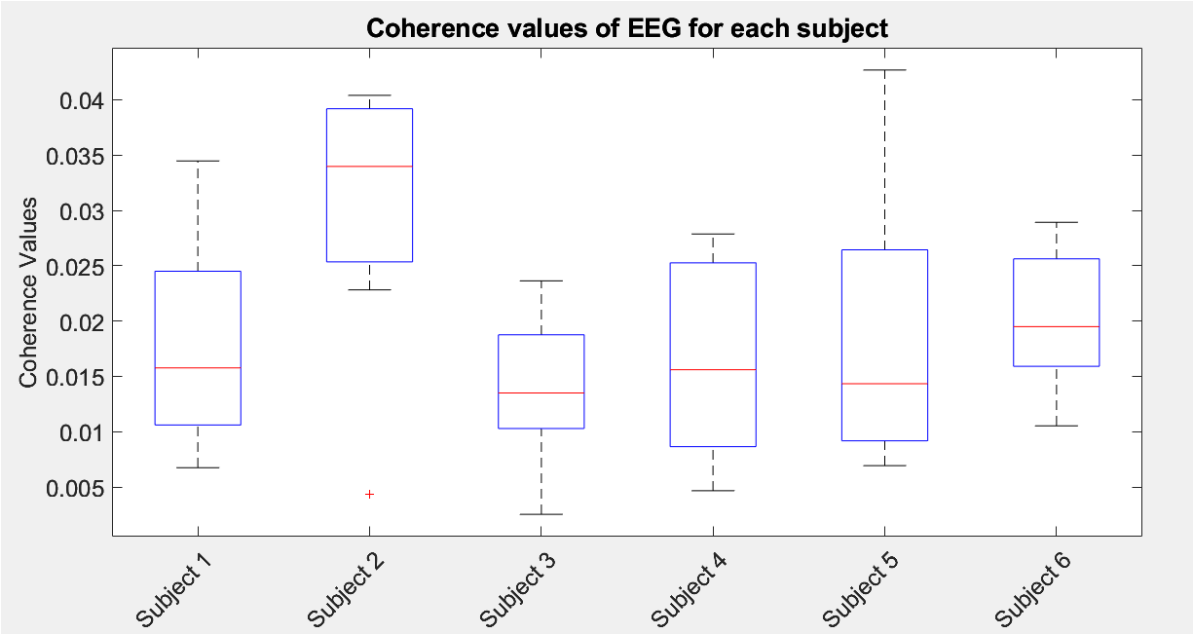

Figure 37: Coherence peak values for each subject with EEG. The coherence peak is the higher coherence value of the electrode with the higher coherence in the movement frequency band.

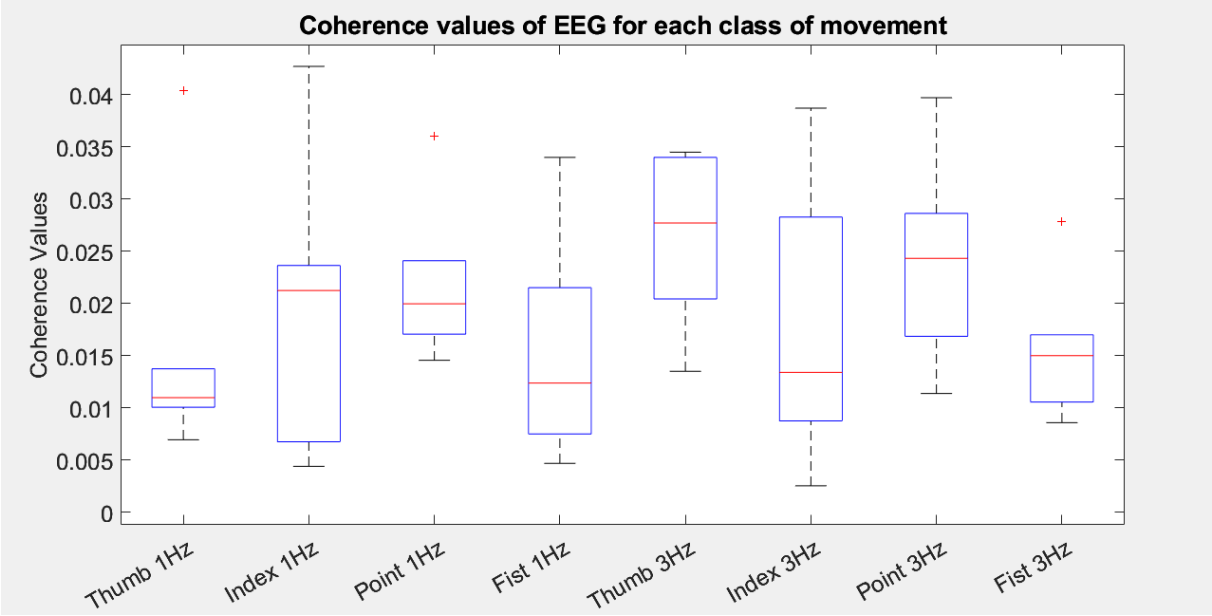

Figure 38: Coherence peak values across subjects for each movement class with EEG. The coherence peak is the higher coherence value of the electrode with the higher coherence in the movement frequency band.

Figure 38 shows that the coherence doesn't change considerably between the different subjects, apart from the Subject 2, who shows a higher coherence compared with the other subjects.

However, the values are much lower than with ECoG, with a mean value across subjects of about 0.02 and of 0.03 for Subject 2. Observing these results, an effort was made to further investigate the causes of such low values by comparing and analyzing similar studies in literature. In particular, it was expected that CKC values obtained from EEG would be lower than those measured with ECoG in this study and also lower than those reported in studies using MEG. However, the coherence in the movement band is even lower than one might have hypothesized when compared to previous EEG-based CKC studies. For instance, Piitulainen et al. (2020) [21] investigated the coherence between the Index finger acceleration during a passive flexion-extension task and the EEG. Their aim was to examine the reliability and reproducibility of CKC estimated from EEG signals using passive index finger movements, which remains uncertain. They employed a pneumatic artificial muscle to ensure precise movement frequency and found CKC values approximately half of those obtained with MEG, with a mean coherence of 0.10 for the dominant hand using a CAR reference (as in our case). Notably, they demonstrated that coherence improved with different referencing methods, reaching mean values of 0.19 and 0.22 using Bipolar and Laplacian references, respectively. Based on these findings, an attempt was made to enhance coherence values by applying Bipolar and Laplacian references. However, this did not lead to any improvement, which is why these attempts are not reported in this thesis. A further comparison can be drawn with the study conducted by Giangrande et al. (2024) [29], which evaluated CKC using ankle kinematics. Similar to the previous study [21], ankle-joint rotations at 2-Hz were induced via a movement actuator. They examined two conditions: one in which subjects kept their foot completely relaxed, resulting in a mean coherence of 0.03, and another where a constant 5-Nm plantar flexion was exerted during movement, which improved coherence to a mean value of 0.13. Finally, Wei et al. [30] analysed CKC during active rhythmic flexion-extension with the index and middle fingers following three task frequencies (0.7 Hz/1.7 Hz/2.5 Hz). They investigated the MotionWithAudio condition, in which a metronome was used to guide the movement

rhythm, and the MotionOnly condition, where the metronome was played only during the first 5 seconds of each 25 seconds trial. In both conditions, peaks at the movement frequency and its harmonics were detectable.

I sought to understand the reasons behind the differences between these studies and the present work, particularly by examining the experimental conditions and the dynamics influencing CKC. The most evident distinction from the first two cited studies [21] [29] is that they employed passive movements controlled by actuators, whereas in this work the movement was active. However, this should not significantly affect coherence, as Piitulainen et al. (2013) [26] demonstrated in a CKC study using MEG. The use of an actuator instead of voluntary movement serves a key purpose: ensuring a perfectly constant movement frequency. A similar goal was pursued in the third study [30] using the metronome, particularly in the MotionWithAudio condition but also in the MotionOnly condition, where the metronome was played only during the first 5 seconds of each trial. While this likely resulted in a movement frequency that was less stable than in the passive movement condition, it was still more consistent than in this work. This consistency in movement frequency is likely the primary factor contributing to the lower coherence values observed. This is reasonable, considering that the coherence formula includes the cross-spectral density of the two signals at each frequency divided by the product of their auto-spectral densities Equation 1. As a result, the ratio between the spectral power at the frequency of interest and the total spectral power (for both signals) is a key determinant of coherence at that frequency. Notably, even in the ECoG data, movement frequency was not perfectly constant due to the self-paced nature of the task. However, the stronger cortical signals provided by ECoG may have mitigated the effects of movement irregularity, as ECoG more directly reflects the activity of the specific motor cortex region involved in the task, which is the one expected to follow the motor movements and, consequently, provide high coherence. In fact, it is widely known that signal-to-noise ratio

of ECoG is superior compared to EEG [59]. In addition to the issue just discussed, signals may not generally have a high signal-to-noise ratio, impacting on the coherence values obtained. All these hypotheses on the causes of the results were also confirmed by Professor Piitulainen, author of most of the studies in the literature on CKC (cited in Section 1.6).

Also in this case, the topographic maps based on the coherence peaks within the movement band of each channel were examined for each subject and movement class. While EEG electrode localization followed the 10-10 system precisely (as in Figure 10), this time it was possible to generate average maps. Specifically, average topographic maps were obtained for each subject, averaging across all subjects (Figure 39), for each movement class, averaging across movement fingers (Figure 40), and a final map representing the mean CKC across all subjects and movements (Figure 41). As before, the coherence of each channel is the peak coherence within the movement band.

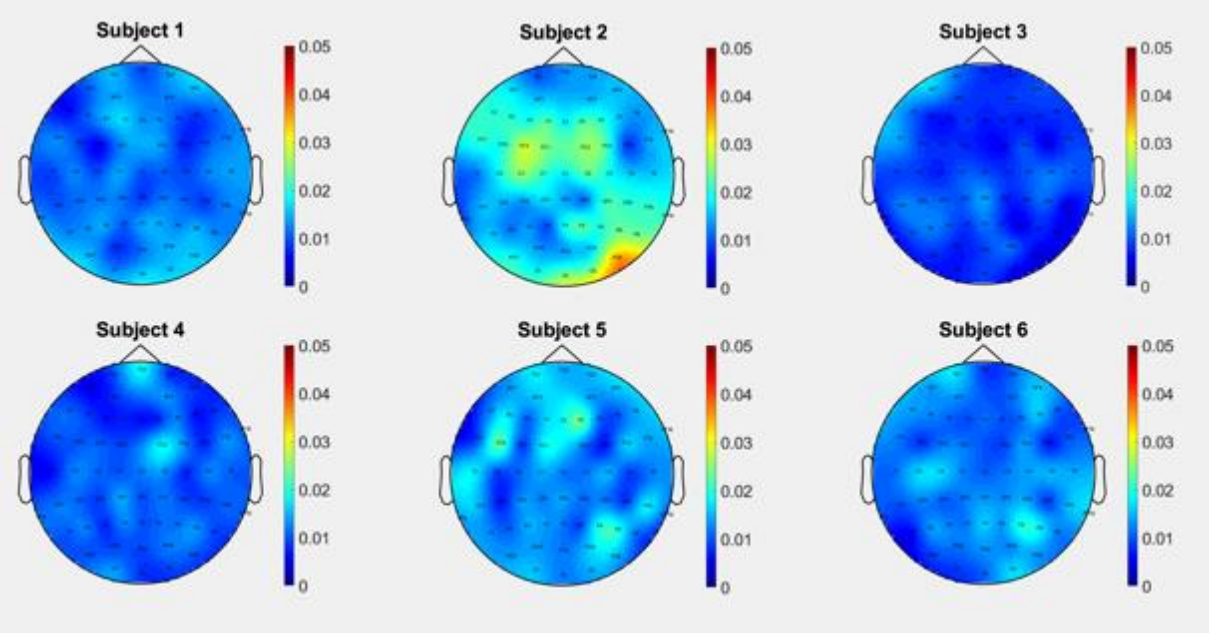

Figure 39: Coherence topographic maps of the EEG for each subject. Each electrode shows the mean coherence across all movement classes of the subject in the movement band. Each plot corresponds to a different subject.

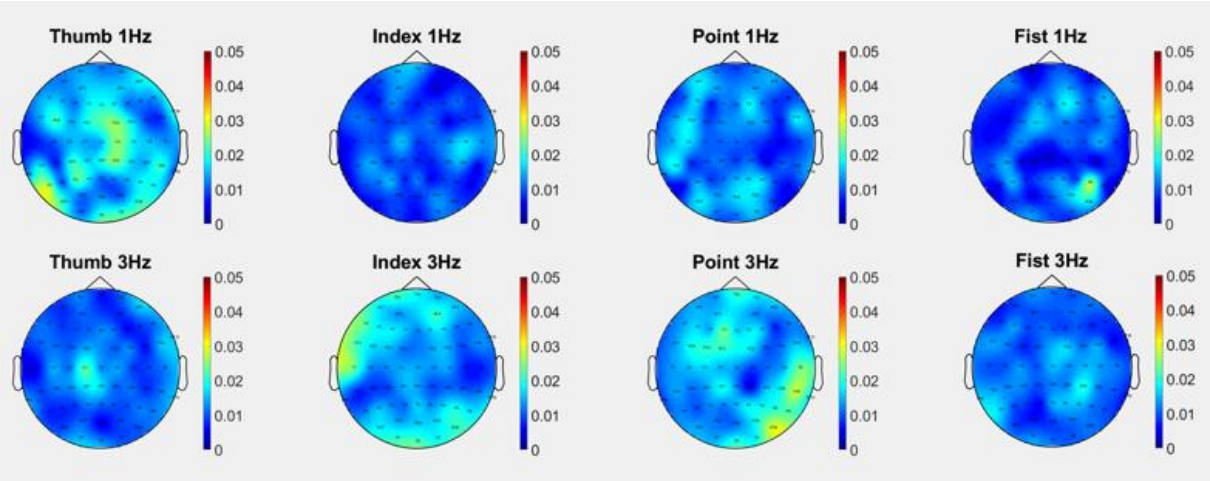

Figure 40: Coherence topographic maps of the EEG for each movement class. Each electrode shows the mean coherence across all subjects of the movement class in the movement band. Each plot corresponds to a different movement class.

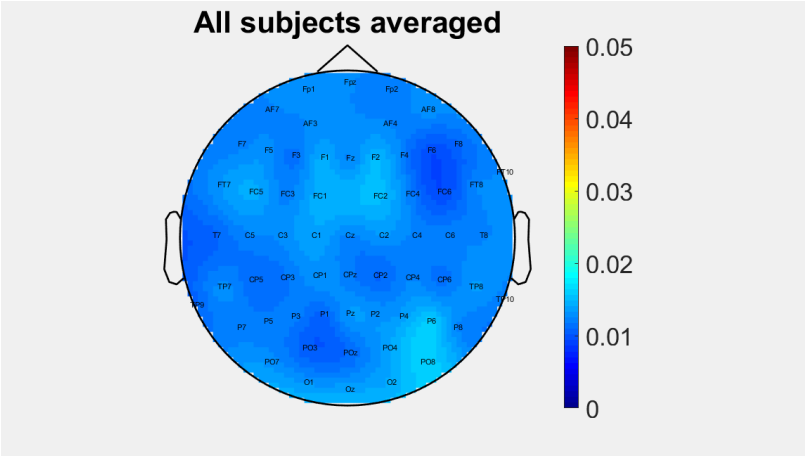

Figure 41: Coherence topographic map of the EEG averaged across all subjects and movement class.

As expected, given the low coherence values, the topographic maps generally do not show a clear increase in coherence over the contralateral sensorimotor cortex, often lacking distinguishable spatial patterns. This region should be primarily responsible for finger movement, as cited before [58] and as observed in the ECoG topographic maps (Figure 24 for

example). If the coherence results had been more consistent, a more physiologically plausible distribution would likely have emerged, as in the ECoG case. Instead, the observed patterns appear more random. This is reasonable, as having relatively low coherence peaks, the values of the contralateral motor cortex area are covered by other channels. Among the topographic maps of different subjects (Figure 39), none exhibit a clear physiological distribution. However, Subject 2, who had the highest coherence values, shows relatively higher coherence near the left motor cortex compared to other channels, even if with elevated values in unrelated areas as well. Similarly, Subjects 5 and 6 present slightly higher coherence near the expected region, though their distributions remain suboptimal. When considering the topographic maps averaged across different movement classes, the spatial patterns remain usually unclear, except for the 'Thumb 3 Hz' movement, which exhibits the physiological distribution.

4.2 Decoding results and discussions

4.2.1 Multiple Linear Regression results with LMPs

Below are the decoding results obtained with the Multiple Linear Regression using LMPs. By 'results', we mean the Pearson correlation between the original and predicted trajectories, metric used to evaluate the goodness of the decoding, as discussed in Section 3.5. Each boxplot below includes the correlation values between the predicted and actual trajectory of all fingers of a subject, each obtained as the average of the correlations across 3 folds of the corresponding finger and subject.

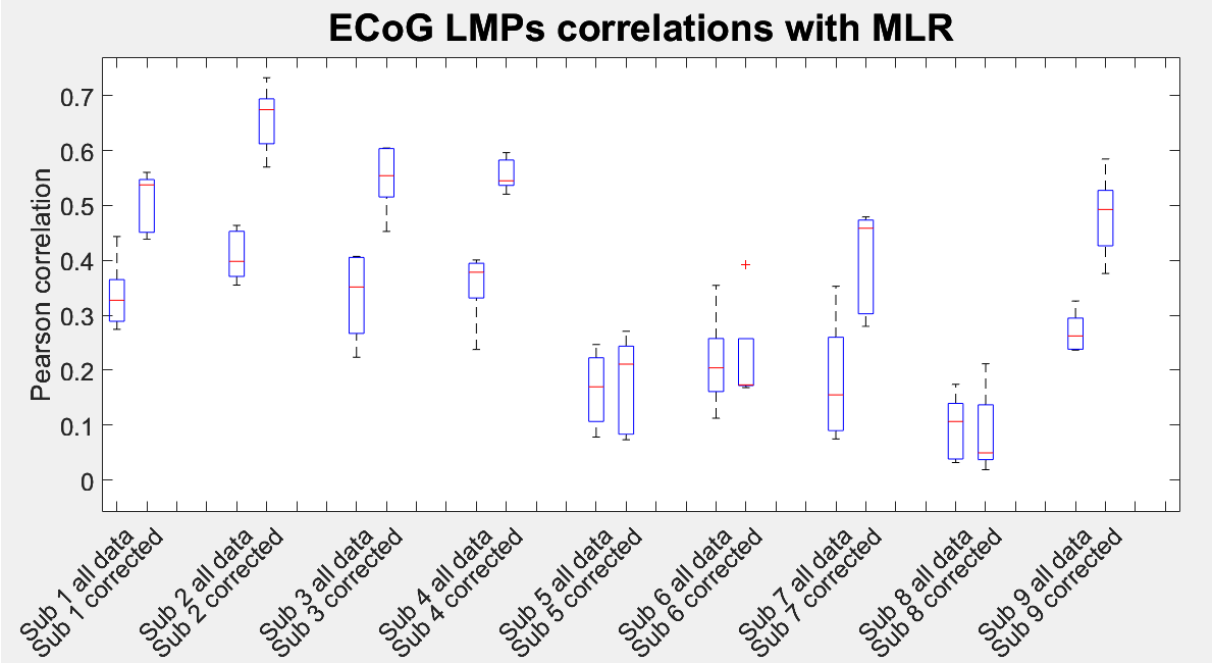

Figure 42: Results of the decoding of ECoG LMPs using the MLR. Each boxplot includes the correlations between the predicted and actual trajectory of all fingers of a subject. For each subject, the boxplot 'all data' refers to the results of the model the trained with the entire trajectories, while 'corrected' refers to the models trained with trajectories without the movement intervals of other fingers.

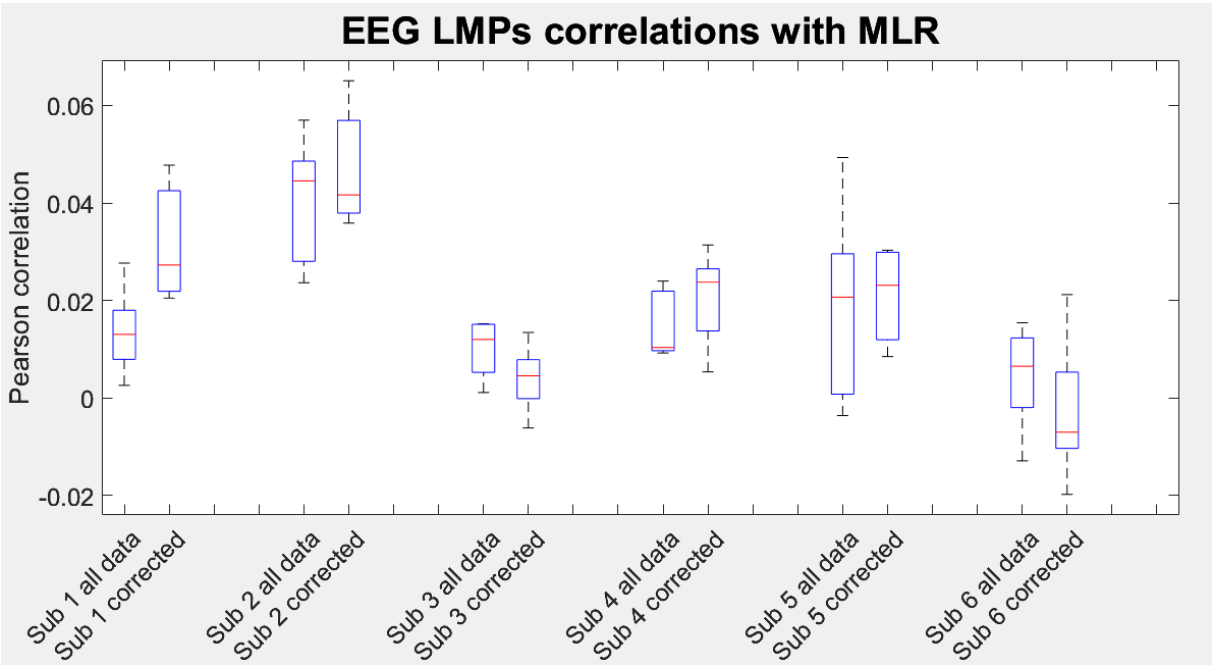

Figure 43: Results of the decoding of EEG LMPs using the MLR. Each boxplot includes the correlations between the predicted and actual trajectory of all fingers of a subject. For each subject, the boxplot 'all data' refers to the results of the model trained with the entire trajectories, while 'corrected' refers to the models trained with trajectories without the movement intervals of other fingers.

Figure 42 shows the results obtained with the ECoG dataset, while Figure 43 refers to the decoding with EEG. For each subject, the boxplot 'all data' refers to the results of the model trained with the entire trajectories, while 'corrected' refers to the models trained with trajectories without the movement intervals of other fingers (as detailed in Section 3.5). Notably, the performance was consistently better with corrected data, again as already discussed in Section 3.5. For ECoG, good performance was achieved, with a median correlation of 0.46 across subjects. In contrast, EEG yielded poor results, with a median correlation of 0.02. It is interesting to note that these decoding results exhibit a similar ranking of subjects as observed in the coherence analysis. Specifically, the subjects who performed better or worse in terms of coherence values tend to show comparable performance trends in decoding correlation. This consistency suggests a potential relationship between coherence measures and decoding performance, reinforcing the findings discussed earlier. This can be observed by comparing Figure 42 and Figure 43 with Figure 22 and Figure 37 respectively, which show coherence results for each subject. In particular, with ECoG, Subject 2 is the best-performing participant, with correlations ranging between 0.57 and 0.73 across fingers, while with EEG the best performance was obtained with EEG dataset Subject 2, exhibiting correlations between - 0.02 and 0.07.

The permutation test, discussed in Section 3.5.2, was performed only for EEG Subject 2, the best performing participant, to assess whether his decoding performance was above chance level. For the other subjects, the performance was so low that conducting the test would not have been meaningful. Results were often above chance level, indicating that the MLR model still captured some meaningful information in its predictions from EEG LMPs, but the p-value was equal to 0.23, indicating that this result do not have statistical significance.

As previously discussed, a relationship was observed between the CKC analysis results across subjects and their respective decoding performance. To further investigate this relationship, a linear fit was performed between the decoding results (correlations) obtained for each channel in a decoding attempt using a single channel as input and the corresponding coherence values for each of these channels. This linear fit is shown in Figure 44, which clearly illustrates a strong linear relationship between coherence and decoding performance. This finding is further supported by a p-value of 0.00 and a correlation coefficient of 0.72 between the two variables, confirming the statistical significance of this relationship.

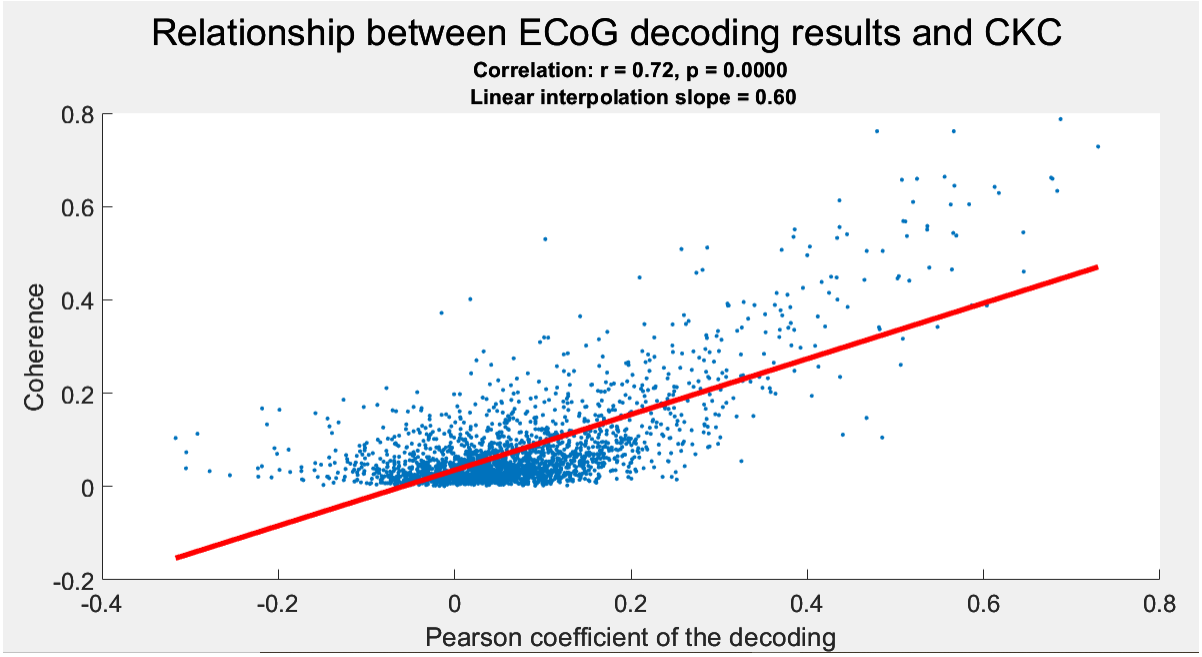

Figure 44: Linear relationship between the results of the MLR using just one channel with LMPs of ECoG, and the correspondent CKC values of the channels.

This provides a quantitative and statistical confirmation of the previously discussed observation that higher CKC values are associated with better decoding performance. However, this analysis does not explain the underlying causes of this relationship or whether one variable directly influences the other. The observed linear relationship could simply result from the fact

that higher-quality LMPs signals lead to both stronger CKC and more accurate decoding. The causality between these variables is challenging to interpret, as multiple factors may contribute to their relationship. For instance, previous studies [28] suggest that CKC is primarily driven by proprioceptive feedback rather than direct motor-related cortical activity.

The correlation between the original and predicted trajectories was then calculated by considering only the finger movement intervals, aiming to investigate how well the model specifically tracks the movement.

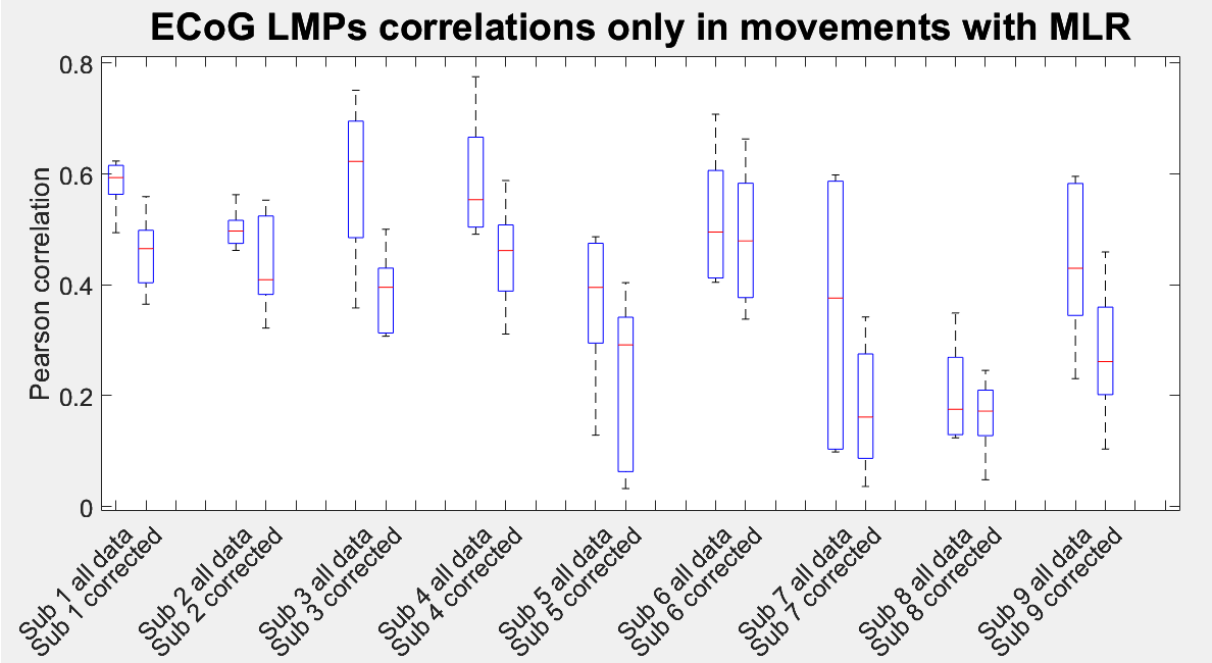

Figure 45: Results of the decoding of ECoG LMPs using the MLR only in the movement intervals. Each boxplot includes the correlations between the predicted and actual trajectory of all fingers of a subject calculated by considering only the finger movement intervals. For each subject, the boxplot 'all data' refers to the results of the model trained with the entire trajectories, while 'corrected' refers to the models trained with trajectories without the movement intervals of other fingers.

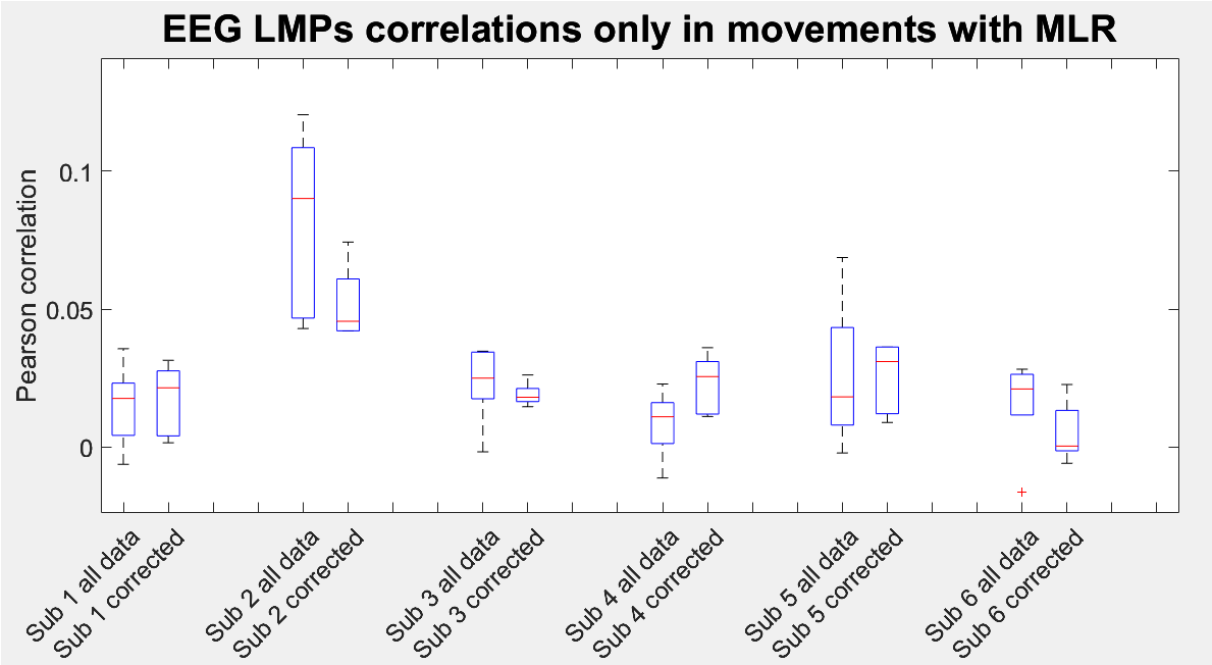

Figure 46: Results of the decoding of EEG LMPs using the MLR only in the movement intervals. Each boxplot includes the correlations between the predicted and actual trajectory of all fingers of a subject calculated by considering only the finger movement intervals. For each subject, the boxplot 'all data' refers to the results of the model trained with the entire trajectories, while 'corrected' refers to the models trained with trajectories without the movement intervals of other fingers.

Figure 45 and Figure 46 show the results of the decoding only in the movement intervals respectively for ECoG and EEG. Again, for each subject, there are two boxplots: one representing the results of the model trained with all data and the other for the model trained without the movement of other fingers. It is important to note that these results come from the same models trained in these two ways; the only difference compared to the previous two figures is the portion of the trajectories considered for the correlation calculation. Figure 45 shows that ECoG performance is consistently better for 'all data' models respect to the results of 'all data' considering the whole trajectory in the correlation in Figure 42, with an improvement of about 0.15 - 0.20 in correlation. Unexpectedly, the models trained with 'corrected' data performed worse than those considering also no-movement intervals (Figure 42). Additionally, their performance was lower than the correlations of the 'all data' models when calculated only within the movement intervals (boxplots 'all data' of Figure 45). Also for

EEG, results improved in this case, considering only movement intervals, while the performance remained quite similar between the 'all data' and 'corrected data' conditions.

Overall, these findings suggest that MLR with LMPs is more effective in tracking ongoing movements (as indicated by the correlation calculated including no-movement portions) than in precisely distinguish movement events from rest (as reflected in the correlation computed only within movement intervals). These results align with previous findings reported in the literature [18] [19].

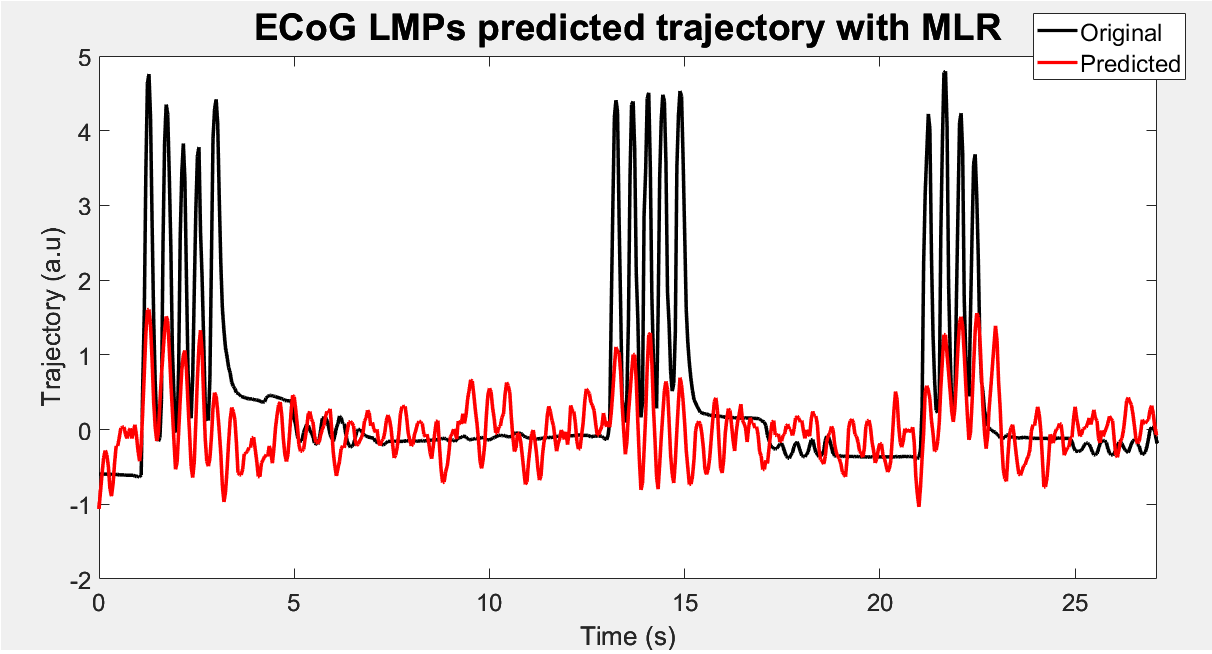

Figure 47: Example of reconstructed trajectory with MLR from ECoG LMPs.

Figure 47 shows an example of a trajectory predicted using MLR from ECoG data. This example is provided to show one of the best cases obtained with this model. As previously discussed, it can be observed that the predicted trajectory follows the movement phases relatively well, while it struggles to remain stable during the no-movement intervals.

4.2.2 Temporal Convolutional Network results with LMPs

Below are the results of the decoding performed using the TCN model with LMPs signals as input. Again, the results are also shown for both version of data for each subject in Figure 48 for ECoG, and in Figure 50 for EEG, while Figure 49 and Figure 51 show a comparison between MLR and TCN results for each subject considering only the 'corrected' version, respectively for ECoG and EEG data.

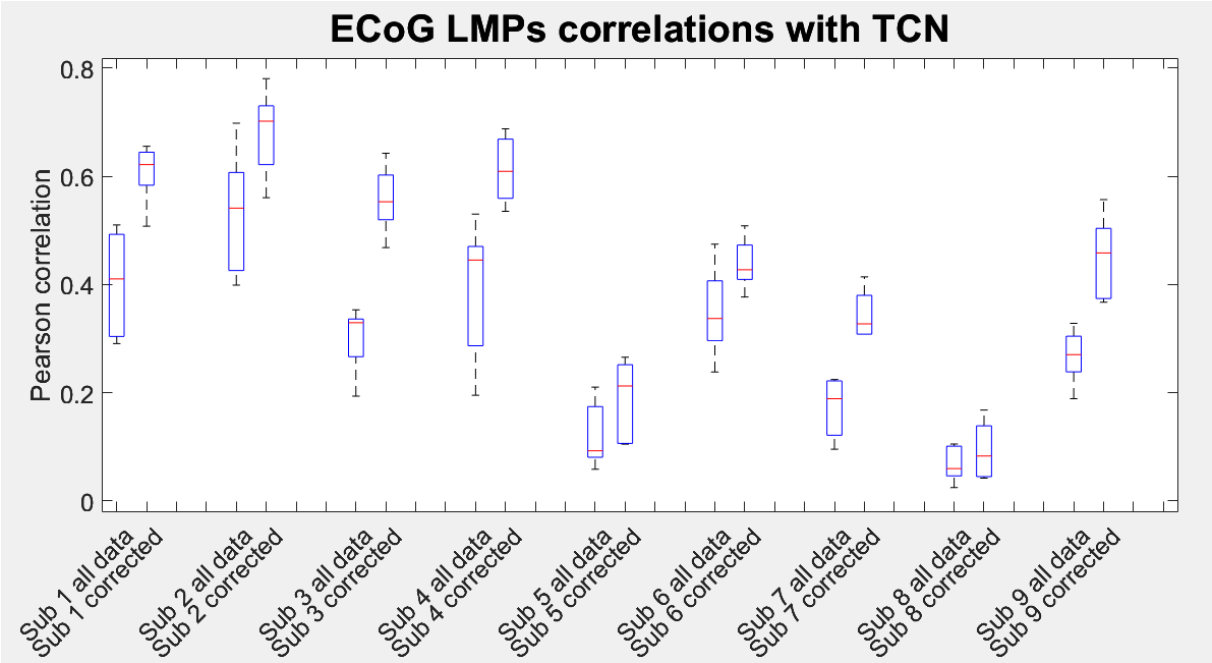

Figure 48: Results of the decoding of ECoG LMPs using the TCN. Each boxplot includes the correlations between the predicted and actual trajectory of all fingers of a subject. For each subject, the boxplot 'all data' refers to the results of the model the trained with the entire trajectories, while 'corrected' refers to the models trained with trajectories without the movement intervals of other fingers.

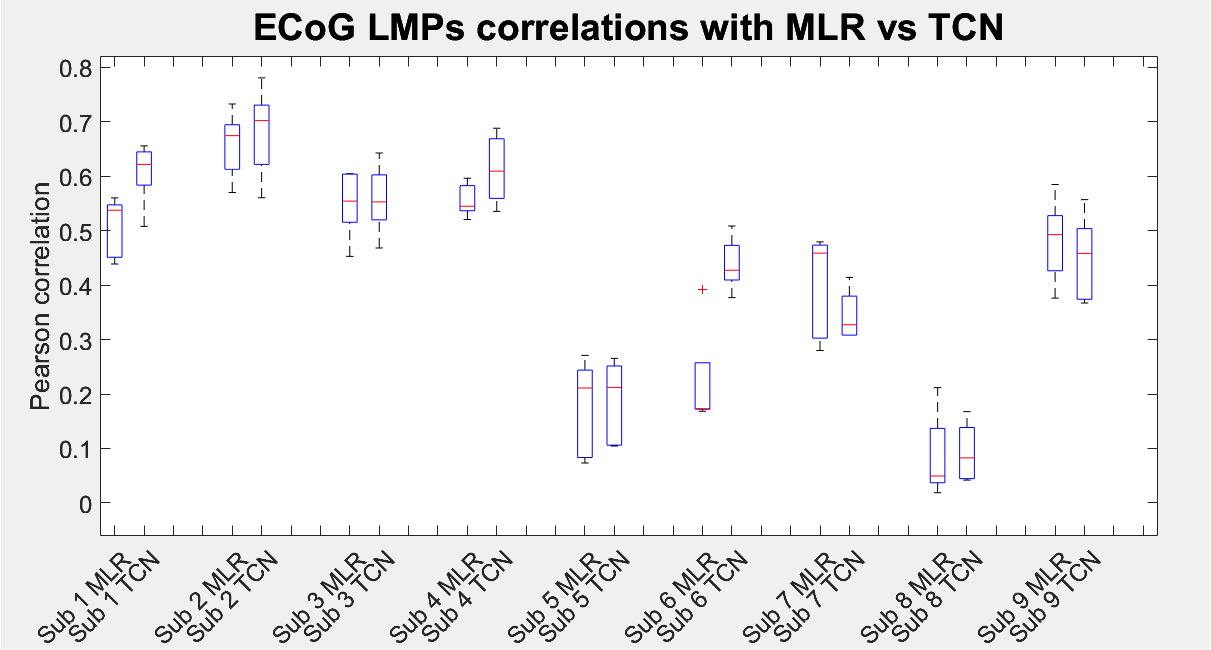

Figure 49: Comparison of decoding performances of ECoG LMPs using the MLR or TCN. Each boxplot includes the correlations between the predicted and actual trajectory of all fingers of a subject for the 'corrected' version (models trained with trajectories without the movement intervals of other fingers).

An improvement in decoding performance using the TCN can be observed, as highlighted in Figure 49. In particular, considering all subjects in the 'corrected' condition, the MLR model achieved a median correlation of 0.46, with a range from 0.02 to 0.73, whereas the TCN model slightly improved the performance, reaching a median correlation of 0.47, ranging from 0.04 to 0.78. To compare the different models more effectively, it is more informative to focus on the best-performing subject (who is the same across models). When considering all subjects, the overall performance is heavily influenced by the lowest-performing cases, which tend to mask the differences between models. For this reason, from this point forward, comparisons will be made based on the best-performing subject for each dataset (ECoG and EEG). For completeness, at the end of this section, a summary is included in Table 4, reporting the results for all subjects, alongside a separate table specifically for the best-performing subject in both datasets (Table 5). In this case, with the TCN model, Subject 2 (the best performer) achieved a median correlation of 0.70, with a range from 0.56 to 0.78, whereas with MLR, the median was

0.67, ranging from 0.57 to 0.73. Overall, TCN provided a slight improvement for ECoG LMPs, even if not particularly substantial.

The same boxplots are shown below for EEG LMPs with TCN.

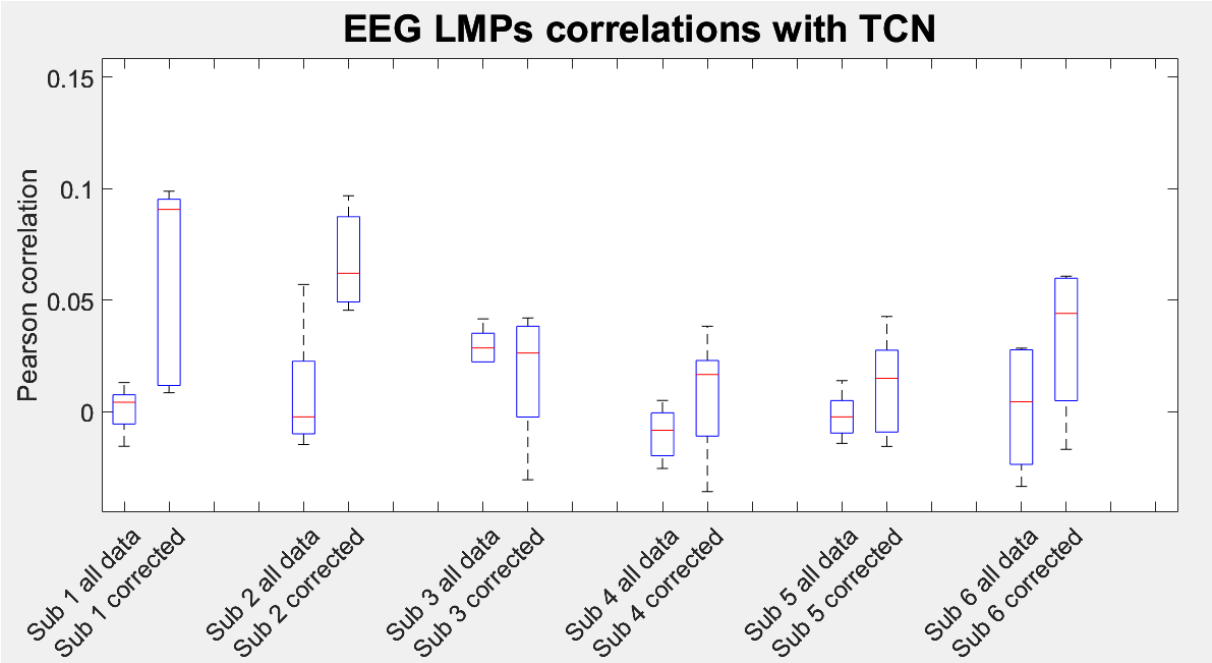

Figure 50: Results of the decoding of EEG LMPs using the TCN. Each boxplot includes the correlations between the predicted and actual trajectory of all fingers of a subject. For each subject, the boxplot 'all data' refers to the results of the model the trained with the entire trajectories, while 'corrected' refers to the models trained with trajectories without the movement intervals of other fingers.

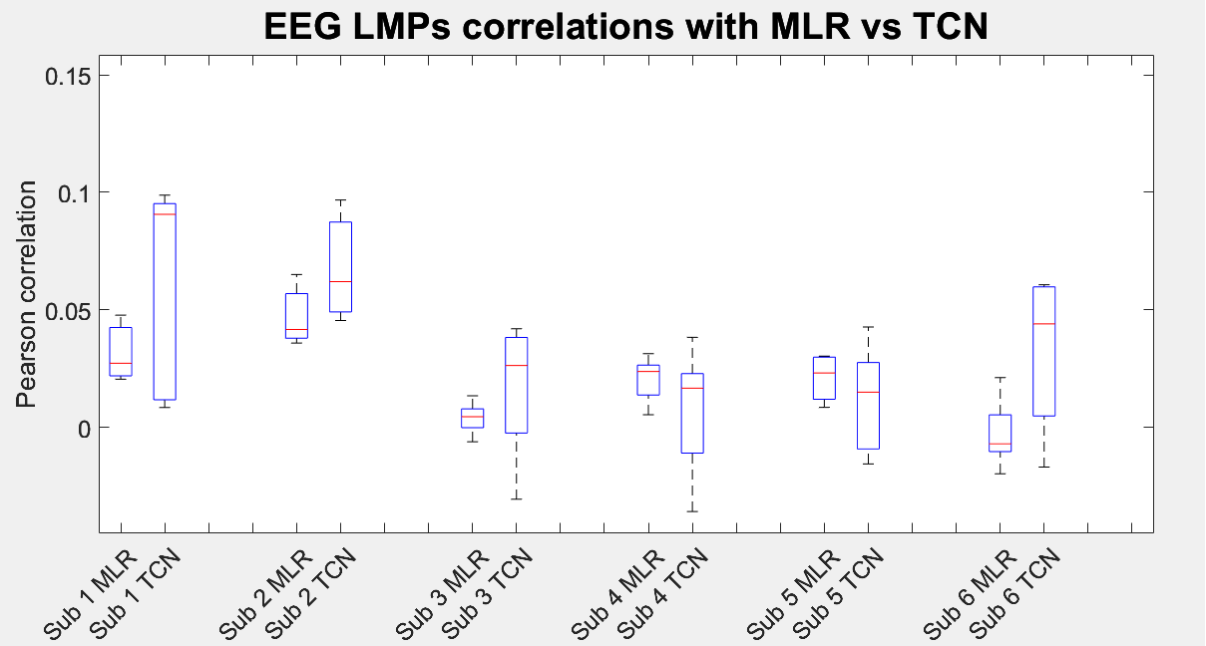

Figure 51: Comparison of decoding performances of EEG LMPs using the MLR or TCN. Each boxplot includes the correlations between the predicted and actual trajectory of all fingers of a subject for the 'corrected' version (models trained with trajectories without the movement intervals of other fingers).

Observing the results for EEG LMPs, a slight improvement with the TCN model compared to MLR can also be noticed in Figure 51. However, despite this minor enhancement, the correlation values between predicted and original trajectories remain very low, with a median correlation of 0.06 and a range from 0.05 to 0.10 for the best-performing subject 'corrected' data (Table 5). Due to these low decoding performances, it was then decided to further investigate the use of brain signals that also included higher frequency bands, as previously discussed in Section 3.5, attempting to achieve better results.

4.2.3 Results with full-band signals

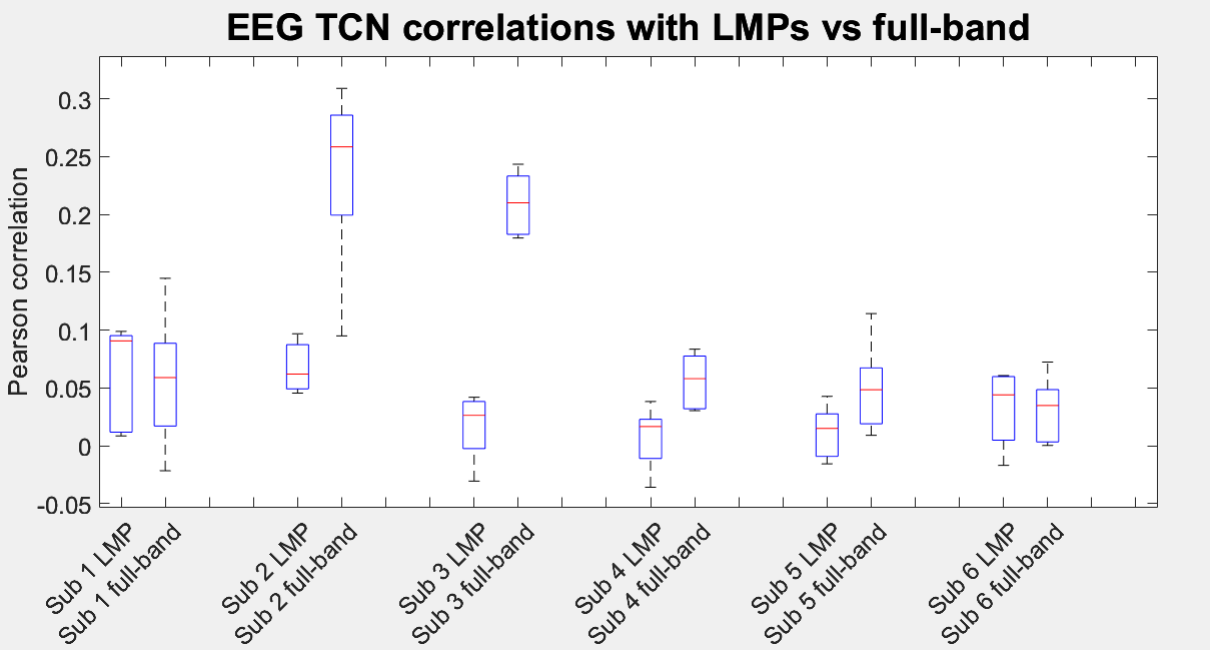

Figure 52: Comparison of decoding performances of EEG using LMPs or full-band signals with TCN. Each boxplot includes the correlations between the predicted and actual trajectory of all fingers of a subject for the 'corrected' version (models trained with trajectories without the movement intervals of other fingers).

Figure 52 shows the results obtained using EEG signals that included frequencies up to 40 Hz as input to the TCN model, compared to the results obtained using EEG LMPs with the same model (both from 'corrected' trajectories). A clear improvement in performance can be observed, particularly for Subject 2 (the best-performing subject) and Subject 3. The correlation with the original trajectories reaches a median value of 0.24, ranging from 0.08 to 0.31 of the best-performing subject (Table 5).

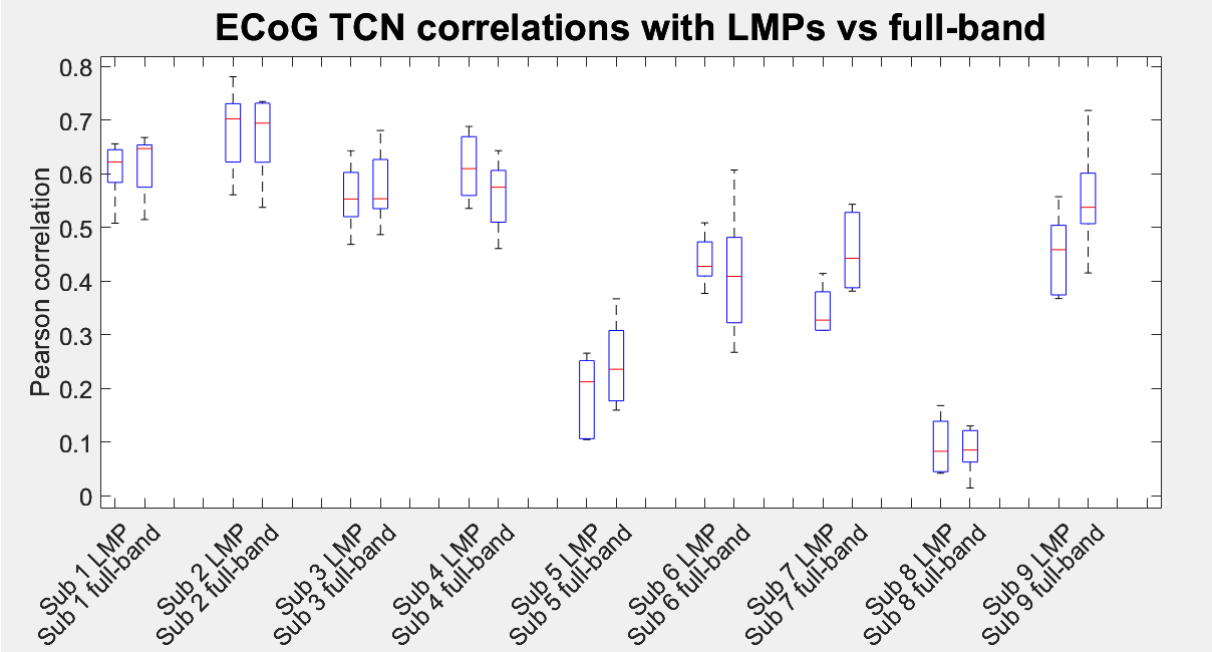

Figure 53: Comparison of decoding performances of ECoG using LMPs or full-band signals with TCN. Each boxplot includes the correlations between the predicted and actual trajectory of all fingers of a subject for the 'corrected' version (models trained with trajectories without the movement intervals of other fingers).

Figure 53 presents the same comparison as the previous one, but for ECoG signals. In this case, while using full-band signals led to an improvement over LMPs, the difference was not as substantial as with EEG.

These results suggest that, in the case of ECoG signals, where we already observed strong CKC and good decoding performance using LMPs, retaining the entire signal bandwidth does not provide additional useful informations to the decoder. Conversely, for EEG signals, LMPs appeared to be less informative, as they resulted in poor performance both in terms of CKC at the movement-related frequencies (1 Hz and 3 Hz, which fall within the LMPs range) and in terms of trajectory decoding. The significant improvement obtained using full-band EEG signals with the TCN model suggests that a deep learning model like TCN is capable of extracting relevant information from these signals that was not accessible when using only LMPs. In particular, these additional features led to a notable performance increase, indicating that when LMPs are unclear or less informative (as in our case with EEG), incorporating a TCN

with full-band signals can enhance decoding. On the other hand, when LMPs are more distinct and interpretable (as seen with ECoG), they contain the most relevant frequency band for decoding, and adding higher frequencies does not further improve trajectory reconstruction.

The decoding process was also repeated using MLR with full-band signals, even though these signals were originally intended for the TCN model. This is because feeding raw signals directly into a Deep Learning model like TCN is more common, whereas with a simpler model like MLR, a prior feature extraction step is typically performed. This attempt was made only to confirm that including additional frequency bands in the input signals does not inherently improve decoding performance. This hypothesis is supported by results in Figure 54 (for ECoG) and Figure 55 (for EEG), which show that MLR did not benefit from the full-band signals. These results further confirm that LMPs are an effective feature for decoding and that adding higher frequency bands only makes the signals less interpretable for MLR, without providing additional useful information.

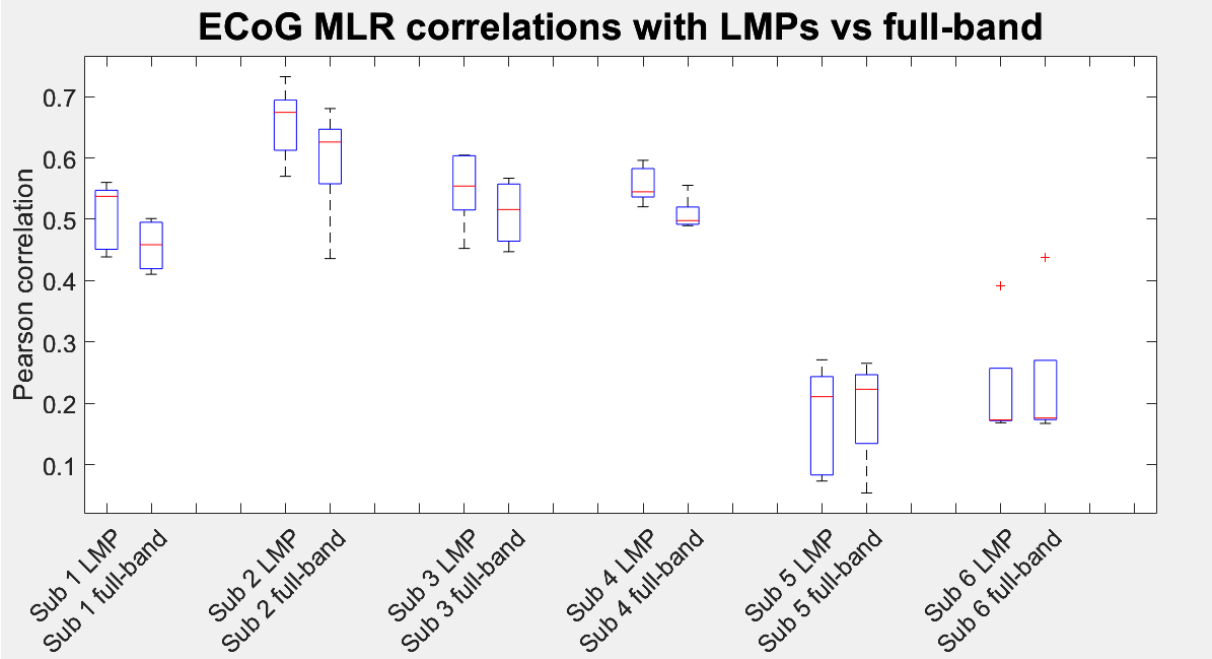

Figure 55: Comparison of decoding performances of EEG using LMPs or full-band signals with MLR. Each boxplot includes the correlations between the predicted and actual trajectory of all fingers of a subject for the 'corrected' version (models trained with trajectories without the movement intervals of other fingers).

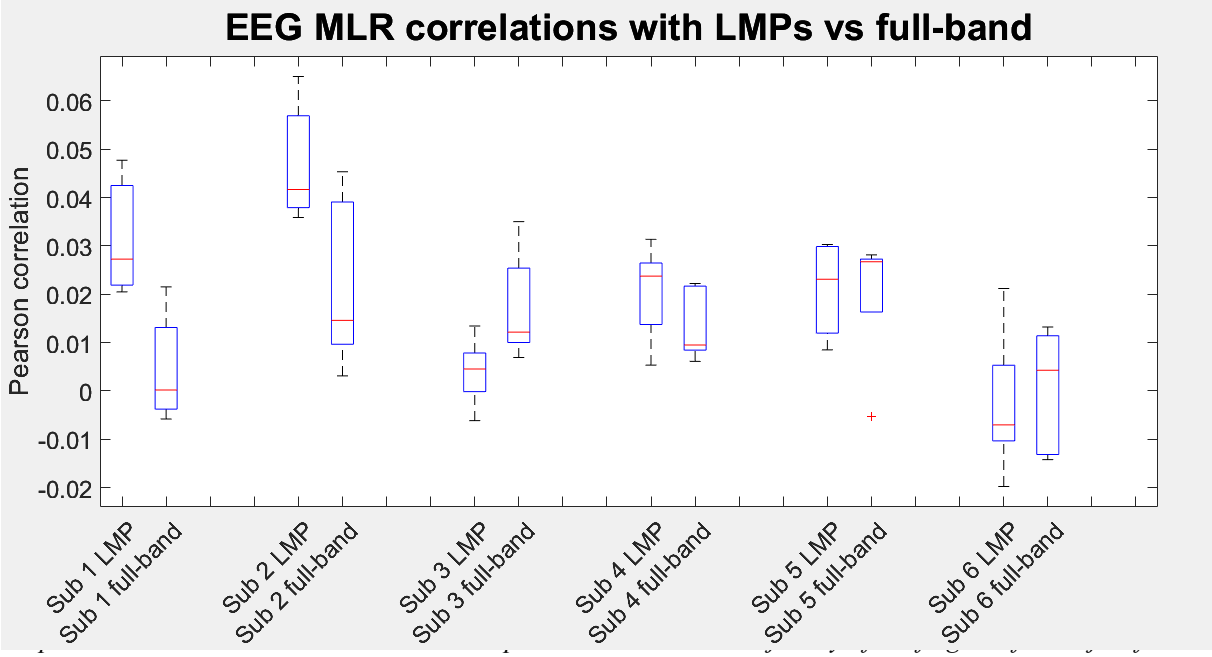

'corrected' version (models trained with trajectories without the movement intervals of other fingers).

Figure 55: Comparison of decoding performances of EEG using LMPs or full-band signals with MLR. Each boxplot includes the correlations between the predicted and actual trajectory of all fingers of a subject for the 'corrected' version (models trained with trajectories without the movement intervals of other fingers).

Two tables summarizing the results obtained for each case study are shown below, with Table 4 containing the performances referring to all subjects, and Table 5 referring to the best subject of the two datasets. Additionally, Figure 56 and Figure 57 provides another summary comparison for ECoG and EEG respectively, allowing for an easier visual assessment of performance across the different cases.

All subjects		ECoG LMP	ECoG full band	EEG LMP	EEG full band
MLR	*Range*	0.02 – 0.73	-0.02 – 0.68	-0.02 – 0.07	-0.01 – 0.05
	Median	0.46	0.42	0.02	0.01
TCN	*Range*	0.04 – 0.78	0.01 – 0.73	-0.04 – 0.10	-0.03 – 0.31
	Median	0.47	0.53	0.03	0.07

Table 4: Comparison of the different decoding cases. The table shows the correlation results across all subjects and fingers with models trained on data without other movements intervals ('corrected'). The blue part is about ECoG, the red is about EEG.

Best subject		ECoG LMP	ECoG full band	EEG LMP	EEG full band
MLR	*Range*	0.57 – 0.73	0.44 – 0.68	0.04 – 0.07	0.00 – 0.05
	Median	0.67	0.63	0.04	0.01
TCN	*Range*	0.56 – 0.78	0.54 – 0.73	0.05 – 0.10	0.08 – 0.31
	Median	0.70	0.69	0.06	0.24

Table 5: Comparison of the different decoding cases for the best subject. The table shows the correlation results of ECoG Subject 2 and EEG Subject 2 across all fingers with models trained on data without other movements intervals ('corrected'). The blue part is about ECoG, the red is about EEG.

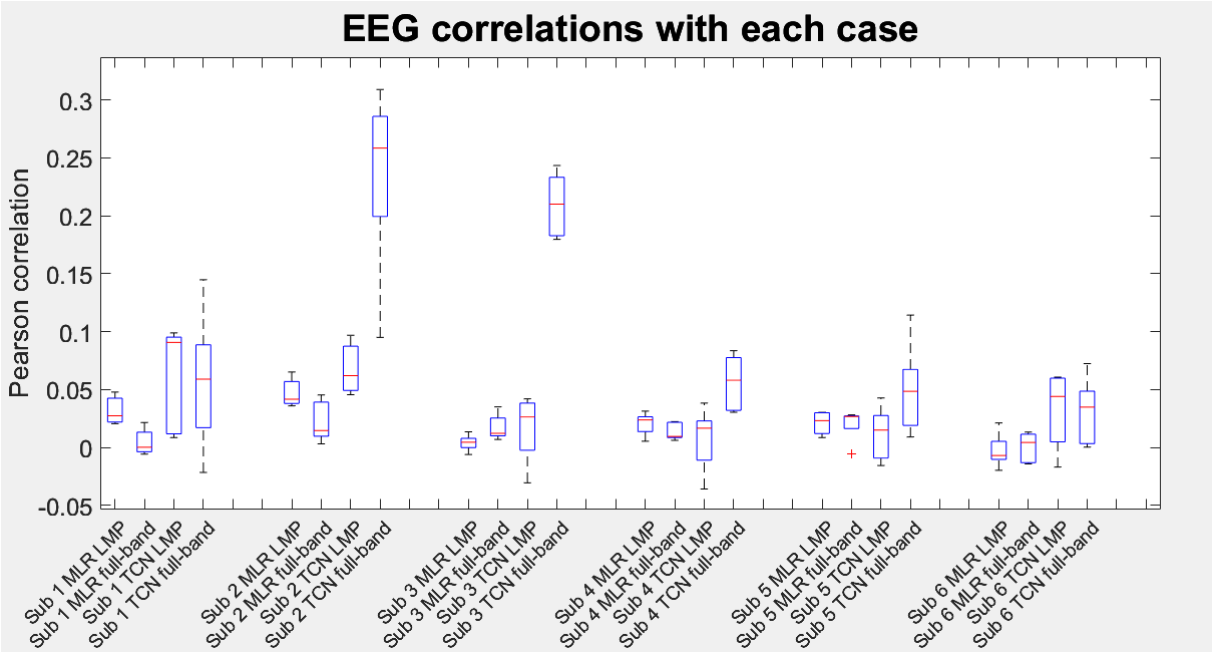

Figure 56: Comparison of all four decoding cases for each subject of EEG dataset. Each boxplot includes the correlations between the predicted and actual trajectory of all fingers of a subject for the 'corrected' version (models trained with trajectories without the movement intervals of other fingers).

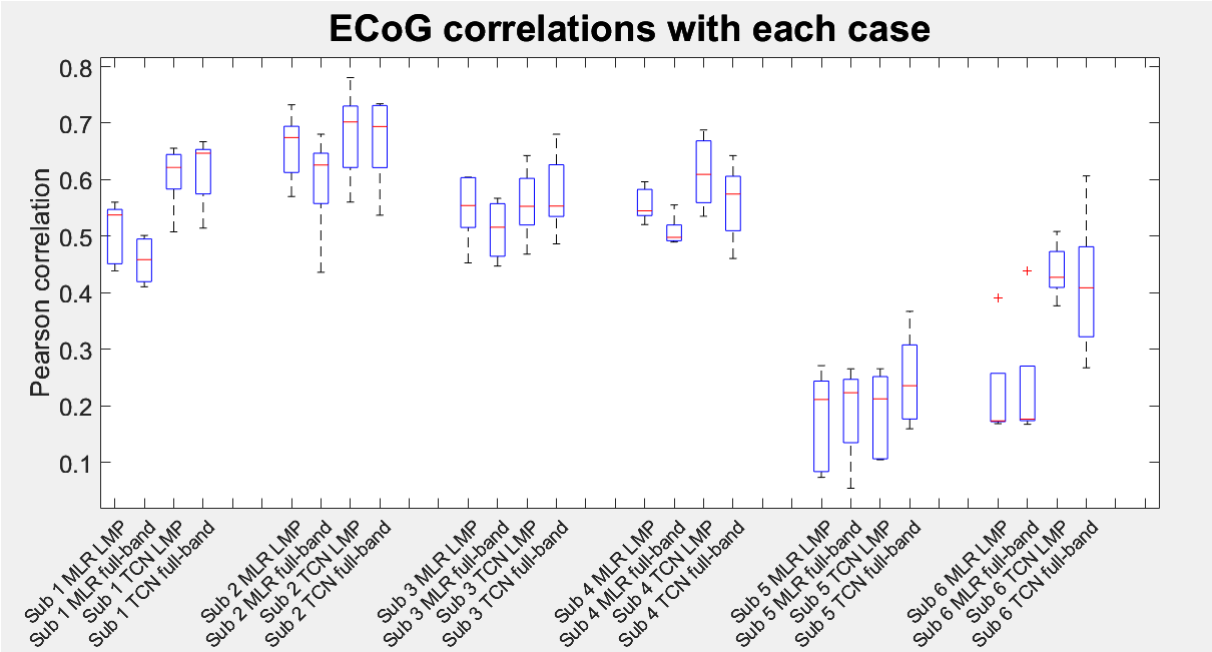

Figure 57: Comparison of all four decoding cases for each subject of EEG dataset. Each boxplot includes the correlations between the predicted and actual trajectory of all fingers of a subject for the 'corrected' version (models trained with trajectories without the movement intervals of other fingers).

5 Conclusion

This study examined the role of low-frequency activity in motor decoding for Brain-Computer Interfaces (BCIs), comparing invasive ECoG and non-invasive EEG signals during repetitive finger movements. The analysis focused on CorticoKinematic Coherence (CKC) and finger trajectory decoding, utilizing both Multiple Linear Regression (MLR) and Temporal Convolutional Networks (TCN).

- **CKC analysis:**

The CKC analysis revealed a stark difference between ECoG and EEG signals. ECoG exhibited strong coherence values, consistently reflecting the expected frequency patterns and showing a clear relationship with movement dynamics. In contrast, EEG demonstrated significantly lower CKC at movement-related frequencies (1 Hz and 3 Hz), with weak and inconsistent coherence patterns. One of the main reasons for this could be the poor frequency stability of the movement. Additionally, the poor CKC performance in EEG can likely be attributed to weaker signal-to-noise ratio (SNR), volume conduction effects, and lower spatial resolution, which made it difficult to capture clear movement-related cortical activity. These factors likely contributed to the observed inconsistencies. On the other hand, with ECoG, the higher SNR, better spatial resolution, and reduced volume conduction effects made the impact of frequency instability in movement-related frequencies less pronounced, highlighting how signal quality is very impactful for CKC calculation. Given that CKC at 1 Hz and 3 Hz serves as a metric describing the LMPs, these results led to the assumption that the LMPs in EEG signals were not as clear and informative as those observed in ECoG.

- **Decoding analysis:**

The decoding analysis further reinforced these findings. ECoG signals allowed for reliable movement trajectory reconstruction, particularly when using LMPs. The inclusion of higher frequencies did not enhance decoding performance, suggesting that LMPs contain the most relevant information. Conversely, EEG decoding performance was generally poor when using LMPs alone, aligning with the weak CKC results. However, an improvement was observed when using full-band EEG signals, particularly with the TCN model, indicating that higher-frequency EEG components might contain movement-related information that was not evident in LMPs alone.

The results from the comparison of the two decoding models showed that, for ECoG, both MLR and TCN performed well using only the LMPs, with only a slight improvement from TCN compared to MLR. This suggests that the information provided by the LMPs is easily decodable even with a simple model like MLR. As specified before, with both models the inclusion of higher-frequency bands did not improve decoding performance. For EEG, however, MLR performed poorly both with LMPs and full-band, while TCN showed a significant improvement with full-band signals, highlighting how a Deep Learning approach can extract useful information from higher-frequency components that were not evident in the LMPs.

Implications for BCI Applications:

The results of this study highlight the challenges in developing BCIs based on ECoG or EEG for real-world applications, such as enabling finger movements for individuals with neuro-motor impairments or for rehabilitation following neuro-motor injuries like strokes. In particular, accurately predicting finger trajectories appears to be a significant challenge, making it difficult for these systems to be used in real-world applications. Even with ECoG signals,

which offer better signal quality, various issues related to their invasiveness would make them unfeasible for clinical use. Regarding EEG signals, which have greater applicability due to their non-invasive nature, this challenge remains more difficult to overcome—at least with the methods employed in this study. Moreover, existing literature suggests that continuous decoding of finger movements from EEG signals is still a difficult task, while classifying a limited set of predefined movements seems more achievable.

Notably, using only 0.5-second windows allows for real-time applications, provided the predictions are accurate. The inference time for both models was always lower than the sampling period of the resampled data at 25 Hz and 83.3 Hz for EEG and 25 Hz for ECoG, ensuring real-time feasibility. The only exception was the TCN with ECoG data resampled at 200 Hz, which took 1.09 seconds to predict one second of trajectory, potentially slightly retarding real-time applications.

The results suggest a potential relationship between CKC value and decoding performance, indicating that higher coherence may be associated with improved decoding accuracy. This connection suggests that CKC likely reflects neural signal information that is also relevant for decoding, indicating its potential role as a marker of movement-related features in motor BCIs (at least for repeated movements). However, further investigation is needed to determine whether stronger CKC directly enhances decoding performance or if both are influenced by common factors such as signal quality.

6 Bibliography

[1] S. D. L. a. d. S. F. Lopes, Niedermeyer's Electroencephalography: Basic Principles, Clinical Applications, and Related Fields, Lippincott Williams & Wilkins, 2011.

[2] K. S. Park, Humans and Electricity, Springer Cham, 2023.

[3] E. N. a. F. L. d. Silva., Electroencephalography: Basic principles, clinical applications, and related fields., Lippincott Williams & Wilkins, 2005.

[4] B. Hans, «Über das Elektrenkephalogramm des Menschen,» *Springer Nature,* vol. 87, p. 527–570, 1929.

[5] S. M. A. S. N. A. M. Abo-Zahhad, «A New EEG Acquisition Protocol for Biometric Identification Using Eye Blinking Signals,» *I.J. Intelligent Systems and Applications,* vol. 6, pp. 48-54, 2015.

[6] N. C. S. D. D. J. R. W. W. F. G. S. a. M. M. V. H. Marijn van Vliet, «Single-Trial ERP Component Analysis Using a Spatiotemporal LCMV Beamformer,» *IEEE TRANSACTIONS ON BIOMEDICAL ENGINEERING,* vol. 63, n. 1, 2016.

[7] F. C. F. C. a. P. M. R. Fabio Babilonia, «Spatial enhancement of EEG data by surface Laplacian estimation: the use of magnetic resonance imaging-based head models,» *Clinical Neurophysiology,* vol. 112, pp. 727-727, 2001.

[8] B. P. S. G. Ritaccio AL, «Electrical Stimulation Mapping of the Brain: Basic Principles and Emerging Alternatives.,» *J Clin Neurophysiol.,* vol. 35, n. 2, pp. 86-97, 2018.

[9] A. D. a. S. Ray, «Cortical Electrocorticogram (ECoG) Is a Local Signal,» *Journal of Neuroscience,* vol. 39, n. 22, pp. 4299-4311, 2019.

[10] N. L. a. L. Bougrain, «Decoding finger flexion from band-specific ECoG signals in humans,» *Frontiers in Neuroscience,* 2012.

[11] W. J. R. a. W. E. W., Brain-Computer Interfaces: Principles and Practice, Oxford University Press, 2012.

[12] S. S. a. M. Baumert, «Intra- and Inter-subject Variability in EEG-Based Sensorimotor Brain Computer Interface: A Review,» *Frontiers in Computational Neuroscience,* vol. 13, 2020.

[13] J. M. A. D. F. a. M. S. Andrés Úbeda, «Estimation of Neuromuscular Primitives from EEG Slow Cortical Potentials in Incomplete Spinal Cord Injury Individuals for a New Class of Brain-Machine Interfaces,» *Frontiers in Computational Neuroscience,* vol. 12, 2018.

[14] J. M. A. R. C. a. J. d. R. M. Andrés Úbeda, «Classification of upper limb center-out reaching tasks by means of EEG-based continuous decoding techniques,» *JournalofNeuroEngineeringandRehabilitation,* vol. 14, n. 9, 2017.

[15] G. R. a. C.-V. J. Bradberry TJ, « Reconstructing three-dimensional hand movements from non-invasive electroencephalographic signals,» *Journal of Neuocience,* vol. 30, n. 9, 2010.

[16] A. H. a. C.-V. JL, «Reconstructing hand kinematics during reach to grasp movements from electroencephalographic signals,» in *Annu Int Conf IEEE Eng Med Biol Soc*, 2011.

[17] O. P. a. M.-P. GR, «Decoding of velocities and positions of 3D arm movement from EEG,» in *Conf IEEE Eng Med Biol Soc*, 2012.

[18] E. C. M. L. Y. a. M. M. V. H. Qiang Sun, «Unraveling EEG correlates of unimanual fnger movements: insights from non-repetitive fexion and extension tasks,» *Journal of NeuroEngineering and Rehabilitation,* vol. 21, n. 228, 2024.

[19] A. F. a. M. M. V. H. Eva Calvo Merino, «The role of distinct ECoG frequency features in decoding finger,» *Journal of Neural Engineering,* vol. 20, 2023.

[20] C. E. K. A. S. J. J. L. M. S. F. P. H. S. J. S. D. E. M. C. Y. L. L. A. C. Z. N. a. A. H. D. Po T. Wang, «Electrocorticogram encoding of upper extremity movement trajectories,» in *6th Annual International IEEE EMBS Conference on Neural Engineering*, San Diego, 2013.

[21] M. I. V. J. a. M. B. Harri Piitulainen, «Feasibility and reproducibility of electroencephalography-based corticokinematic coherence,» *Journal of Neurophysiology,* vol. 124, p. 959–1967, 2020.

[22] X. W. R. L. X. M. S. L. a. J. M. Yuxuan Wei, «Decoding movement frequencies and limbs based on steady-state movement-related rhythms from noninvasive EEG,» *Journal of Neural Engineering,* vol. 20, 2023.

[23] J. L. K. N. D. P. R. L. L. G. S. B. K. Jerbi, «Coherent neural representation of hand speed in humans revealed by MEG imaging,» *Proc. Natl. Acad. Sci. U.S.A.,* vol. 104, n. 18, pp. 7676-7681, 2007.

[24] D. T. X. O. d. B. M. P. B. V. B. P. G. S. H. R. J. V. Bourguignon M, «Functional motor-cortex mapping using corticokinematic coherence,» *Neuroimage,* vol. 55, n. 4, pp. 1475-9, 2011.

[25] M. B. X. D. T. R. H. V. J. Harri Piitulainen, «Coherence between magnetoencephalography and hand-action-related acceleration,,» *NeuroImage,* vol. 72, pp. 83-90, 2013.

[26] M. B. X. D. T. R. H. A. V. J. H. PIITULAINEN, «CORTICOKINEMATIC COHERENCE DURING ACTIVE AND PASSIVE,» *Neuroscience,* vol. 238, pp. 361-370, 2013.

[27] V. J. M. O. d. B. P. V. B. S. G. a. X. D. T. Mathieu Bourguignon, «Neuronal network coherent with hand kinematics during fast repetitive hand movements,» *Neuroimage,* vol. 59, pp. 1684-1691, 2012.

[28] H. P. X. D. T. V. J. R. H. Mathieu Bourguignon, «Corticokinematic coherence mainly reflects movement-induced proprioceptive feedback,» *Neuroimage,* vol. 106, pp. 382-390, 2015.

[29] G. L. C. A. B. a. H. P. Alessandra Giangrande, «Volitional muscle activation intensifies neuronal processing of proprioceptive afference in the primary sensorimotor cortex: an EEG study,» *Journal of Neurophysiology,* vol. 131, pp. 28-37, 2024.

[30] Y. W. e. al, «Decoding movement frequencies and limbs based on steady-state movement-related rhythms from non invasive EEG,» *Journal of Neurophysiology,* vol. 20, 2023.

[31] S. V. H. P. M. B. V. J. R. H. Eero Smeds, «Corticokinematic coherence as a new marker for somatosensory afference in newborns,» *Clinical Neurophysiology,* vol. 128, n. 4, pp. 647-655, 2017.

[32] M. H. R. I. R. J. K. J. &. L. O. V. Hämäläinen, «Magnetoencephalography–Theory, instrumentation, and applications to noninvasive studies of the brain.,» *Reviews of Modern Physics,* vol. 65, n. 2, pp. 413-497, 1993.

[33] K. J. D. H. C. J. H. A. O. H. N. F. R. R. T. K. J. G. O. a. E. E. F. Miller, "Human cortical motor activity is selectively phase-entrained on underlying rhythms," *PLoS computational biology 8, no.9,* 2012.

[34] M. R. Nuwer, «10-10 electrode system for EEG recording,» *Clin Neurophysiol.,* vol. 129, n. 5, 2018.

[35] S. H. P. F. H. S. N. K. a. S. Nur Faadhilah Afif, «Comparison of Wet and Dry EEG Electrodes Based On Brain Signals Characterization In Temporal and Anterior Frontal Areas Using Audio Stimulation,» *Journal of Physics,* vol. 1505, 2020.

[36] Mathworks, «https://www.mathworks.com/help/matlab/,» [Online].

[37] «https://www.python.org/,» [Online].

[38] Google, «https://colab.research.google.com/,» [Online].

[39] M. R. L. N. J. M. A. D. K. D. Ludwig KA, "Using a common average reference to improve cortical neuron recordings from microelectrode arrays," *J Neurophysiol,* vol. 101, no. 3, pp. 1679-89, 2009 Mar.

[40] P. F. E. M. a. J.-M. S. Robert Oostenveld, «FielTrip: : Open Source Software for Advanced Analysis of MEG, EEG, and Invasive Electrophysiological Data,» *Computational Intelligence and Neuroscience,* vol. vol. 2011, p. 9 pages, 2011.

[41] A. J. &. S. T. J. Bell, «An information-maximization approach to blind separation and blind deconvolution,» *Neural Computation,* vol. 7, n. 6, pp. 129-1159, 1995.

[42] S. C. A. &. Y. H. Amari, «A new learning algorithm for blind signal separation,» *Neural Networks,* vol. 8, n. 4, pp. 803-810, 1996.

[43] T. W. G. M. &. S. T. J. Lee, «Independent component analysis using an extended infomax algorithm for mixed sub-Gaussian and super-Gaussian sources,» *Neural Computation,* vol. 11, n. 2, pp. 417-441, 1999.

[44] M. Zibulevsky, «Blind source separation in the frequency domain,» *IEEE Transactions on Signal Processing,* vol. 48, n. 10, pp. 2938-2948, 2000.

[45] R. L. a. J. C., "Blinking Artifact Removal in Cognitive EEG Data Using ICA," in *2006 International Conference of the IEEE Engineering in Medicine and Biology Society*, New York, 2006.

[46] L. Z. B. &. S. M. Yao, «Fast and accurate decoding of finger movements from ECoG through Riemannian features and modern machine learning techniques,» *Journal of Neural Engineering,* vol. 19, n. 1, 2022.

[47] K. V. B. a. M. A. Azeez, «Optimized estimation of power spectral density,» in *2017 International Conference on Intelligent Computing and Control Systems (ICICCS)*, Madurai, India, 2017.

[48] P. S. Radoslav Bortel, «Approximation of statistical distribution of magnitude squared,» *Signal Processing,* vol. 87 (2007) , p. 1100–1117, 2006.

[49] L. G. A. G. O. a. S. R. Davide Anguita, «The 'K' in K-fold Cross Validation,» in *ESANN 2012 proceedings, European Symposium on Artificial Neural Networks, Computational Intelligence*, Bruges (Belgium), 2012.

[50] J. Lu, A rigorous introduction to linear models, 2021.

[51] J. M. A. R. C. a. J. d. R. M. Andrés Úbeda, «Classification of upper limb center-out reaching tasks by means of EEG-based continuous decoding techniques,» *Journal of NeuroEngineering and Rehabilitation,* vol. 14, n. 9, 2017.

[52] J. Q.-D. M. G. C.-J. a. D. A. A. Marcano-Cedeño, «Feature Selection Using Sequential Forward Selection and classification applying Artificial Metaplasticity Neural Network,» in *IECON 2010 - 36th Annual Conference on IEEE Industrial Electronics Society*, Glendale, AZ, USA, 2010.

[53] J. P. R. a. M. A. Tirlea, «Permutation Testing for Dependence in Time Series,» *arXiv:2009.03170,* 2020.

[54] J. Z. K. a. V. K. Shaojie Bai, «An Empirical Evaluation of Generic Convolutional and Recurrent Networks for Sequence Modeling,» 2018.

[55] S. K. a. R. Casper, «Applications of Convolution in Image Processing with MATLAB,» *University of Washington,* pp. 1-20, 2013.

[56] R. Philippe, «Temporal Convolutional Networks for Keras,» *GitHub repository,* 2020.

[57] P. Nakkiran, «Learning Rate Annealing Can Provably Help Generalization, Even for Convex Problems,» *arXiv preprint arXiv:2005.0736,* 2020.

[58] J. V.-S. E. M. W. M. H. Alvaro Pascual-Leone, «Responses to rapid-rate transcranial magnetic stimulation of the human motor cortex,» *Brain,* vol. 117, n. 4, pp. 847-858, 1994.

[59] B. W. E. K. A. L. E. C. I. D. A. M. P. B. D. V. R. M. M. V. H. Mansoureh Fahimi Hnazaee, «Localization of deep brain activity with scalp and subdural EEG,» *NeuroImage,* vol. 223, pp. 1053-8119, 2020.

[60] K. S. Luiz A. Baccalá, «Partial directed coherence: twenty years on some history and an appraisal,» *Biological Cybernetics,* vol. 115, p. 195–204, 2021.

[61] T. N. a. H. P. Toni Mujunen, «Corticokinematic coherence is stronger to regular than irregular proprioceptive stimulation of the hand.,» *Journal of Neurophysiology,* vol. 126, p. 550–560, 2021.